AFCRL-64-179

A COMMUNICATION SYSTEM AND THEORY FOR INVESTIGATION OF EM WAVE PROPAGATION IN THE EARTH AT FREQUENCIES FROM 0 TO 3000 CPS

Darrell R. Ward
Frederick W. Patrick

Electrical Engineering Research Laboratory
The University of Texas
Austin, Texas

Contract AF 19(604)-8513

FINAL REPORT
Technical Report No. 6-60
28 February 1964

Prepared
for
AIR FORCE CAMBRIDGE RESEARCH LABORATORIES
OFFICE OF AEROSPACE RESEARCH
UNITED STATES AIR FORCE
Bedford, Massachusetts

REPRODUCTION QUALITY NOTICE

This document is the best quality available. The copy furnished to DTIC contained pages that may have the following quality problems:

- Pages smaller or larger than normal.
- Pages with background color or light colored printing.
- Pages with small type or poor printing; and or
- Pages with continuous tone material or color photographs.

Due to various output media available these conditions may or may not cause poor legibility in the microfiche or hardcopy output you receive.

☐ If this block is checked, the copy furnished to DTIC contained pages with color printing, that when reproduced in Black and White, may change detail of the original copy.

Requests for additional copies by Agencies of the Department of Defense, their contractors, and other Government agencies should be directed to the:

DEFENSE DOCUMENTATION CENTER (DDC)
CAMERON STATION
ALEXANDRIA, VIRGINIA 22314

Department of Defense contractors must be established for DDC services or have their 'need-to-know' certified by the cognizant military agency of their project or contract.

All other persons and organizations should apply to the:

U.S. DEPARTMENT OF COMMERCE
OFFICE OF TECHNICAL SERVICES
WASHINGTON 25, D.C.

AFCRL-64-179

A COMMUNICATION SYSTEM AND THEORY FOR INVESTIGATION OF EM WAVE PROPAGATION IN THE EARTH AT FREQUENCIES FROM 0 TO 3000 CPS

Darrell R. Word
Frederick W. Patrick

Electrical Engineering Research Laboratory
The University of Texas
Austin, Texas

Contract AF 19(604)-8513

FINAL REPORT

Technical Report No. 6-60

28 February 1964

Prepared

for

AIR FORCE CAMBRIDGE RESEARCH LABORATORIES
OFFICE OF AEROSPACE RESEARCH
UNITED STATES AIR FORCE
Bedford, Massachusetts

TABLE OF CONTENTS

LIST OF FIGURES
Text

List of Figs., cont'd.

LIST OF FIGURES - Appendix A

LIST OF FIGURES -Appendix B

ABSTRACT

This report describes a 40 kilowatt transmitter designed for investigating electromagnetic wave propagation in the earth at frequencies from DC to 3000 cps. The transmitter uses a dipole antenna consisting of two surface electrodes between which a current can be passed through the earth. A brief description of the receiving equipment and some experimental data are included, and a discussion of the related theory and field strength prediction is given in the last section.

I. INTRODUCTION

The primary purpose of the transmitter described in this report is to provide a signal source for investigation of signal strength and attenuation in the earth as a function of frequency and position relative to the transmitter at the lower audio and sub-audio frequencies. A similar experimental investigation has been performed by Dunn[1] at a higher power and at a fixed frequency of 400 cps in which the radiation field was considered; however, with the relatively lower power and the one kilometer electrode spacings used here, the radiation field at the frequencies in question is essentially zero and measurements deal with only the induction field of the antenna. As shown in Figure 1, the electric field produced by the transmitter at electrodes A and B is detected by a receiver which measures the potential between two receiving electrodes m and n. The receiving system is located at some distance R and angle θ with respect to the transmitting electrodes and electrodes m and n are at some angle β. The potential measured at the receiving electrodes is a function of R, θ and β; the electrode spacings; the transmitting electrode current; and the character of the earth in the general vicinity of the transmitter and receiver. The dependence of the signal on the earth structure affords the possibility of determining at least the gross features of the earth structure beneath the measuring site. This is accomplished by matching experimental results

with theoretical results based on assumed earth models. This procedure is sometimes referred to as the dipole-dipole method[2] of subsurface resistivity sounding, and a special case is the four-electrode method[3] in which the transmitting and receiving electrodes are along a common line.

The transmitter design incorporates three basic considerations; namely, reasonably high output power capability, with continuously variable operating frequency and portability.

Following a description of the basic transmitter components, a brief discussion of the receiving equipment and examples of data taken in the Austin area will be given.

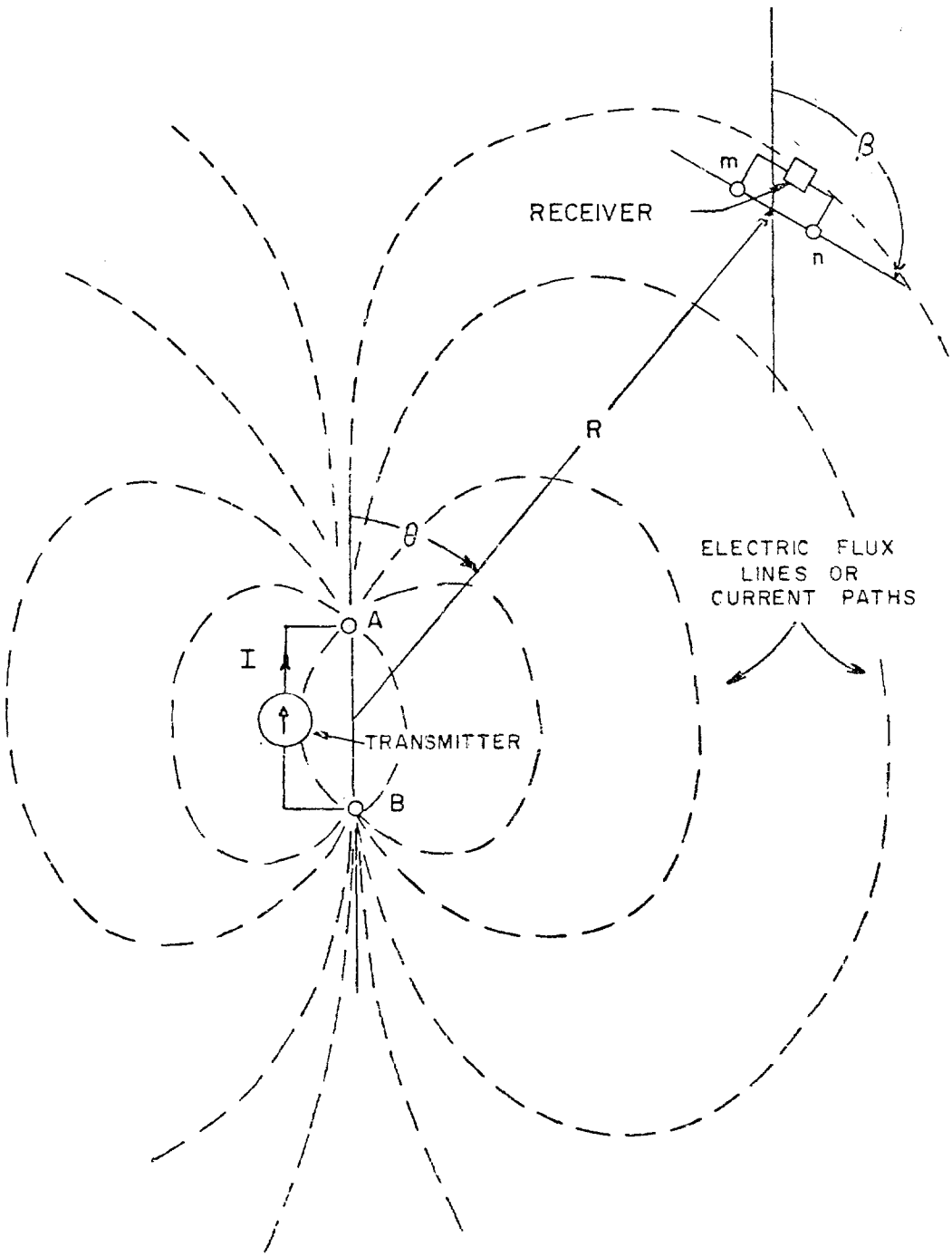

PLAN VIEW OF TRANSMITTER AND
RECEIVER ARRANGEMENT

FIG. 1.

II. TRANSMITTER

The basic function of the transmitter is to inject into the transmitting electrodes a high direct current (up to 100 amperes) which can be reversed at will, or can be periodically reversed at any frequency up to a maximum, to produce a square wave alternating current (up to 200 amperes peak to peak) in the electrodes and through the ground. The transmitter can switch up to 400 volts for a full output power of 40 kw. The basic components of the transmitter designed to accomplish this are given in block diagram form in Figure 2, and complete circuit diagrams are given in the Appendix. Direct current from a high current DC supply is applied to the transmitting electrodes through a silicon controlled rectifier (SCR) switching bridge circuit, which is capable of reversing on command the power supply polarity at the electrodes. Switching command is given by voltage pulses from the switching bridge control circuit, which may be either controlled manually, or driven periodically by a function generator.

A fast circuit breaker, also an SCR circuit, is inserted in series with the switching bridge. Actuated by the circuit breaker control, this breaker opens if the current exceeds a preset limit or if the temperature of any one of the SCR's gets too high. The breaker can be operated manually with "on" and "off" buttons.

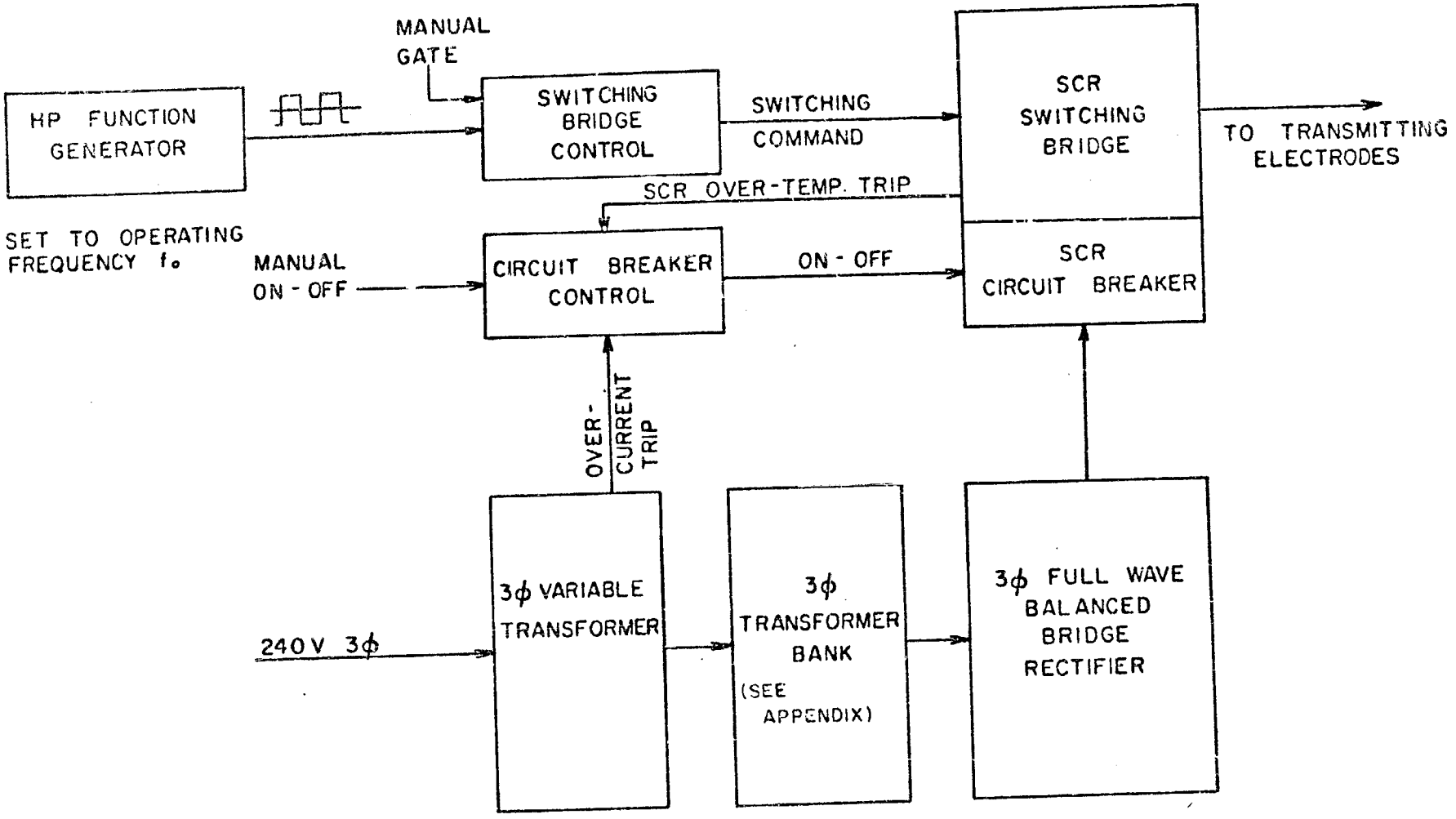

BLOCK DIAGRAM OF TRANSMITTER

FIG. 2.

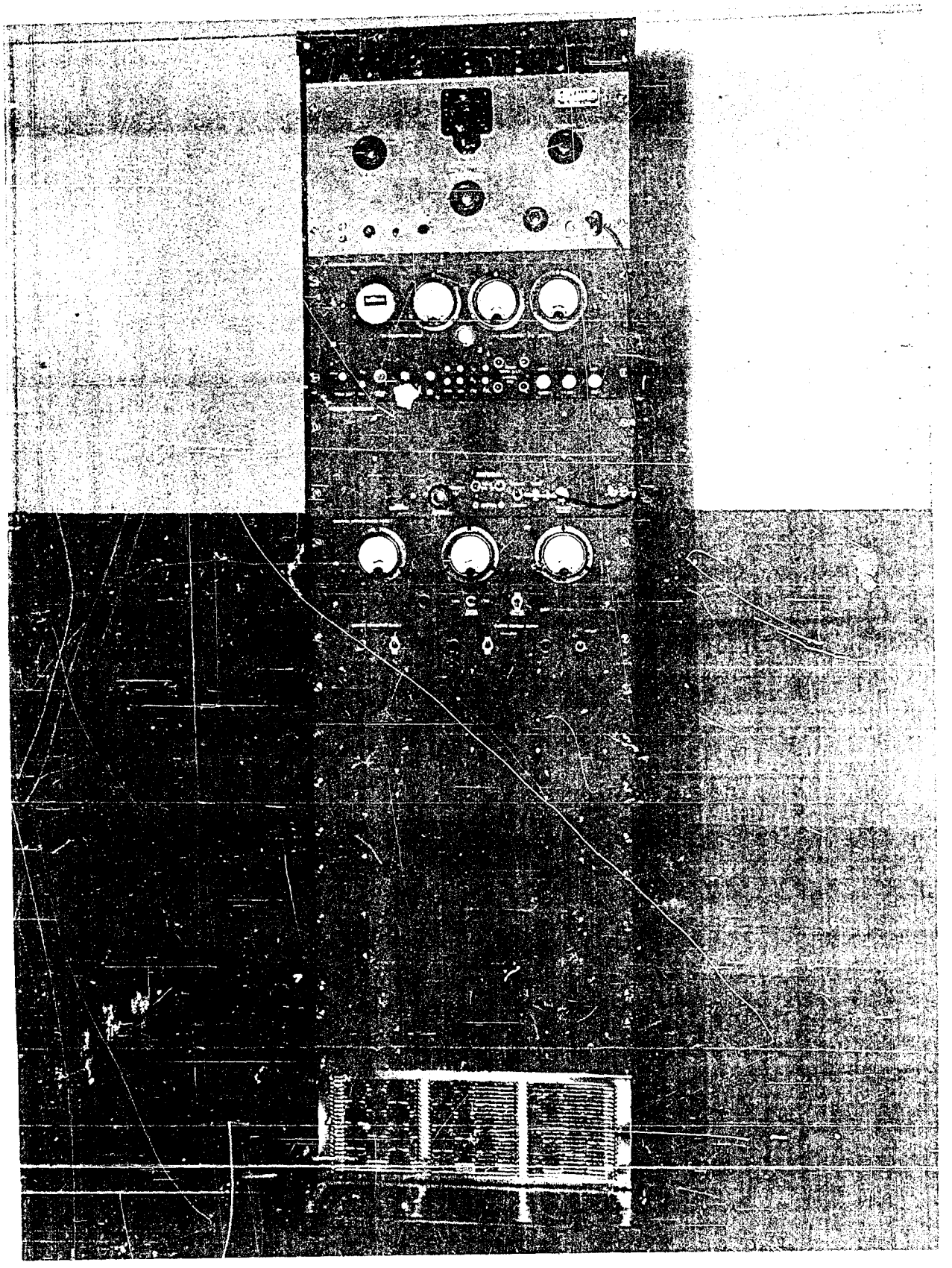

COMPLETE TRANSMITTER

FIG. 3.

The transmitter, except for the two power transformers, is entirely contained in one standard 19-inch relay rack as shown in Figure 3. The lower half of the rack contains the switching bridge, the power supply rectifier, and the cooling fan. In the upper half are the control circuits. They are, from top to bottom, the Hewlett-Packard function generator, the circuit breaker control, the switching bridge control, and the control circuitry power supply.

The silicon controlled rectifiers and the ordinary silicon rectifiers for the high current power supply are stud mounting devices which require external heat sinks. Figure 4 shows the chassis containing the switching bridge, which has four SCR's and the circuit breaker, which has two SCR's. The forced-air-cooled heat sinks, the tops of which can be seen in Figure 4, are mounted in vertical air passages made of insulating material. The nearest four are for the switching bridge. Figure 5 shows the power supply rectifier chassis with the cover removed. The heat sinks are in mountings similar to the SCR heat sinks and the spacing is the same. When mounted in the rack, as shown in Figure 6, the rectifier and the switching bridge chassis are stacked so that the cooling air blower (bottom of rack) can force air up through both. The SCR and rectifier junctions dissipate about 100 watts each at full current and the heat sinks are designed to dissipate this power while maintaining the rectifier junction temperatures below the maximum ratings in ambients up to 130° F..

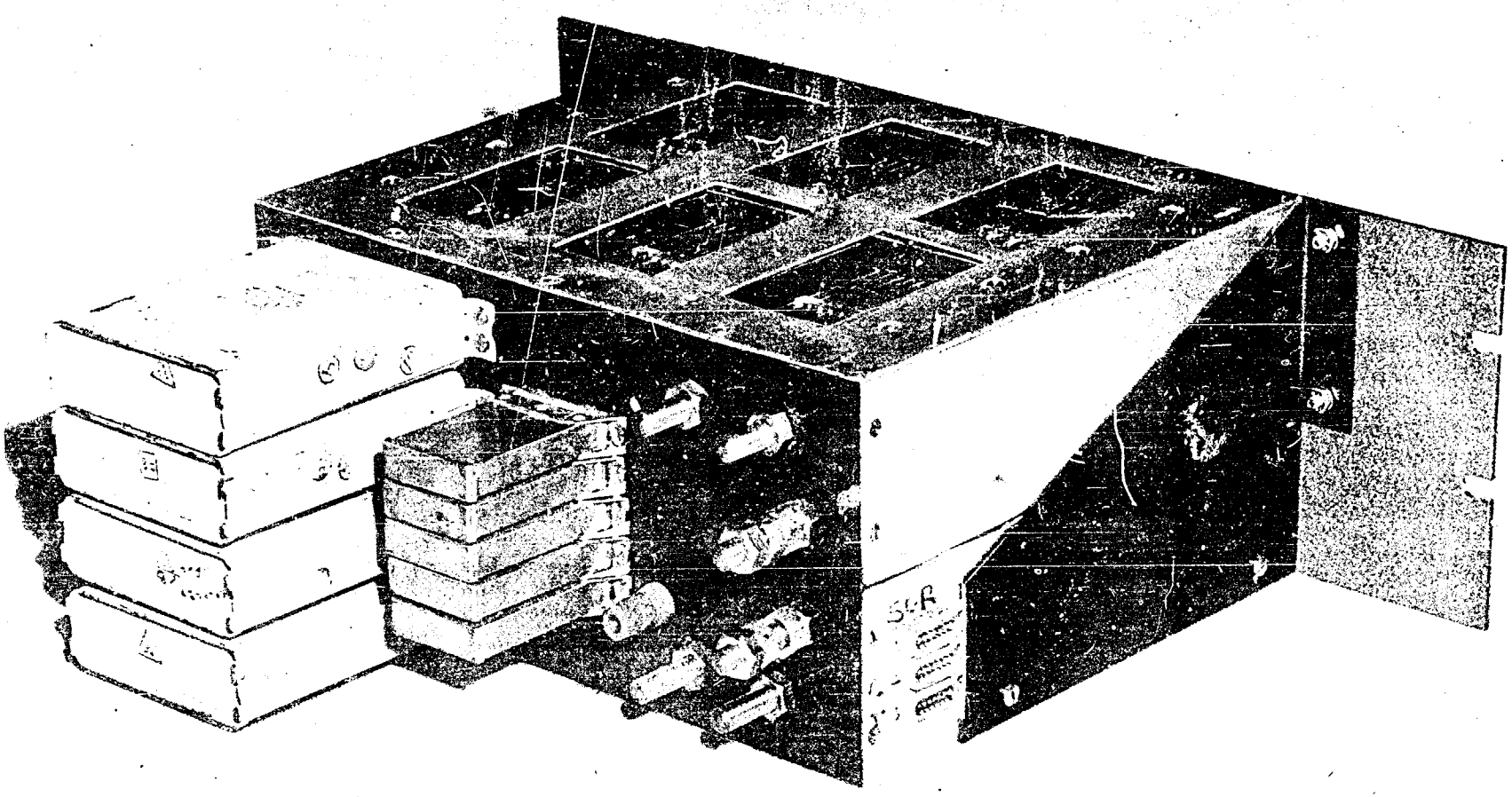

SCR SWITCHING BRIDGE

FIG. 4.

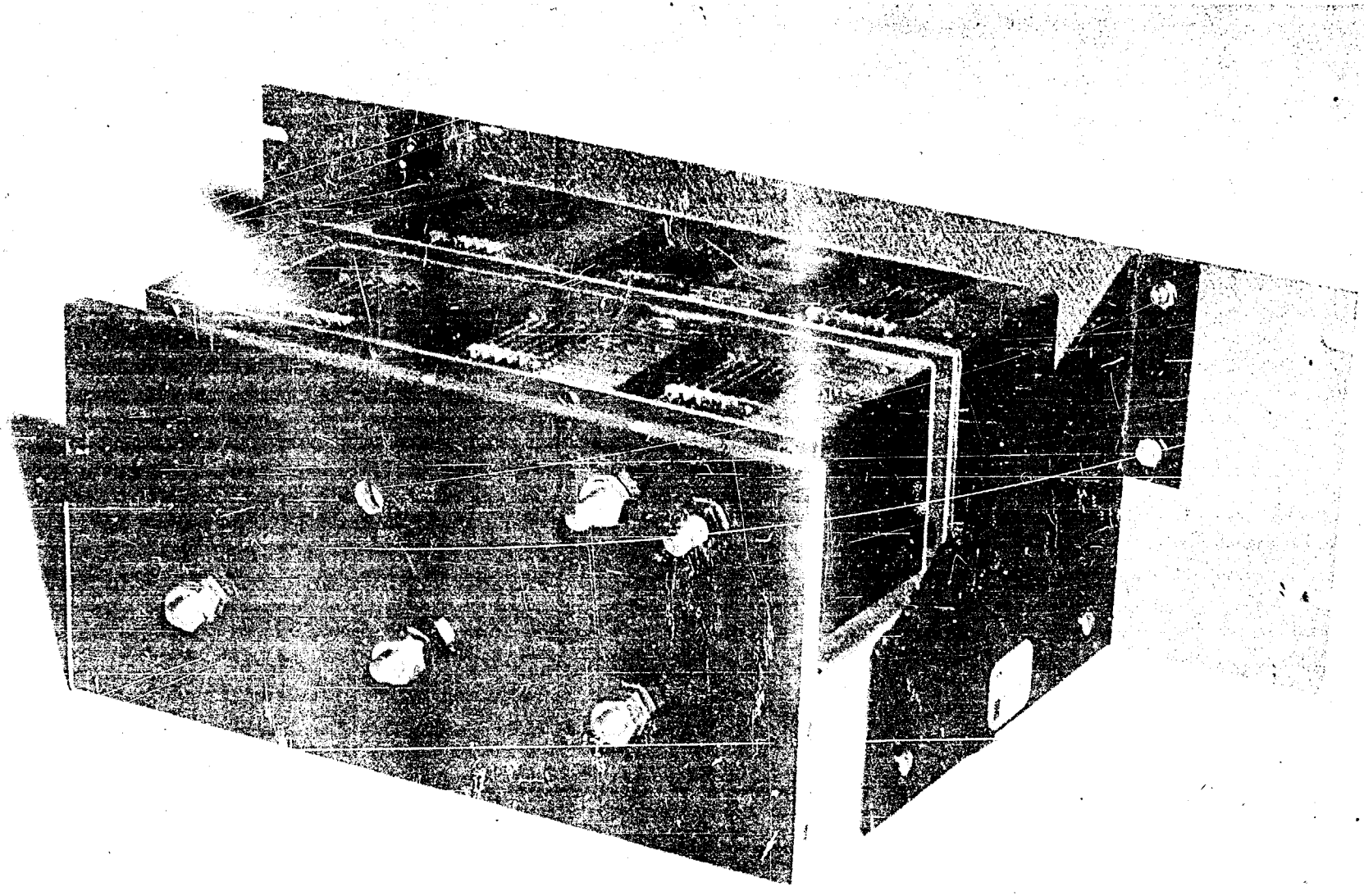

POWER SUPPLY RECTIFIER BRIDGE

FIG. 5.

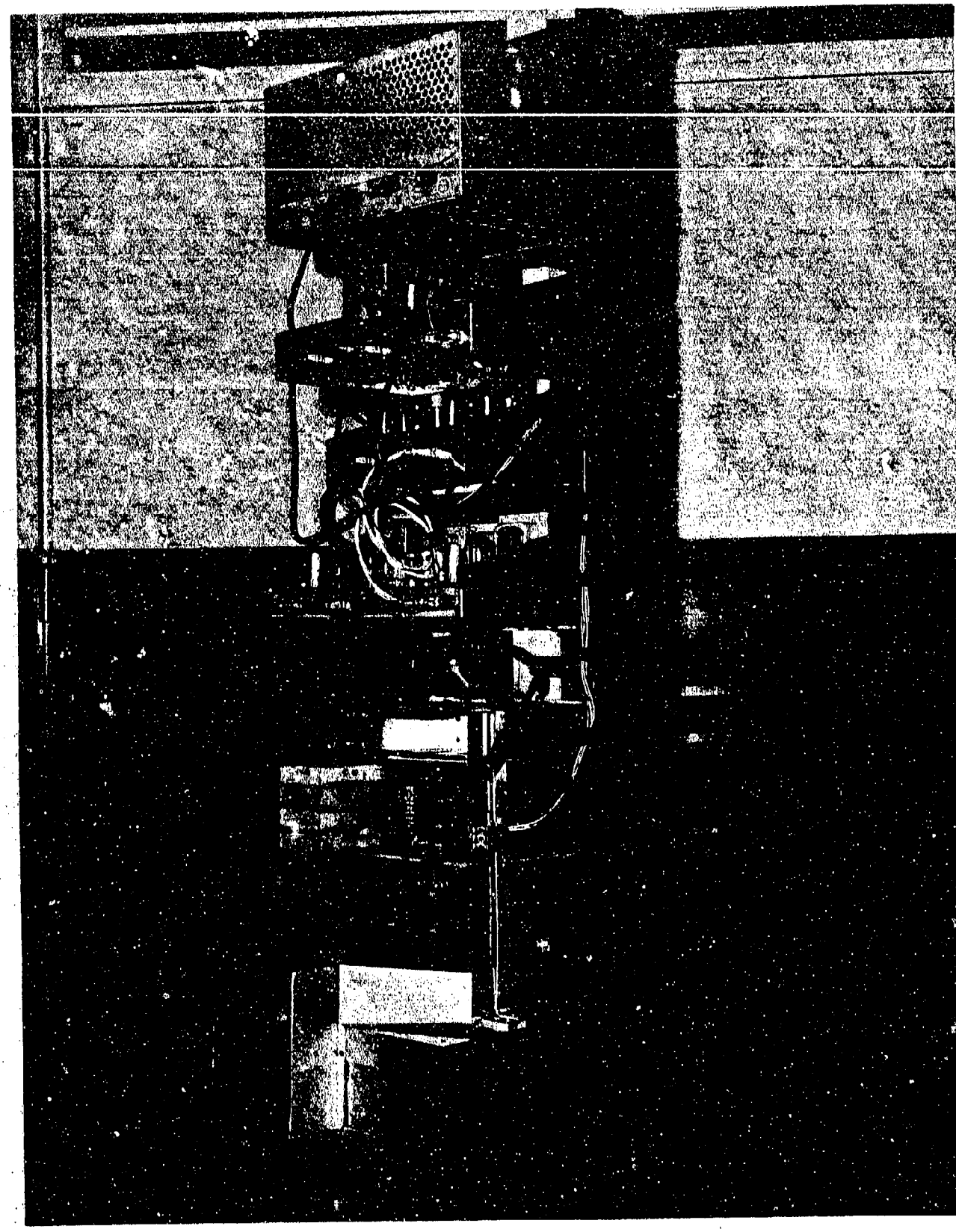

REAR OF TRANSMITTER RACK

FIG. 6.

A. DC Power Supply

A detailed schematic diagram of the power supply, along with the output voltage wave-form, is shown in Figure A-2 of the Appendix. Transmitter power is derived from a 240 volt, 60 cps, 3-phase source which must be capable of deliverying over 40 kw if the transmitter is used at maximum power. For portability, a diesel-powered generator has been used with this system. AC power is passed through a 3-phase variable autotransformer capable of continuously varying the output voltage from 0 to 280 volts rms at 90 amperes. The output of the variable transformer is fed through a 3-phase 30 kva continuous duty transformer bank which can be wye- or delta-connected with 1:1 or 1:2 primary to secondary turns ratios. This transformer bank provides possible voltage step-up and DC isolation between the transmitter and the AC power source. This transformer bank limits the transmitter to intermittent operation at full power of 40 kw.

The output of the 3-phase transformer bank is rectified by a full-wave, balanced bridge circuit using 100 ampere silicon rectifiers. The DC component of the output voltage is 95.5% of the peak line to line voltage at the input to the rectifier. The peak to peak ripple voltage is 14% of the DC voltage and is at a frequency of six times the power frequency or 360 cps in this case.

No attempt is made to filter this ripple voltage; however, since the rectifier bridge has a very high impedance to reverse voltage at

the output terminals, a capacitance of 50 μf is placed across the output to lower the impedance to reverse voltage spikes and to fast forward voltage spikes which could exist across the source inductance.

The power supply output is continously variable from 0 to over 400 volts DC so that the transmitter current may be set to any value up to the maximum.

A .005 ohm resistor R_b is inserted next to the neutral in one phase of the variable transformer to serve as a current sensor for the circuit breaker control.

B. The Silicon Controlled Rectifier

The silicon controlled rectifier (SCR) is a triode semiconductor switching device which has two stable states of conduction. The circuit symbol is shown in Figure 7 with an outline drawing of a high current SCR. The SCR can block forward or reverse anode to cathode voltage with very small leakage current or can be made to conduct relatively high forward (anode to cathode) current with extremely low voltage drop. The SCR operation is somewhat analogous to the thyratron in that forward conduction is initiated by applying a brief signal to the control gate. The SCR can then be turned off only by reduction of the forward current to a low level known as the holding current.

1. Conduction states

First consider the p-n junction shown in Figur . 8. When electrically neutral p- and n-doped semiconductor materials are

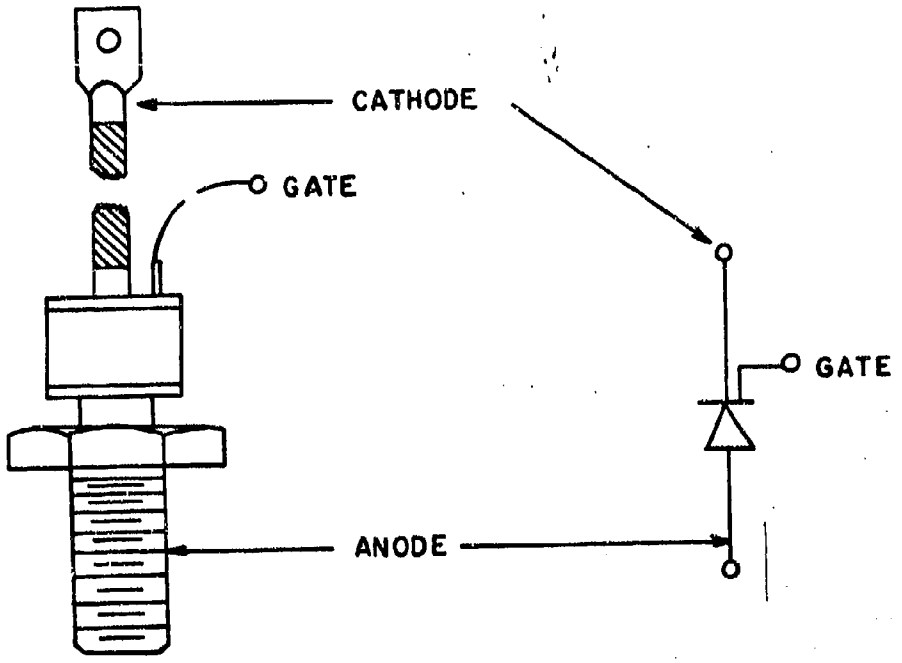

SCR OUTLINE DRAWING AND CIRCUIT SYMBOL

FIG. 7.

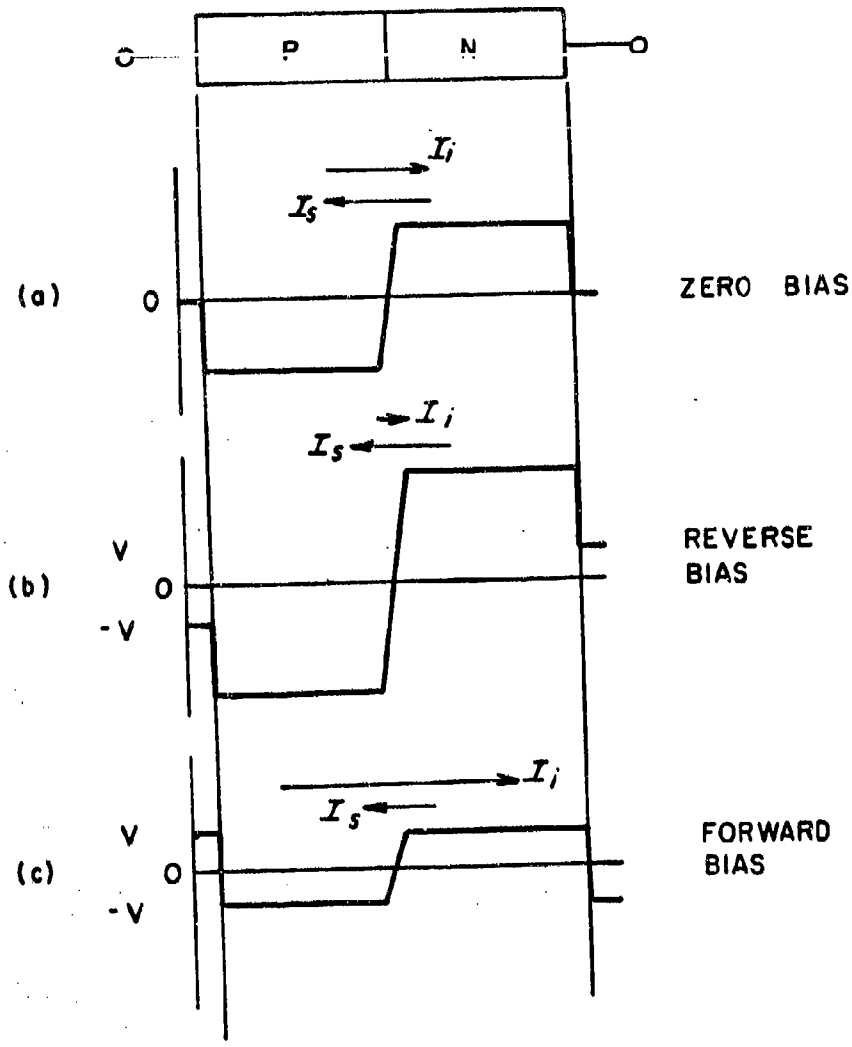

P-N SEMICONDUCTOR JUNCTION

FIG. 8.

placed together, the majority carriers (holes in the p-material and electrons in the n-material) diffuse across the junction into the adjacent material. An electric field is produced across the junction between the diffused carriers and the medium from which they came; and this field, which is in the direction from the n-material to the p-material, tends to confine the diffused carriers to the region of the junction. It is in the direction to oppose the flow of majority carriers across the junction, but minority carriers are accelerated by the field and therefore cause a steady flow of minority current across the junction. This current, which is the saturation current I_s of the junction, is primarily dependent upon the minority carrier density and does not change appreciably as the field at the junction varies.

If there is no externally applied voltage, as in Figure 8a, the saturation current tends to reduce the field at the junction and increase the flow of majority carriers, or the injection current I_i, in the opposite direction, such that equilibrium is finally reached when the injection current equals the saturation current and the net current flow across the junction is zero.

If reverse voltage is applied externally to the p-n junction, as in Figure 8b, the field at the junction will be increased and the injection current will be reduced. There will then be a net reverse current flowing through the junction which is $I_r = I_s - I_i$. This will be a very small current since the minority carrier density is low.

If forward voltage is applied, Figure 8c, the junction field will be reduced, and injection current will be increased so that there is a net forward current of $I_f = I_i - I_s$. This forward current can be quite high compared to the reverse current if the majority carrier density is high enough. This corresponds to the conduction state of the junction, whereas the junction is in the blocking state when reverse voltage is applied.

The SCR is composed of our layers of alternated p- and n-type silicon as shown in Figure 9a, producing three p-n junctions. Due to majority carrier diffusion across the p-n junctions, the potential distribution from anode to cathode in absence of externally applied voltage will be as shown in Figure 9b.

Now consider the application of a forward voltage (positive from anode to cathode). Referring to the nomenclature of Figure 9, the anode and cathode junctions will now be forward biased, but the control junction will be reversed biased, blocking forward current. However, there will be a small current flow equal to the saturation current at the control junction, since the injection current of the reversed biased control junction is near zero. This saturation current flows as injection current at the anode and cathode junctions. This condition corresponds to the "off" state of the SCR.

If reverse voltage is applied across the SCR, the control junction will be forward biased, but the anode and cathode junctions will both be reverse biased, blocking the flow of current. Again a small leakage current will flow. This reverse current in the SCR will be the saturation

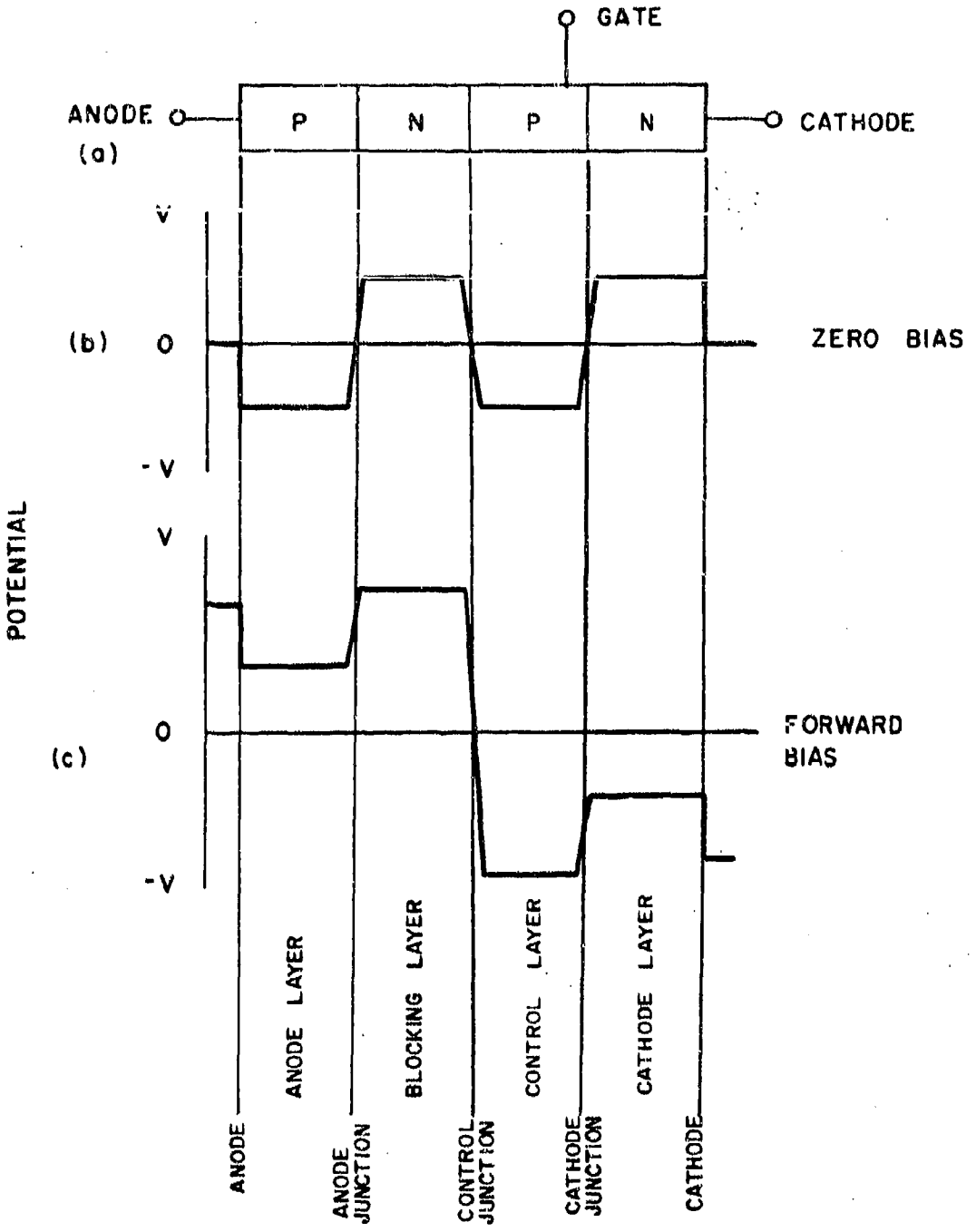

SCR POTENTIAL DISTRIBUTION

FIG.9.

current at the anode and cathode junctions and will be approximately the same as the forward leakage current.

Now suppose that forward voltage is applied to the SCR and a high forward current is somehow made to flow. This current must flow in the control and blocking layers as minority carrier current. These minority carriers are accelerated by the field of the reverse biased control junction, and if the current density is high enough, the accelerated minority carriers will multiply by collision in an avalanche effect and produce excess majority carriers in the control and blocking layers near the control junction. At the same time, the high injection current at the anode and cathode junctions produces clouds of minority carriers in the blocking and control layers near the anode and cathode junctions respectively. These charge clouds are of opposite polarity to the ones on the other side of the respective layers. The majority and minority carrier charge clouds are accelerated toward each other across the blocking and control layers by mutual attraction and by their own concentration gradients, thus supporting the high current. The carrier life is of sufficient length in the control and blocking layers that charge production by injection and multiplication far exceeds the loss by recombination. Forward current in the anode and cathode layers is due to majority carriers.

This condition, in which forward voltage drop across the SCR goes to a very low value, corresponds to the "on" state of the SCR and will be maintained until the forward current is reduced to the holding

current, below which carrier multiplication by collision is low enough and recombination is high enough that the process is no longer regenerative. The SCR will then revert to the forward blocking (off) state.

2. Turn-on and turn-off

When the SCR is in the off state, blocking forward voltage, it can be turned on or made to conduct forward current by initiating the previously described avalanche effect in a small area of the control junction and letting this condition propagate over the entire control junction. In this way, the SCR may be turned on with an amount of power which is very small compared to the power handled by the SCR. Turn-on is accomplished by applying a forward voltage to a small region of the cathode junction by means of a gate lead attached to one edge of the control layer (the gate lead is made positive with respect to the cathode lead), causing a high density cloud of electrons to be injected into one edge of the control layer from the cathode layer. This cloud of electrons is attracted and greatly accelerated by the nearby electric field of the reverse biased control junction; the electrons begin producing carriers by collision in a small region of the control junction and this condition spreads itself over the entire junction. A finite time, in the neighborhood of 5 μ sec, is required for the SCR to be fully on. The gate no longer has any effect after the avalanche condition begins in the control junction.

Turn-on will also occur if the rate of increase of forward voltage, $\frac{de_f}{dt}$, is too high, causing a displacement current at the junction

large enough to initiate the multiplication of carriers by collision. Therefore, this derivative must be considered when applying forward voltage if it is intended for the SCR to remain off. For most SCR's, the maximum rate of increase is 20 volts/μ sec.

Turn-off is accomplished when the SCR is again made capable of blocking externally applied forward voltage. This means that the charge carrier density must be lowered below the value needed to sustain the carrier multiplication condition that exists during the on state. Turn-off will occur if the current is reduced below the holding value, but it is accomplished more rapidly by applying a brief reverse voltage to the SCR. Upon doing so, a short pulse of current flows in the reverse direction as the carriers are swept from the anode and cathode layers; however, due to the now reverse biased anode and cathode junctions, the charge carriers cannot flow from the blocking and control layers and can disappear by recombination only. Therefore it is necessary to wait a short length of time for recombination to reduce the carrier density to a low enough value, after which forward voltage may again be applied. The waiting time depends on the carrier life of the material used, but is normally around 25 μ sec for most large SCR's.

C. SCR Circuit Breaker

The silicon controlled rectifier circuit breaker electronically switches the DC power supplied to the SCR switching bridge by the power

supply. This breaker can be opened and closed manually by push-buttons on the control panel, and it will automatically open if either the power supply current or the temperature of any of the SCR's gets too high. All "off" and "on" commands for the breaker are supplied by the circuit breaker control chassis to be considered in a later section.

Consider the breaker circuit shown in Figure 10a. SCR S5 is in series with the load and carries the full load current. When the breaker is open, both SCR's S5 and S6 are in the off state and are blocking forward voltage. The capacitor C_b is charged to V_b by a charging voltage supplied by the breaker control chassis. Note that S6 must block a forward voltage equal to the source voltage $e_s(t)$ plus V_b. To close the breaker, a gate voltage pulse is applied to S5, causing it to turn on and close the circuit. S6 remains off. To open the breaker, a gate voltage pulse is applied to S6, causing it to turn on and place the capacitor voltage V_b across S5 in the reverse direction. A short pulse of reverse recovery current flows through S5, after which it becomes a high impedance, and circuit current is momentarily diverted through S6 and C_b. The equivalent circuit for the time after gating S6 is shown in Figure 10b. S5 remains reverse biased as long as C_b is charged with the polarity shown, or as long as $e_b(t)$ is positive. For S5 to recover its forward blocking ability, this reverse bias must last for a time $\Delta t \geq 25\mu s$.

Unfortunately, the capacitor voltage time constant, and thus the reverse bias time, is dependent upon the circuit breaker load and source

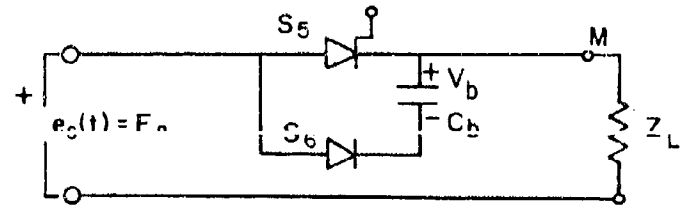

(a)

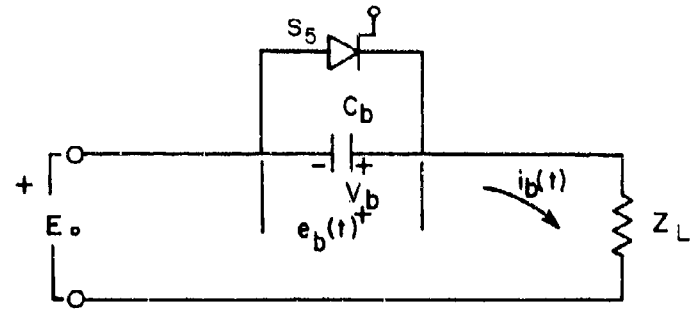

(b)

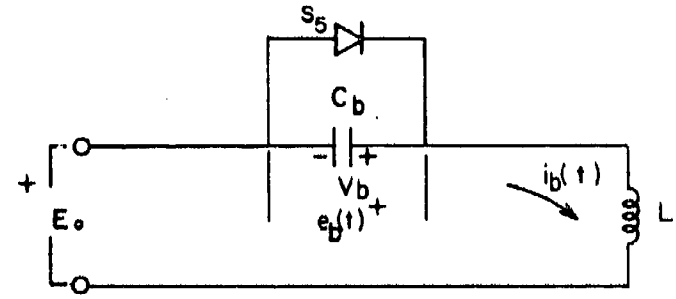

(c)

BASIC CIRCUIT BREAKER AND EQUIVALENT CIRCUITS DURING COMMUTATION

FIG. 10.

impedance. If the source impedance were zero, and if the load impedance were to suddenly drop to zero due to a short circuit, the reverse bias voltage time constant would go to zero and S5 would not be given time to recover. However, as will be seen in the next section, the SCR switching bridge circuit has a series inductance of L = 1 mh in the line coming from the power supply. This inductance, which also functions in the commutation of the switching bridge, is more than large enough to limit the rate of rise of fault current to a reasonable value. The source impedance, which is always greater than zero, will also limit the fault current; however, since this impedance will not always be known, the circuit breaker parameters were determined using a worst case condition.

As a worst case, consider the equivalent circuit of Figure 10c in which the load has been shorted past the commutating inductor L. Also consider a zero source impedance. During the time that $e_b(t)$ is going from V_b to zero, the circuit current may be approximated by

$$i_b(t) \cong \left(\frac{E_o + V_b}{L}\right) t + I_o \qquad (1)$$

where I_o is the value of circuit current at which the breaker control senses the overload and turns on S6 at t = 0. The capacitor voltage and the reverse voltage on S5 can then be approximated by

$$e_b(t) \cong V_b - \frac{1}{C} \int_o^t i_b(t)\,dt$$

$$= V_b - \frac{E_o + V_b}{2LC} t^2 - \frac{I_o}{C} t. \qquad (2)$$

It is desired that $e_b(t)$ go to zero in a minimum of $\Delta t = 25\ \mu s$; therefore

$$V_b - \frac{E_o + V_b}{2LC} (\Delta t)^2 - \frac{I_o}{C} \Delta t = 0 \qquad (3)$$

relates the circuit parameters which satisfy the cut-off conditions.

Since the maximum forward blocking voltage for S6 is 500 volts, this is the maximum allowable value for $E_o + V_b$. Let the trip current $I_o = 150a$. This gives

$$0 = V_b - \frac{500}{2 \times 10^{-3} C} (25 \times 10^{-6})^2 - \frac{150}{C} (25 \times 10^{-6})$$

$$V_b = \frac{3806 \times 10^{-6}}{C} \qquad (4)$$

If $C = 40\ \mu f$, $V_b = 95$ volts. The source voltage $e_s(t) = E_o$ can then be as high as 400 volts and, as is seen in the section on the switching bridge, it is undesirable to operate the bridge above 400 volts. Therefore, the above values seem reasonable.

Since an SCR cannot turn on without the flow of forward current through its junctions, the breaker cannot be closed without a load. Likewise, the SCR's of the switching bridge cannot be turned on until the breaker is closed. To overcome this locked state, a small resistance R_1, consisting of five 110 volt panel lamps connected in series, is connected across the breaker. This provides a load resistance that begins low enough to allow the breaker SCR to turn on, and then rises to a much higher value as the lamp filaments heat up, so that little power is dissipated in this resistance.

D. SCR Switching Bridge

DC power from the circuit breaker output is applied to the transmitting electrodes by a silicon controlled rectifier bridge circuit which determines the electrode polarity. This switching bridge is shown in Figure 11a where the transmitting electrode resistance is represented by R in the circuit. Voltage is applied across R by turning on either the SCR's S1 and S2 or S3 and S4; the polarity depends on which pair is on. The bridge is self-commutating so that when one pair is turned on, the other is automatically turned off. The self-commutation is made possible by proper adjustment of the commutating inductance and capacitance, L and C, for a given value of R, so that the SCR's of the pair being turned off have the necessary reverse bias time and a slow enough application of forward voltage.

1. Commutation

Consider the conditions of the circuit prior to commutation. When the breaker is closed, there is at first no voltage across R since all the SCR's are off. Now if gate pulses are applied simultaneously to the SCR pair S1 and S2, these SCR's turn on (represented by solid arrows in Figure 11b) and the voltage e(t) rises to the source voltage with a wave form determined by R, L, and C. If $\frac{de(t)}{dt}$ is not too large (less than about 20 volts/μs) the SCR pair S3 and S4 will remain off (represented by outlined arrow). Since the forward resistance of the SCR's is very low (about .01 ohms for the ones used) compared to acceptable values of R, it can be neglected here. The switching bridge is now in one of its stable "on" states. C is charged to

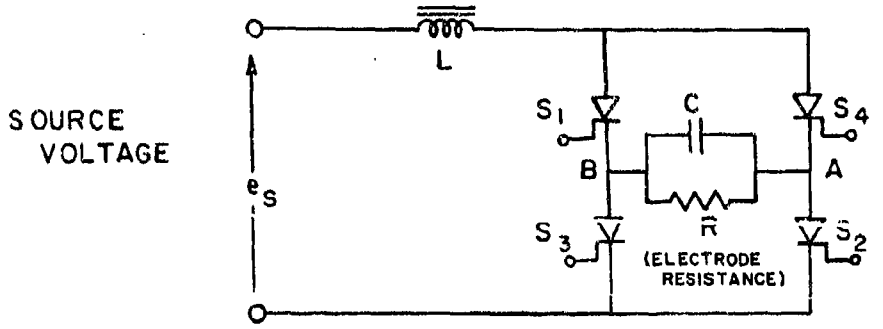

(a) OFF

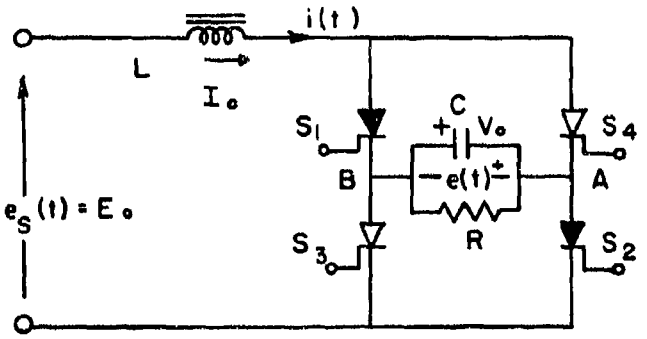

(b) TERMINAL B POSITIVE

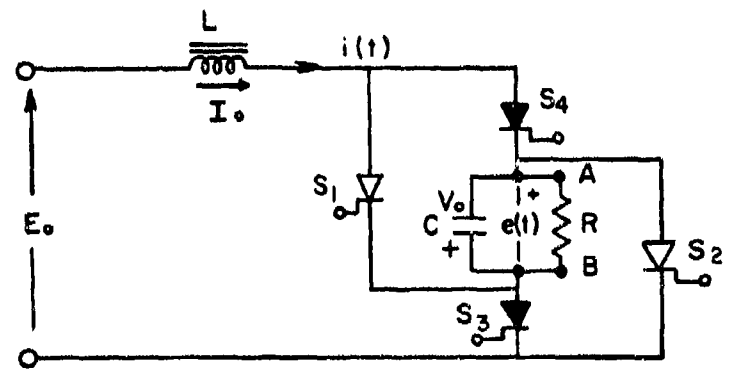

(c) SWITCHING TO TERMINAL
A POSITIVE

SCR SWITCHING BRIDGE AND CONDUCTION STATES

FIG. 11.

$V_o = E_o$ with the polarity shown and a current of $I_o = \frac{E_o}{R}$ flows through L. To make the bridge switch and reverse current through R, gate pulses are applied simultaneously to SCR's S3 and S4, causing them to turn on and apply the capacitor voltage e(t) (initially equal to $-E_o$) across S1 and S2 in the forward direction as shown in Figure 11c. S1 and S2 are reverse biased during the time that e(t) is negative. After a short pulse of reverse recovery current through S1 and S2, the internal impedance of these SCR's becomes very high. If certain conditions are met, S1 and S2 remain off as e(t) proceeds to its final value of $+E_o$, and the switching will be completed.

The first condition to be met is that e(t) must remain negative for the time Δt which is equal to or greater than the time Δt_{min} required for S1 and S2 to recover. Secondly, after e(t) reaches zero, $\frac{de(t)}{dt}$ must be less than a given maximum to avoid turning S1 and S2 back on with high forward displacement current. The third condition is that the current i(t) must never be negative, since this would turn off S3 and S4 and cause the voltage across R to go to zero.

Assuming the above conditions are satisfied, the voltage e(t) can be represented by the equivalent circuit of Figure 12a for the time after gating S3 and S4.

2. Expression for switching transients

To get an expression for e(t) after switching begins, consider the circuit of Figure 12a. Let $e_s(t) = u(t)E_o$, where u(t) is the unit step function; L and C have initial conditions I_o and V_o, respectively.

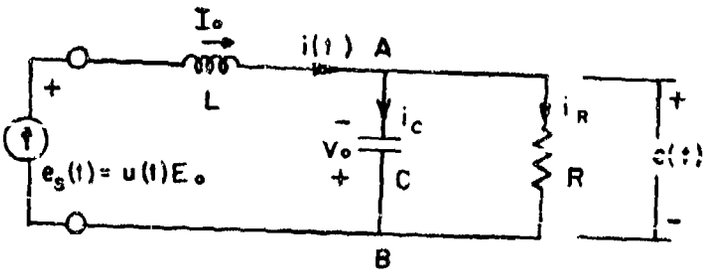

(a)

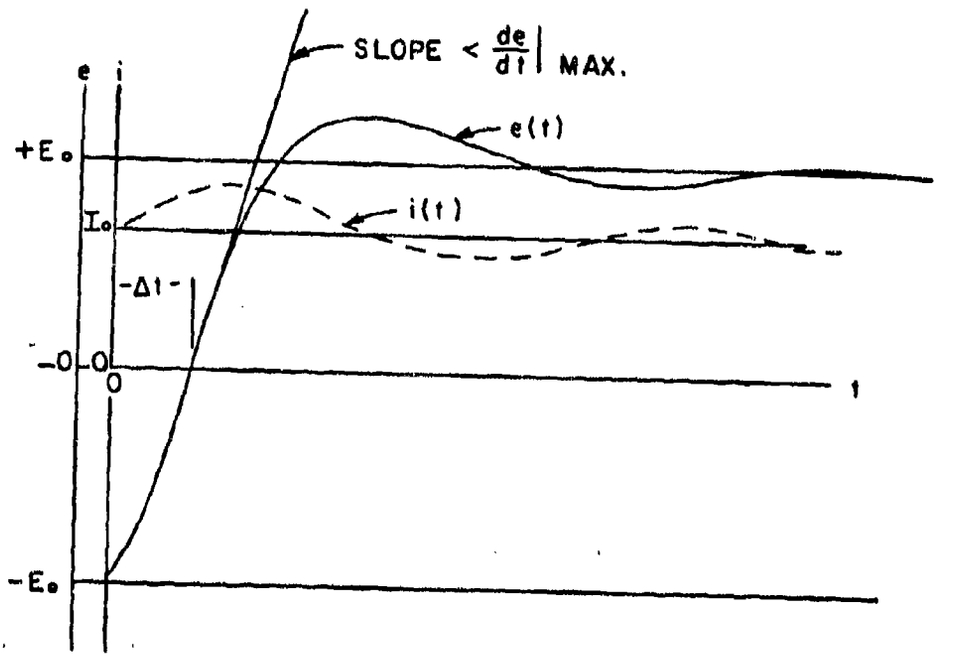

(b)

EQUIVALENT CIRCUIT AND WAVE FORMS OF SWITCHING BRIDGE DURING COMMUTATION

FIG. 12.

Summing the currents at terminal A gives

$$i = i_R + i_C \tag{5}$$

or, written in terms of the voltages,

$$\frac{1}{p}\,\frac{1}{L}\,[e_s - e] = Ge + Cpe, \qquad G = \frac{1}{R} \tag{6}$$

where $\frac{1}{p}$ is the time integral operator and p is the time derivative operator.

Taking the Laplace transform gives

$$\frac{1}{sL}\,\mathcal{L}\{e_s - e\} + \frac{1}{sL}\int_{-\infty}^{o} [e_s - e]\,dt = GE(s) + C_s E(s) - Ce(o^+)$$

where $E(s) = \mathcal{L}\{e(t)\}$.

Since

$$\frac{1}{L}\int_{-\infty}^{o} (e_s - e)\,dt = I_o \quad \text{and} \quad e(o^+) = V_o,$$

$$\frac{E_s(s)}{sL} - \frac{E(s)}{sL} + \frac{I_o}{s} = GE(s) + CsE(s) - CV_o. \tag{7}$$

Solving for E(s),

$$E(s) = \frac{E_s(s)/_{LC} + I_o/_C - V_o/_s}{s^2 + G/_C\, s + 1/_{LC}}. \tag{8}$$

The characteristic equation,

$$s^2 + \frac{G}{C}\,s + \frac{1}{LC} = 0 \tag{9}$$

is of the form

$$s^2 + 2\zeta\,\omega_o s + \omega_o^2 = 0 \tag{10}$$

where the natural frequency of the circuit is

$$\omega_o = \frac{1}{\sqrt{LC}} \tag{11}$$

and the damping factor is

$$\zeta = \frac{G}{2}\sqrt{\frac{L}{C}} \tag{12}$$

Now, letting $e_s(t) = u(t)\ E_o$, $V_o = E_o$, and $I_o = GE_o$, where E_o is a constant, the inverse transform of $E(s)$ is found to be

$$E(t) = u(t)\ E_o\left[1 - 2e^{-\zeta\omega_o t}\cos\sqrt{1-\zeta^2}\,\omega_o t + \frac{2\zeta}{\sqrt{1-\zeta^2}}e^{-\zeta\omega_o t}\sin\sqrt{1-\zeta^2}\,\omega_o t\right] \tag{13}$$

The inductor current

$$i(t) = u(t)\frac{1}{L}\int_{-\infty}^{t}[e_s - e]\,dt$$

can be written as

$$i(t) = u(t)\ I_o\left[\frac{\omega_o}{2\zeta}\int_0^t\left(-2e^{-\zeta\omega_o t}\cos\sqrt{1-\zeta^2}\,\omega_o t + \frac{2\zeta}{\sqrt{1-\zeta^2}}\,e^{-\zeta\omega_o t}\sin\sqrt{1-\zeta^2}\,\omega_o t\right)dt \tag{14}$$

The functions e(t) and i(t) have the general shape shown in Figure 12b.

The above expressions were obtained with the assumption that $e_s(t)$ was a constant. The power supply voltage wave form, as shown in Figure A-2, has, actually, a 14% ripple voltage; however, this ripple is at a

frequency of 360 c/s, and each hump on the wave form is 2.8 msec. long. Since Δt of Figure 12b is only about 30 μsec, the natural frequency ω_o of the commutating circuit can be quite high, and the transients during switching will endure for only a short time interval compared to the period of the power supply ripple. Therefore, the source voltage for the switching bridge can be assumed to be essentially constant during the switching transients. E_o will then be just the instantaneous value of the power supply voltage at the time the bridge is switched. Also, due to the comparatively fast response time of the commutating circuit, the initial conditions will follow the power supply wave form and will still be related to E_o in the same manner assumed previously.

If the switching bridge is to work into a given electrode resistance R, the necessary values of L and C must be determined in order that the voltage and current transients meet the conditions necessary for commutation outlined earlier.

Consider the expressions for e(t) and i(t). If they are divided by E_o and I_o, respectively, they can be written as

$$\frac{e(t)}{E_o} = u(t)\left[1 - 2e^{-\zeta\omega_o t}\cos\sqrt{1-\zeta^2}\,\omega_o t + \frac{2}{1-\zeta^2}\,e^{-\zeta\omega_o t}\sin\sqrt{1-\zeta^2}\,\omega_o t\right] \quad (15)$$

and

$$\frac{i(t)}{I_o} = u(t)\left[\frac{1}{2\zeta_o}\int_o^t\left(-2e^{-\zeta\omega_o t}\cos\sqrt{1-\zeta^2}\,\omega_o t + \frac{2\zeta}{\sqrt{1-\zeta^2}}\,e^{-\zeta\omega_o t}\sin\sqrt{1-\zeta^2}\,\omega_o t\right)d\omega_o t + 1\right]. \quad (16)$$

Notice that these are expressions for the voltage and current normalized to one at their steady state values. They are functions of only two variables, $\omega_o t$ and ζ; therefore, by plotting $e(t)/E_o$ and $i(t)/I_o$ as functions of $\omega_o t$ with ζ as a parameter, two families of curves are obtained that represent the commutating circuit under all conditions. These curves can be used in conjunction with Equations (11) and (12) to determine L and C.

A Pace Model 221R general purpose analog computer, connected as shown in Figure 13 was used to obtain the generalized curves for e(t) and i(t). Consider again the differential equation for the output voltage e(t) of the commutating circuit. It can be written in terms of ζ and ω_o as

$$pe = -2\zeta\omega_o e + \frac{\omega_o^2}{p}(E_o - e). \tag{17}$$

Dividing by ω_o and E_o gives

$$\frac{p}{\omega_o}\,\frac{e}{E_o} = -2\zeta\,\frac{e}{E_o} + \frac{\omega_o}{p}\left(1 - \frac{e}{E_o}\right).$$

Let $\frac{p}{\omega_o} = P$, a derivative operator with respect to $\omega_o t$; and let $\frac{e}{E_o} = e'$, the normalized output voltage. Rewriting and multiplying by -1,

$$-Pe' = 2\zeta e' - \frac{1}{P}(1 - e') \tag{18}$$

The inductor current

$$i = i_C + i_R = Cpe + Ge,$$

and since

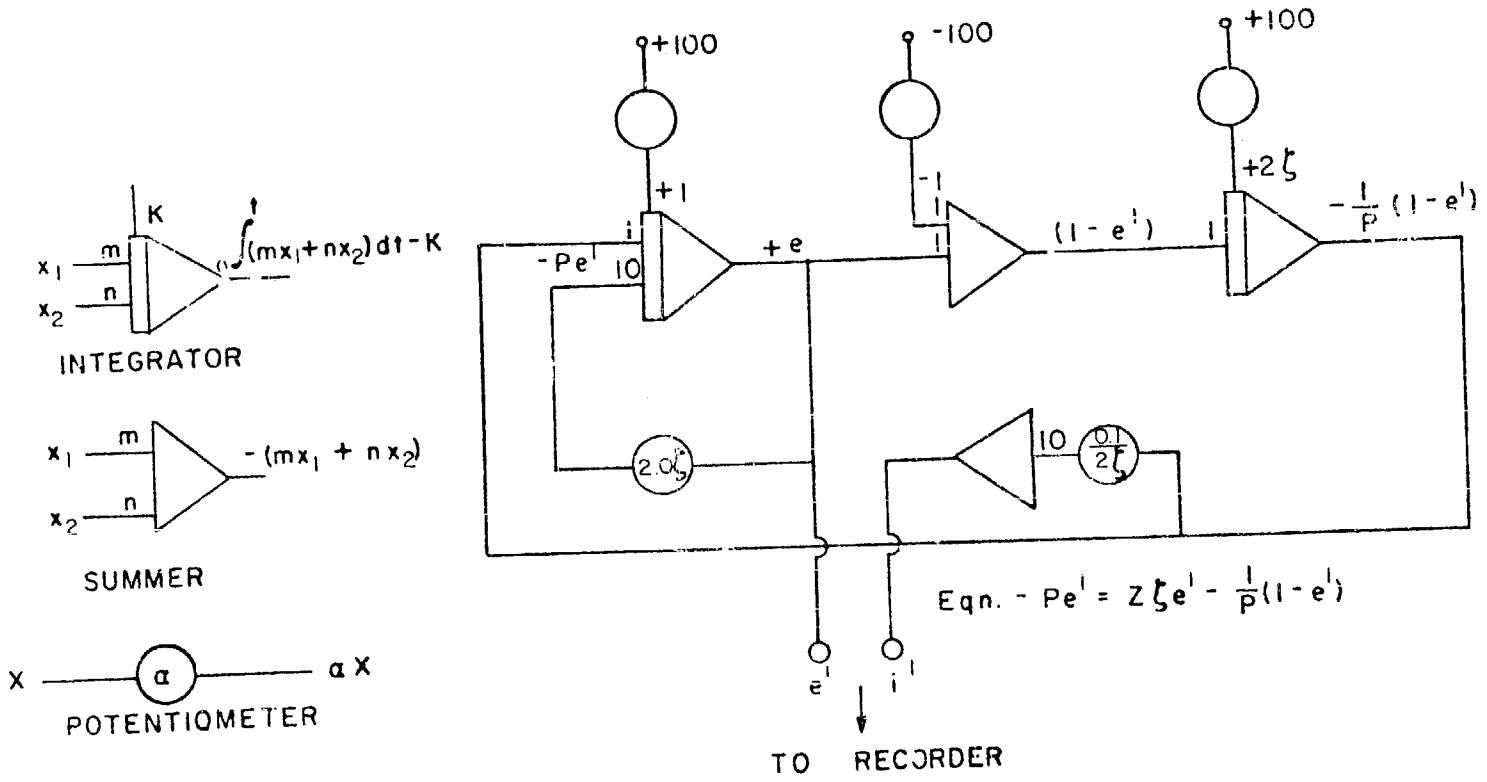

ANALOG COMPUTER CIRCUIT

FIG. 13.

$$p = \omega_o P,$$

$$i = \omega_o C P e + G e = \frac{G}{2\zeta} P e + G e.$$

Multiplying and dividing by E_o

$$i = \frac{G E_o}{2\zeta} P \frac{e}{E_o} + G E_o \frac{e}{E_o}$$

or

$$i = \frac{I_o}{2\zeta} P e' + I_o e',$$

and therefore

$$i' = \frac{1}{2\zeta} P e' + e'.$$

Substituting into Equation (18):

$$i' = \frac{1}{2\zeta} \frac{1}{P} (1 - e'). \qquad (19)$$

Figures 14 and 15 show the outputs of the analog computer recorded values of -1 and +1, respectively. These curves, along with the expressions for ω_o and ζ can be used to determine the circuit values for proper commutation. The voltage e' must go to zero, or cross the $\omega_o t$ axis in a time equal to or greater than $\omega_o t$ axis in a time equal to or greater than $\omega_o \Delta t_{min}$, where Δt_{min} is the minimum reverse bias time which allows the SCR's to recover (this time is 25 μsec for the SCR's used).

It is apparent from the plot of e' that $\frac{de'}{d\omega_o t} = \frac{1}{\omega_o \Delta t}$ at the axis crossings for ζ greater than about 0.4. Therefore

$$\frac{de}{dt} = \frac{E_o}{\omega_o \Delta t} = \frac{E_o}{\Delta t}. \qquad (20)$$

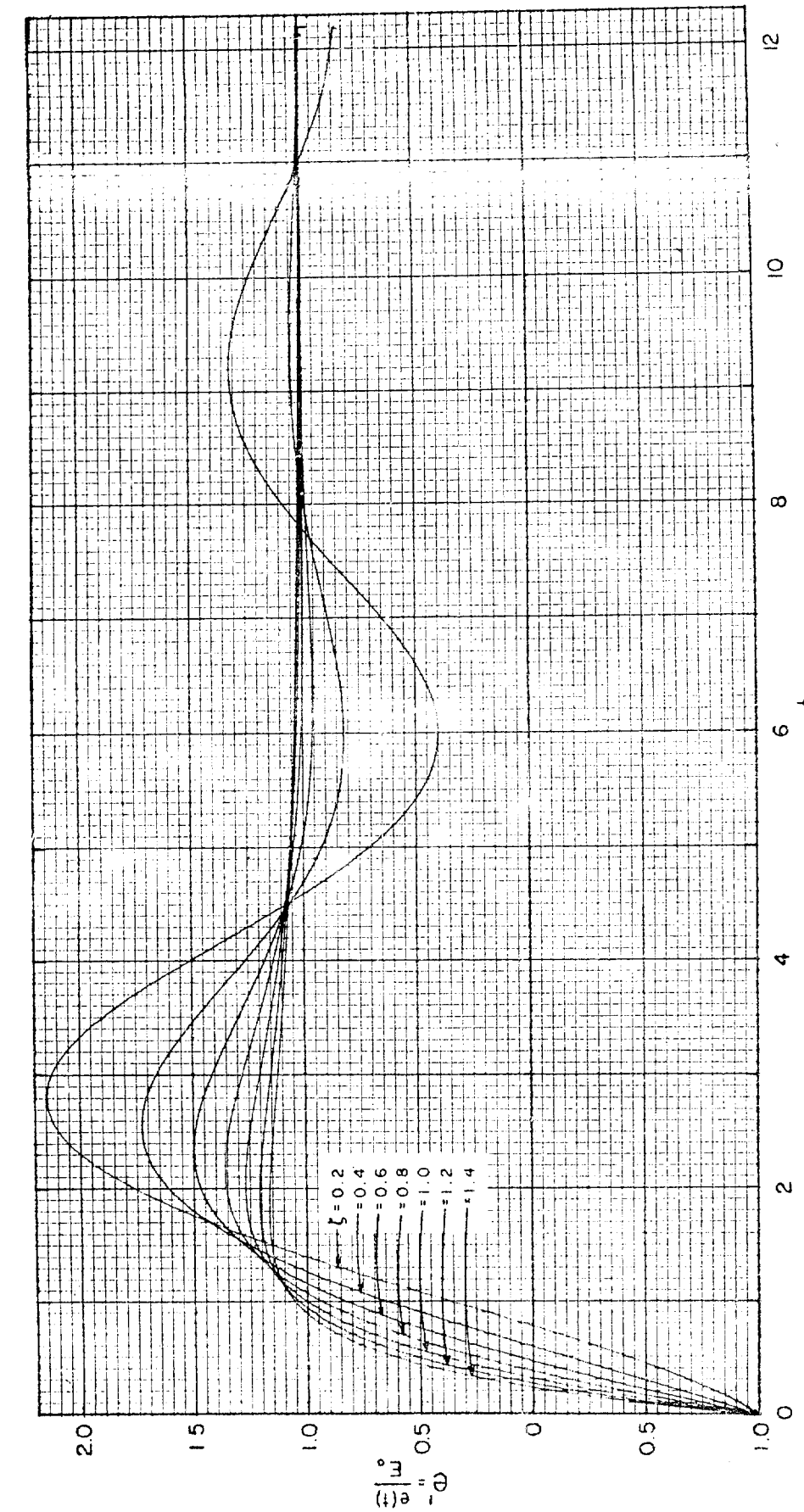

NORMALIZED VOLTAGE TRANSIENT DURING SWITCHING

FIG 14

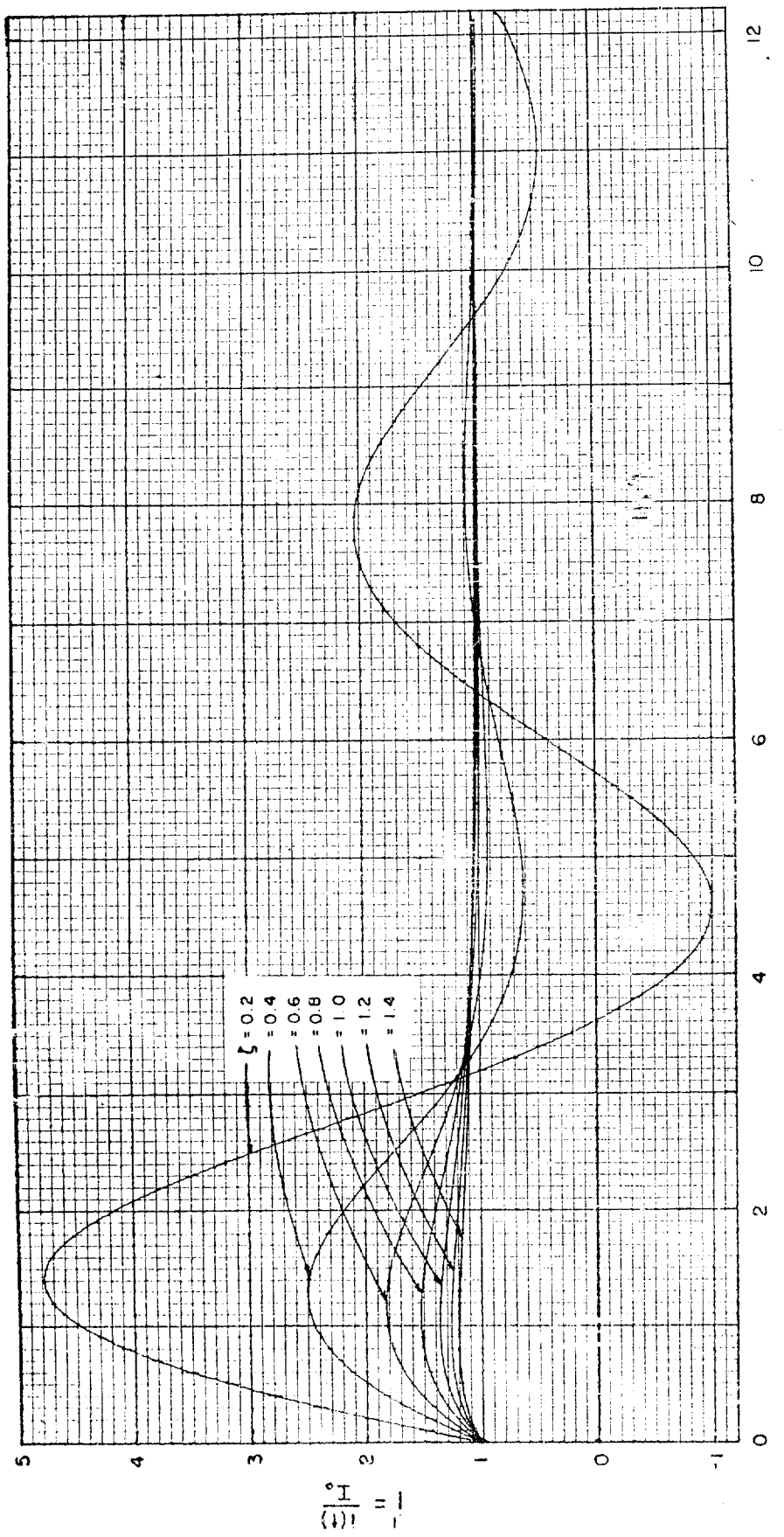

NORMALIZED CURRENT TRANSIENT DURING SWITCHING

FIG. 15.

E_o can never be over 500 volts, since this is the maximum forward and reverse blocking voltage for the SCR's; also, Δt can never be below 25μsec. Therefore $\frac{de}{dt} \leq 20$ volts/μ sec, which is the maximum allowable value. Consequently, if Δt is large enough for commutation, and the damping factor is above 0.4, the forward voltage derivative will be below the maximum allowable value.

From the plot of i', it is seen that the inductor current will not reverse if ζ is kept above 0.3; therefore, any damping factor above this value is permissible providing other conditions are met.

Maximum voltage and current ratings for the SCR's, as given in the appendix, must be considered when adjusting the operating conditions. A source voltage E_o and a damping factor ζ must be chosen which will not allow voltage and current overshoot to exceed the maximum ratings.

For easier reading of the values of $\omega_o \Delta t$, a plot of these values versus damping factor is given in Figure 16. Also, to provide a better view of the effect of the parameters L and C, Figures 17, 18, and 19 show lines of constant Δt and ζ in the LC-plane for three different typical values of load resistance R.

3. Commutating inductor

As seen in the graphs of Figures 17, 18, and 19, for a given R, Δt is primarily a function of the commutating capacitance C, and L mostly serves to vary the damping factor. Since a high damping factor is desirable, L should be as large as possible; however, since this inductor

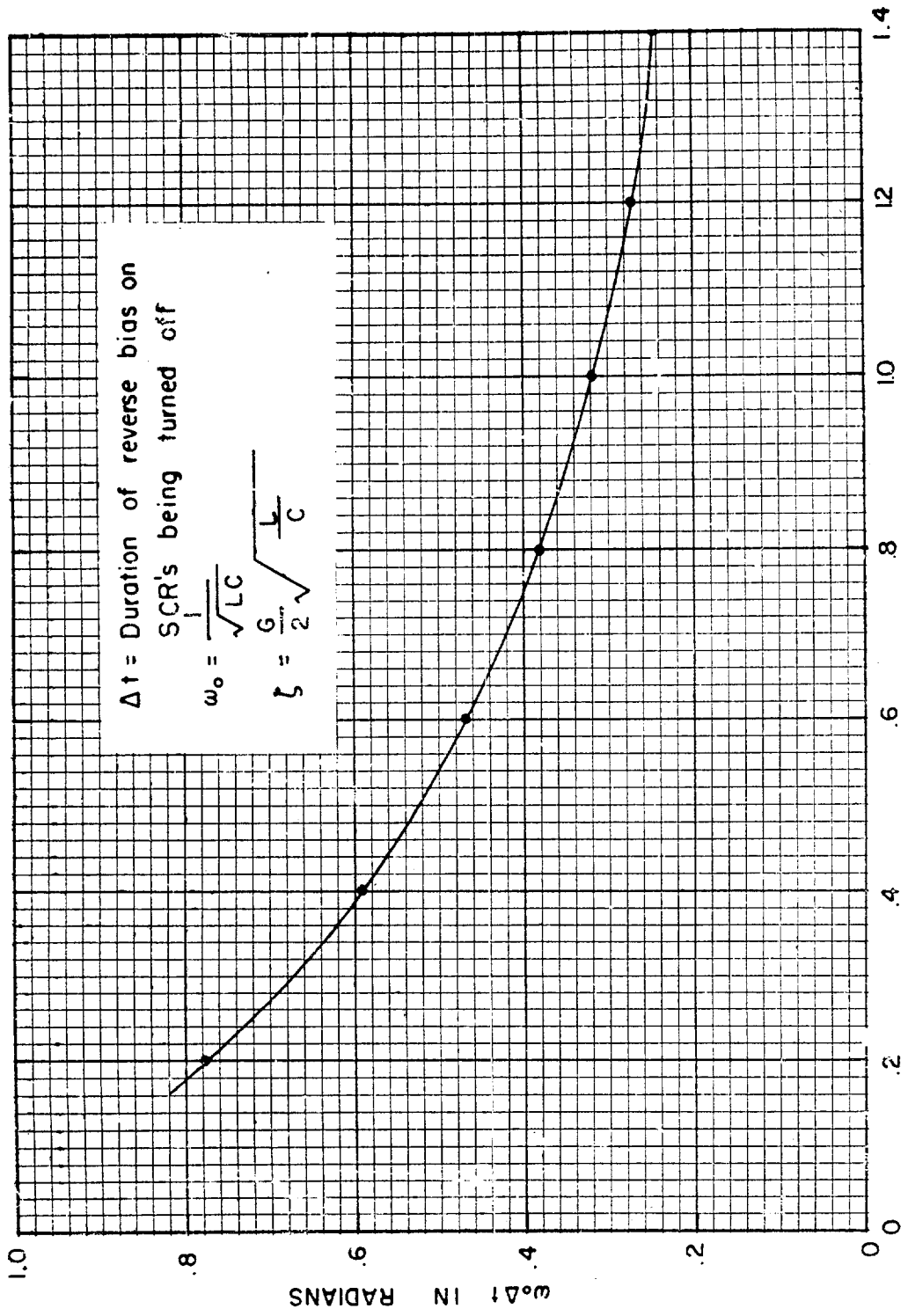

REVERSE BIAS ANGLE V.S. DAMPING FACTOR

FIG. 16.

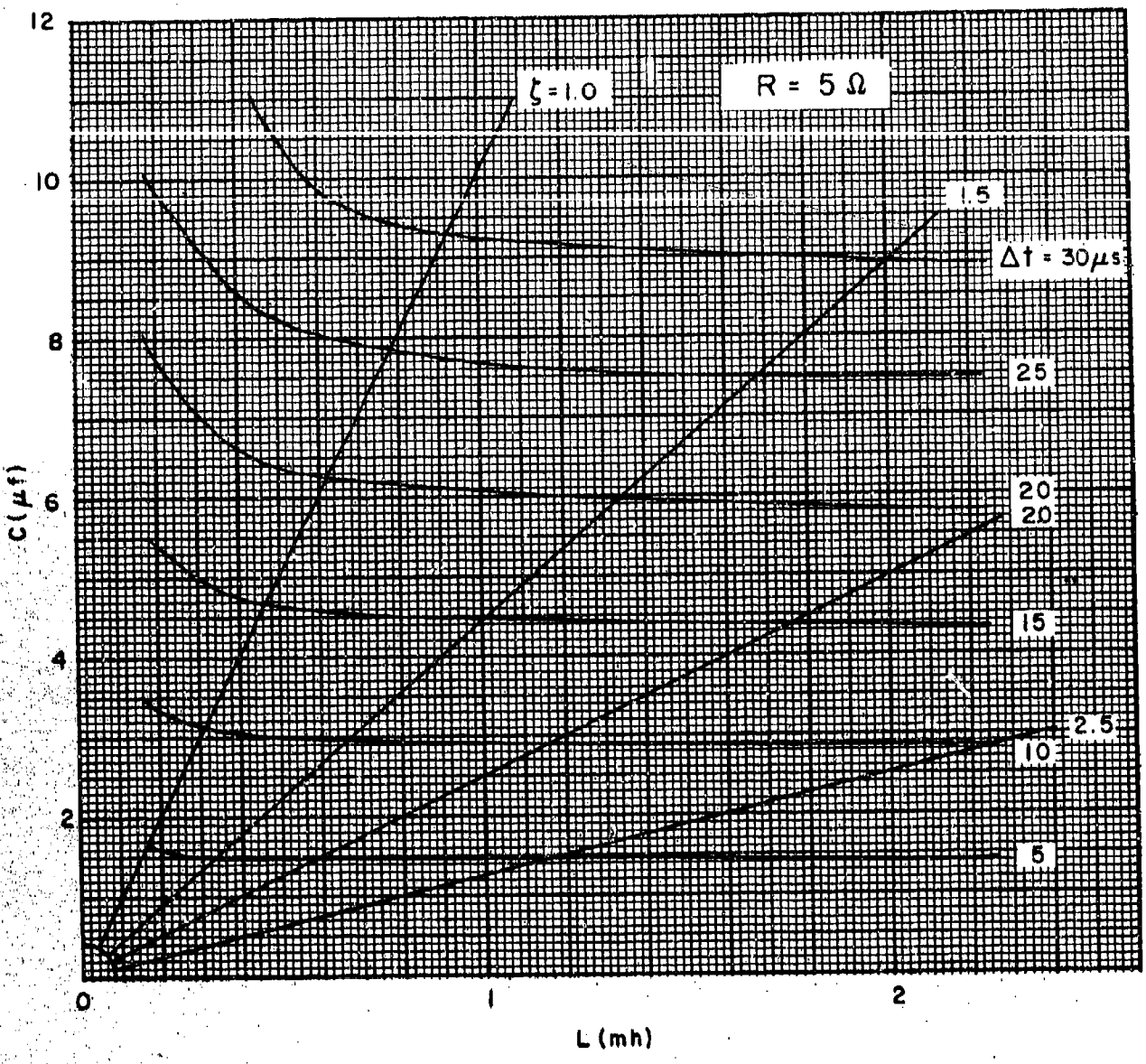

CONSTANT REVERSE BIAS TIMES FOR SCR COMMUTATING CIRCUIT WITH R = 5 OHMS

FIG. 17.

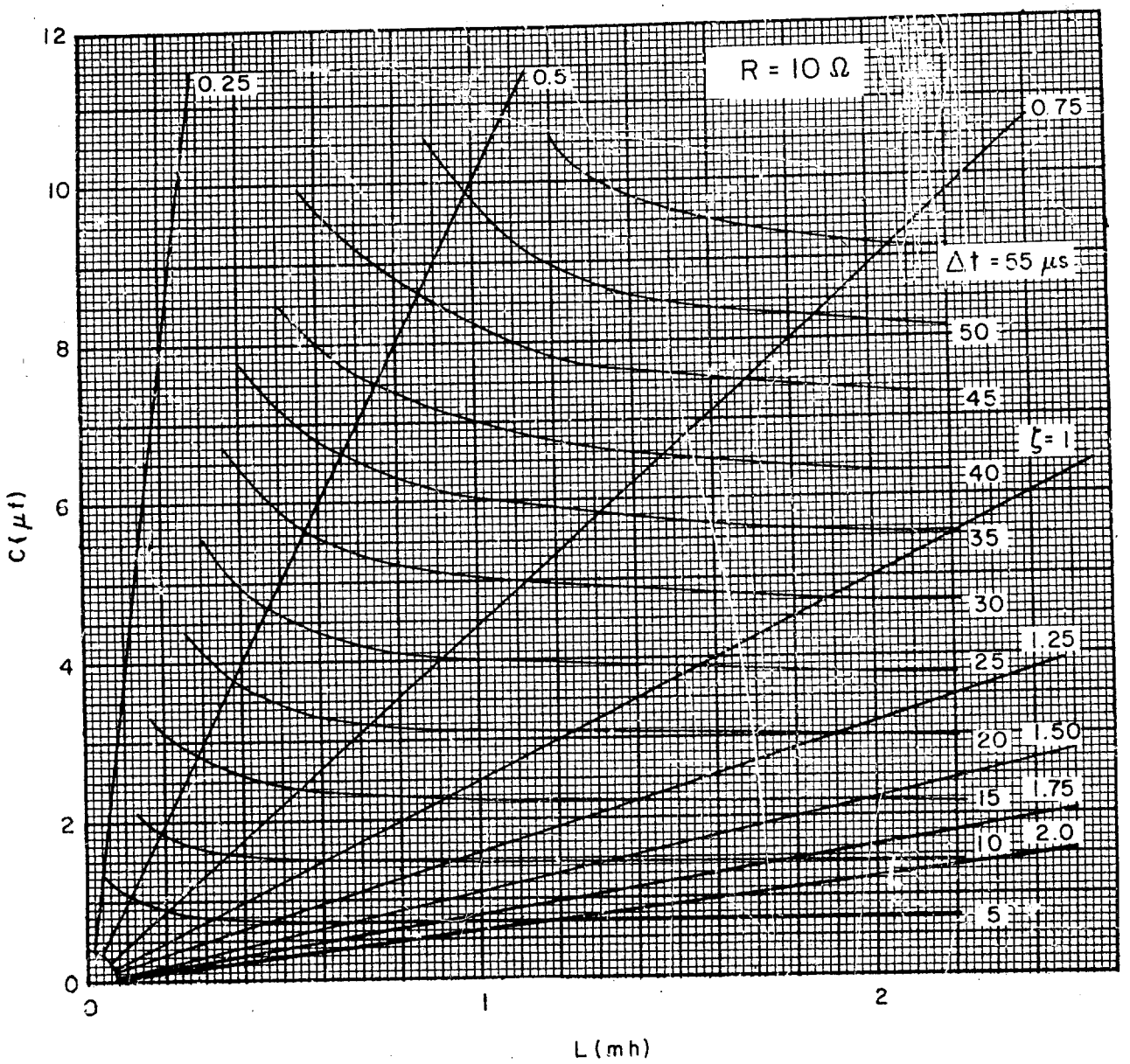

CONSTANT REVERSE BIAS TIMES FOR SCR COMMUTATING CIRCUIT WITH R=10 OHMS

FIG. 18.

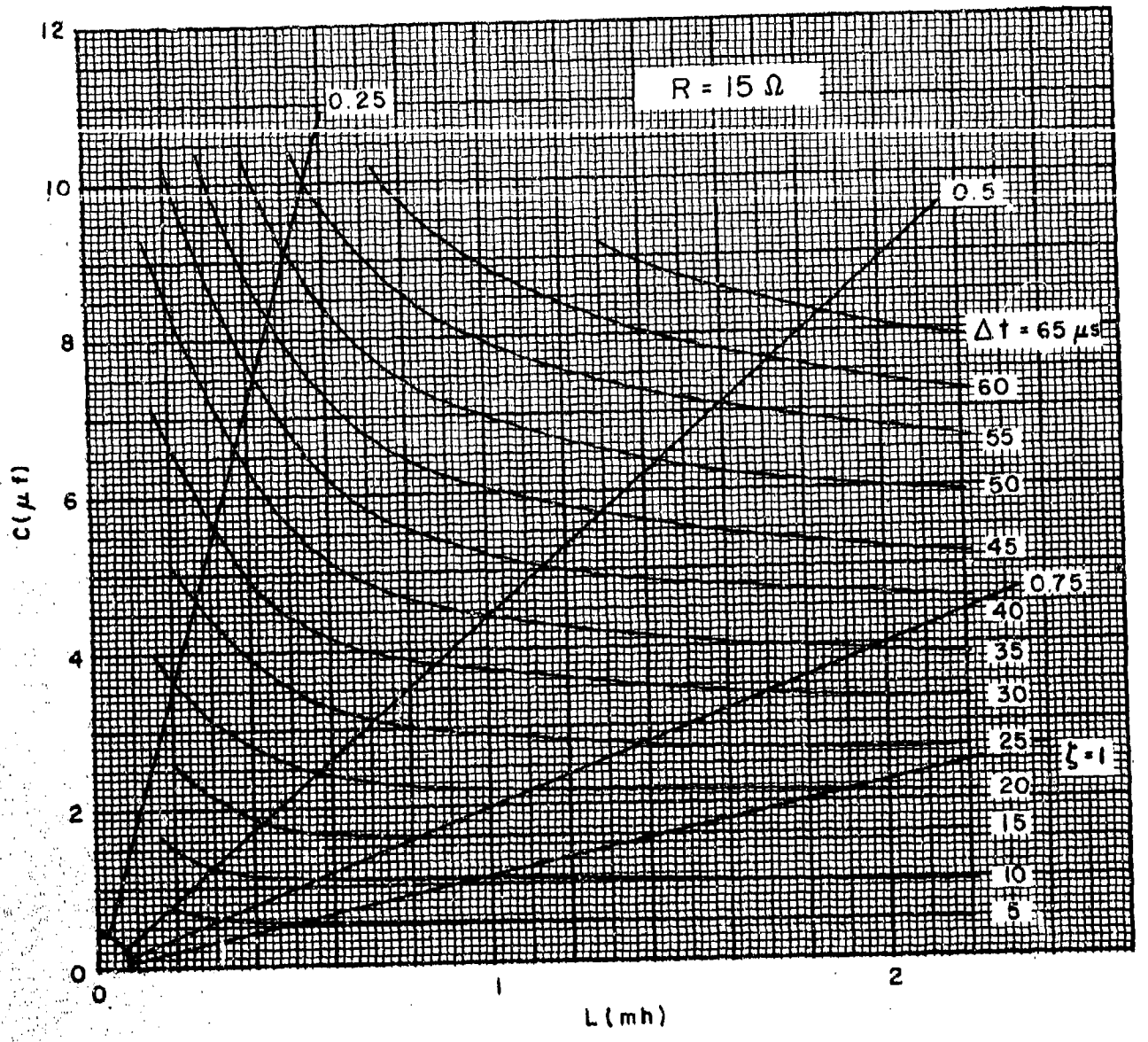

CONSTANT REVERSE BIAS TIMES FOR SCR COMMUTATING CIRCUIT WITH R = 15 OHMS

FIG. 19.

must carry up to 100 amperes its physical size becomes a limitation. A 1 mh inductor was chosen as a good compromise between physical and electrical size. This value of L allows satisfactory operation of the switching bridge into electrode resistances of 15 ohms and below.

The 1 mh commutating inductor (Figure 20) is wound with #4 AWG stranded copper and has an internal resistance of 0.0125 ohms. A large fuse with replaceable inserts for up to 100 amperes is placed in series with the inductor for protection in case of circuit breaker failure.

4. Commutating capacitor

For a given load resistance, Δt is mainly determined by C. The value of C should be chosen to give a Δt of about 30 μ sec, or 5 μ sec safety margin over the 25 μ sec required by the SCR's. Damping factor will decrease with increasing C, and should it be desired to operate the system with a reasonable damping factor with an electrode resistance above about 15 ohms, it would be necessary to increase the value of L. However, in this case it would be more desirable to lower the electrode resistance, if possible, so that a higher electrode current could be attained.

A capacitance of 5 μ f was built into the switching bridge. It is necessary to add external capacitance across terminals A and B if the electrode resistance gets below about 9 ohms. The built-in capacitor can be disconnected if necessary.

The commutating capacitor undergoes a rapid change in voltage during commutation and consequently experiences a large current

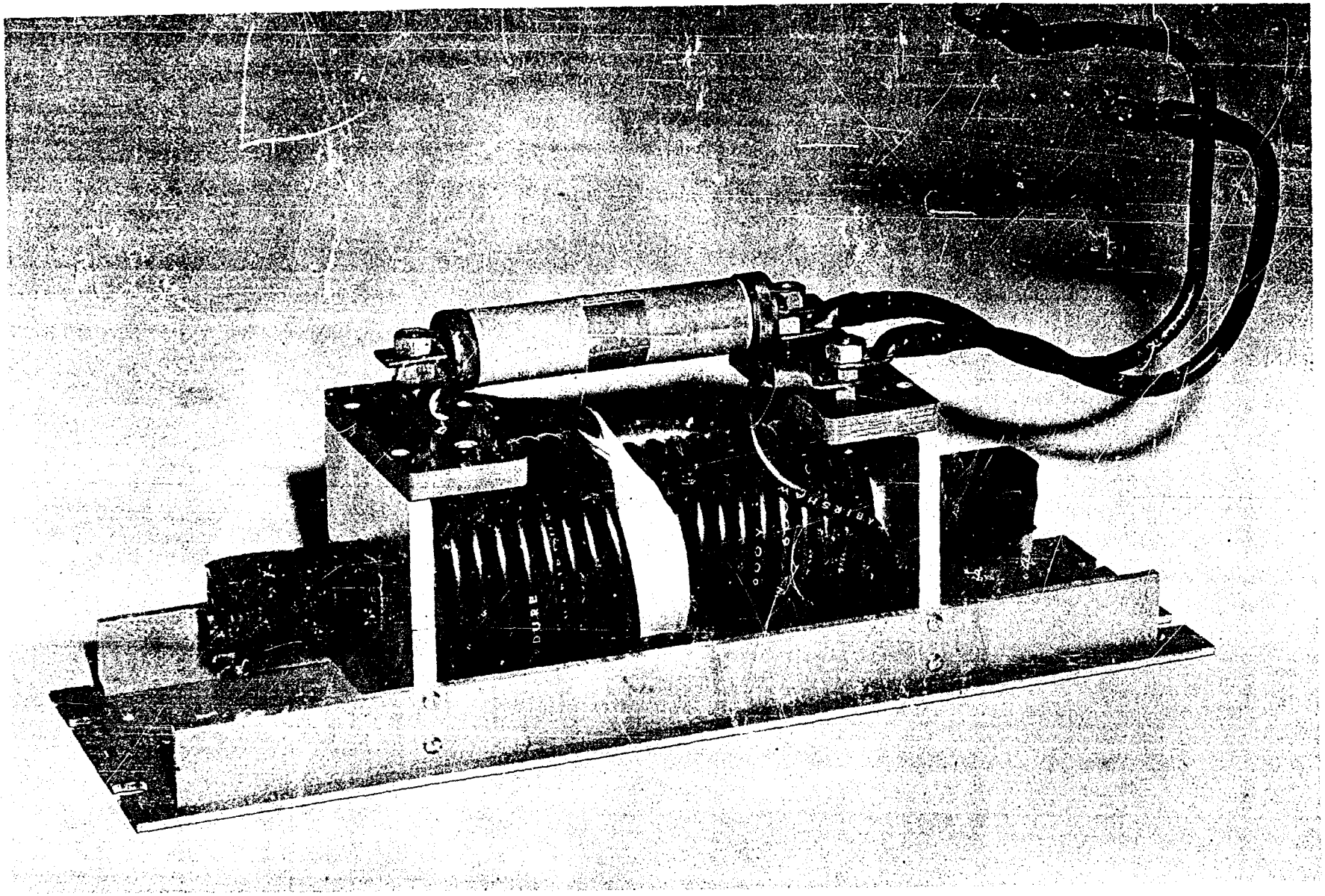

COMMUTATING INDUCTOR

FIG. 20.

pulse. For low operating frequencies the average power loss in the capacitor is very low and the current spikes are of little concern; however, as the operating frequency is increased, the current spikes become closer together in time and the rms current becomes large enough that special consideration must be given the type of dielectric used in the capacitor. The power lost in the capacitor as a function of frequency can be written as

$$P(\omega) = (pf)\, I(\omega)\, E(\omega) \tag{21}$$

where pf is the power factor and $I(\omega)$ and $E(\omega)$ are the rms values of the sinusoidal current and voltage of the capacitor at the frequency ω. Since

$$I(\omega) = E(\omega)\, \omega C, \tag{22}$$

the expression for power loss becomes

$$P(\omega) = (pf)\, \omega C E^2\, (\omega), \tag{23}$$

and for a periodic, non-sinusoidal wave form, the total power dissipated is given by

$$P_c = \sum_{n=1}^{N} P(\omega_n) = \sum_{n=1}^{N} (pf)\, \omega_n\, C E^2(\omega_n) \tag{24}$$

where N is the highest harmonic present.

Consider a capacitor operating at 3000 cps with 500 volt peak sinusoidal voltage; this will be close to the actual conditions with

the transmitter operating at 3000 cps at full voltage, since at this frequency the voltage rise time during commutation is a considerable portion of the half period, and the sharp corners of the voltage wave form are rounded, reducing the harmonic components. For this case

$$P_c = (pf)(2\pi)(3000)[(.707)(500)]^2 C \text{ watts}$$

or

$$\frac{P_c}{10^6 C} = (pf)(2.36 \times 10^3) \text{ watts}/\mu f. \qquad (25)$$

The power factor of most dielectrics is constant with frequency over a wide range. Some dielectrics considered for the commutating capacitor and their power factors are:[4]

	p.f.
Mylar	1%
Teflon	.02%
Polystyrene	.02%
Mica	.02%
Mineral oil impregnated paper	0.2 - 0.3%

If Mylar is used

$$\frac{P_c}{10^6 C} = (.01)(2.36 \times 10^3) = 23.6 \text{ watts}/\mu f$$

or with a 10 μf commutating capacitor 236 watts would be dissipated. If the

internal thermal resistance of the capacitor is very high, overheating and damage to the capacitor will result. For teflon, polystyrene, or mica,

$$\frac{P_c}{10^6 C} = 0.47 \text{ watts}/\mu f;$$

however, due to the relatively high costs, these dielectrics were not chosen. The most favorable compromise seemed to be mineral oil-impregnated paper, which has a loss of 4.7 to 7 watts/μf which has proven to be a tolerable value. Also the thermal resistance of the oil-impregnated paper is lower, allowing the capacitor to dissipate more heat at a lower temperature. Oil-paper dielectric capacitors are used for the circuit breaker as well as the switching bridge.

5. Operating frequency range

During switching, the voltage e(t) goes from $-E_o$ to 0 in a minimum of about 30 μs. Also, if $\frac{de(t)}{dt}$ remains essentially constant until e(t) reaches $+E_o$ as it does for low values of ζ (0.2, 0.4, etc.), another 30 μsec is required to reach $+E_o$. Therefore, this imposes on the operating frequency a minimum half period of about 60 μsec, allowing a possible operating frequency as high as 8.5 kc/s, giving a triangular wave output voltage; however, at the low damping factors, the current i(t) can reach several times I_o in this half cycle, making it necessary to operate at reduced current.

If ζ is large, say 1.4, so that the current is well behaved, the minimum half period becomes about 130 μsec so that the

maximum operating frequency is now 3.8 kc/s. The transient voltage e(t) should be carefully adjusted and monitored when operating at the extreme frequency mimits.

E. Control Circuitry

Both the circuit breaker and the switching bridge are controlled by applying voltage pulses to the SCR gates at the proper time. It seems desirable to first consider the gate driving circuit which is used on all but one of the SCR's of the system.

1. Gate driving amplifier

The positive voltage and current characteristics of an SCR gate are those of a forward biased p-n junction. These characteristics, shown in Figure 21 for the SCR's used in this system, vary widely from one SCR to another of the same type; also, one SCR will not require the same gate voltage and current for turn-on as another. The shaded region in the plot of Figure 21 represents the region above which any SCR of this type will turn on; therefore, if a gate driving circuit is to turn on any SCR of this type, its output load line must pass beyond the shaded region. Other conditions are imposed on the driving circuit by the maximum allowable voltage, current, and instantaneous power which can be applied to the gate without causing damage. The driving circuit load line must be below these limits.

The SCR gate drivers used in this system are cathode followers of the form shown in Figure 22. Their output is coupled to the control gate by 10:1 step-down pulse transformer which provides a lower output

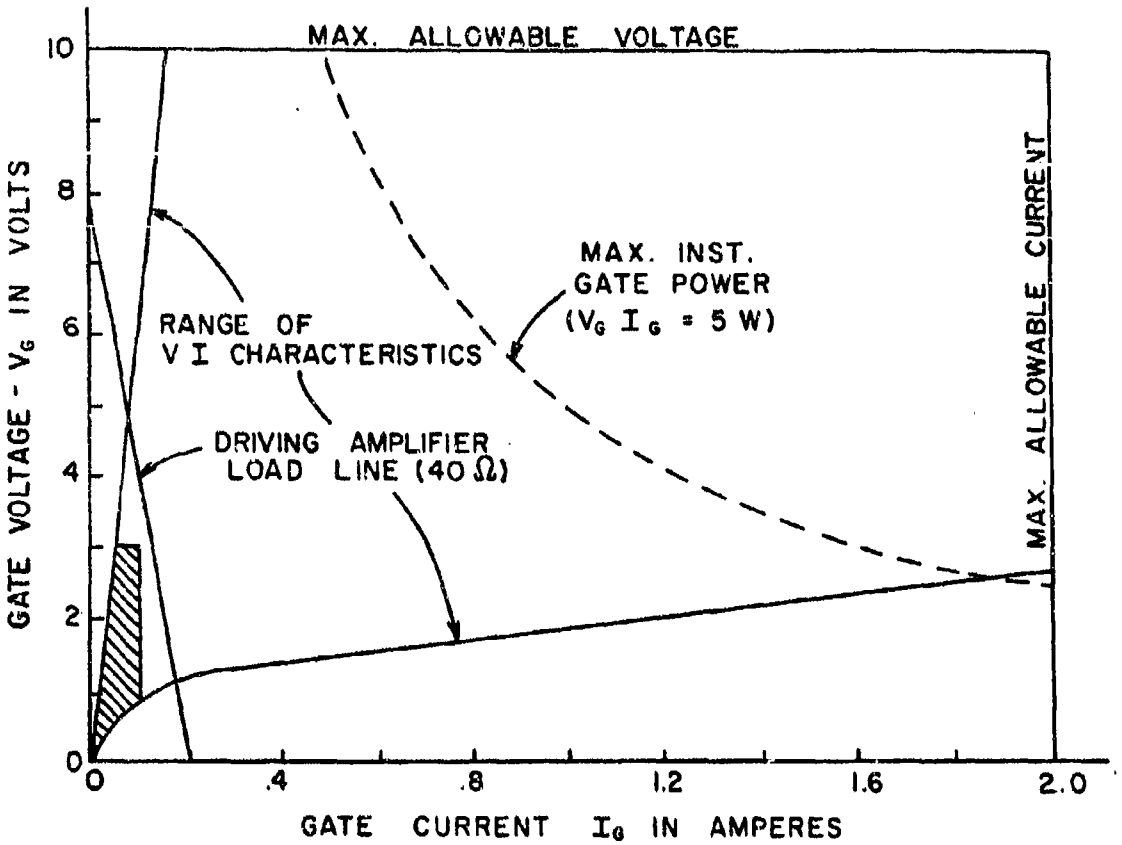

CONTROL GATE CHARACTERISTICS FOR
IR 7IRC50A SCR

FIG. 21.

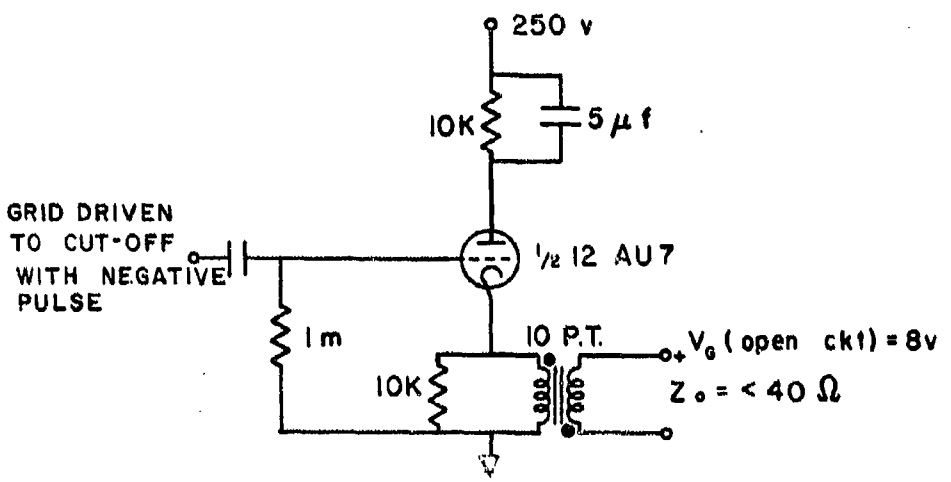

CONTROL GATE DRIVING AMPLIFIER

FIG. 22.

impedance and DC isolation between the SCR and the control circuit. This cathode follower circuit has an open circuit output voltage of 8 volts with an output impedance of under 40 ohms. Its load line, shown in Figure 21, passes just beyond the shaded region of the characteristics so that just over minimum required power is applied to the gate.

The cathode follower circuit of Figure 22, which is used in the circuit breaker control, has zero grid bias and is driven to cut-off by a negative pulse. The cathode followers used to drive the switching bridge SCR's are the same, except that they are biased to cut-off and driven to saturation with a positive grid pulse.

2. Circuit breaker control

The circuit breaker control, shown in block diagram form in Figure 23, provides turn-on and turn-off gate pulses for the SCR circuit breaker, and charges the commutating capacitor C_b. A complete circuit diagram is given in Figure A-4 of the Appendix.

The "on" pulse for SCR S5 is produced manually by pushing the "on" button on the control panel. This causes relay RY-2 to switch a small capacitor, initially charged to 250 volts, onto a 2000 ohm to 50 ohm voltage divider. The gate voltage for S5 is taken from across the 50 ohm resistor.

The "off" pulse for SCR S6 can be produced manually with the "off" button on the control panel, or it can be generated by the temperature or current trip circuits. The "off" pulses from the three possible

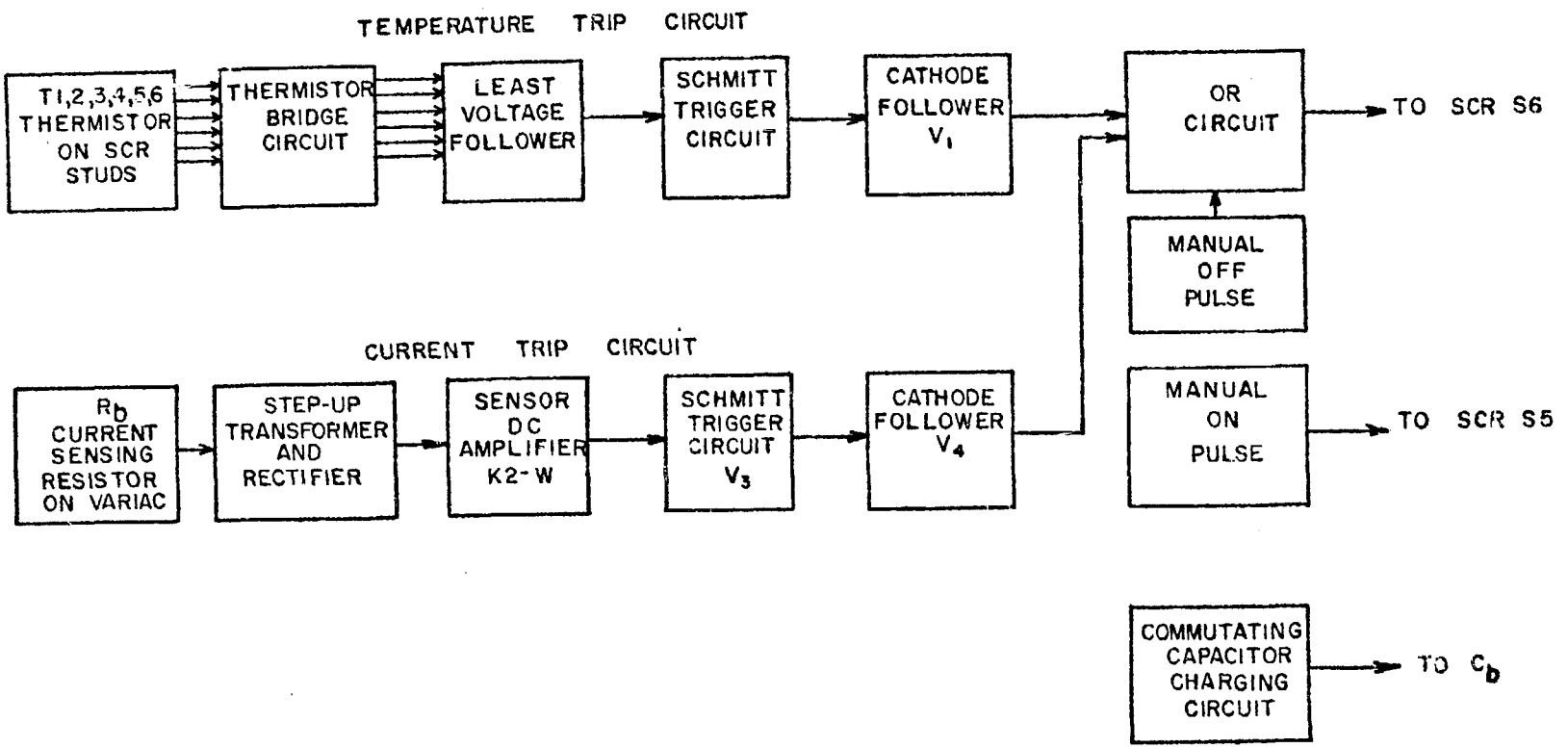

BLOCK DIAGRAM OF CIRCUIT BREAKER CONTROL

FIG. 23.

sources are applied to the gate of S6 through a diode "OR" circuit, which allows any one or more of the three pulses to turn off the breaker.

The temperature trip circuit senses the stud temperature of each of the six SCR's in the transmitter by means of thermistors T1 to T6 fastened to the SCR mounting studs. The thermistors are mounted as shown in Figure A-3 so that they are electrically insulated from the SCR studs; good thermal connection is made through a silicone heat sink paste. As shown in the schematic diagram, each thermistor serves as a element of one of the six AC Wheatstone bridge circuits composed of the 200 ohm resistors and the potentiometer TS-1. The potentiometer serves as two legs that are common to all six bridges. The thermistor resistance goes down with increasing temperature and is approximately represented by

$$R_o(T) = R_o(T_o)\, e^{\beta(\frac{1}{T} - \frac{1}{T_o})}, \qquad (26)$$

where R_o is the thermistor resistance, β is a constant peculiar to a particular thermistor, T is the thermistor temperature in °K, and T_o is a reference temperature in °K. The thermistors used have a resistance of 1000 ohms at 25 C, 67 ohms at 100°C, and 38 ohms at 120°C. Potentiometer TS - 1 is adjusted so that the thermistor bridges are unbalanced at room temperature and approach balance as the temperature rises and the thermistor resistance goes down. The bridge is adjusted to balance at a temperature above that at which the breaker is to trip, so that the bridge output voltage is still decreasing when the temperature passes through the trip level.

The bridge outputs are attached to a diode "OR" circuit which acts as a least voltage follower and its output is exactly the voltage existing on the bridge whose thermistor is at the highest temperature. The "OR" circuit output is rectified and filtered to produce a DC voltage which decreases as the highest temperature rises. This DC voltage serves as the input to a Schmitt trigger circuit V_2 that is biased to switch when the thermistor temperature reaches the desired maximum. Potentiometer TS-2 is adjusted to set the desired switching level, by substituting a resistor, corresponding to the trip temperature, for one of the thermistors and adjusting TS-2 to reduce the Schmitt trigger input until it switches. The Schmitt circuit switches at about 12 volts input with respect to ground.

The Schmitt trigger output, which falls in potential when the circuit switches states, is coupled to a cathode follower V_1 which drives the SCR gate.

The current trip circuit derives its input from the .005 ohm current sensing resistor R_b in one phase of the variable transformer. The voltage drop across this resistor is stepped-up by a 48:1 transformer, full wave rectified, and passed through a DC operational amplifier and onto the input of the Schmitt circuit V_3. This Schmitt circuit drives the cathode follower V_4 in the same manner as does the temperature trip circuit.

To adjust the trip current level, the DC amplifier input is first shorted by energizing relay RY-4, and the balance potentiometer Z-1 is turned to unbalance the amplifier until the meter M-5, on the breaker

control panel, reads the trip current. With RY-4 still closed, potentiometer CS-1 is then adjusted in the direction to decrease the output voltage until the Schmitt circuit V_3 switches states. The amplifier is then rebalanced with its input shorted.

The DC operational amplifier in the current trip circuit was added to achieve flexibility in deriving breaker inputs from other sources or sensors than the current sensor shown. The AC current sensor presently used measures only one phase of the source current, and is inherently slow. Since the circuit breaker can open in about 50 μ sec it is planned to build a current sensor of comparable response time.

The charging supply, powered by transformer T-1, is connected across the circuit breaker commutating capacitor C_b, keeping it charged to 100 volts. The reset relay RY-1 is used to disconnect the charging supply in the event that SCR S6 is held in the "on" state by current through the DC circuit consisting of S6, the charging supply, and the circuit breaker load and source. This usually does not occur.

On the front panel of the circuit breaker control are meters for indicating the DC power supply voltage and current, and the voltage and frequency of the AC source. The neon indicator lights N-1, N-2, N-3, and N-4, shown in the schematic diagram, also appear on the front panel. These lights indicate the condition of the circuit breaker. If all four indicators are lighted, the commutating capacitor is charged, the commutating SCR S6 is off, the two Schmitt trigger circuits are in the proper state, and the breaker is ready to be turned on.

3. Switching bridge control

Two sets of pulse trains are provided for the switching bridge. One set of simultaneous pulses is applied to the gates of SCR's S1 and S2 of the bridge. The second set is applied to S3 and S4. For symmetrical, periodic switching of the electrode current, the pulses of each set are periodic with a period $T = 1/f_o$, where f_o is the operating frequency, and the two sets are 180° out of phase in time. For manual switching, a pulse is produced in one set when the control button is down and in the other set when the button is up, so that electrode polarity depends upon whether the button is up or down. A block diagram of the control circuit is shown in Figure 24, and a detailed schematic diagram is given in the Appendix.

The control circuit contains a Schmitt trigger with hysteresis. The output plate of the Schmitt circuit switches up when the input voltage reaches 84 volts and down when the input reaches 76 volts. A voltage divider biases the input to 80 volts, which is halfway between the switching levels. The input voltage to the bridge control circuit is capacitor coupled to the center of the input biasing divider (point "a" of Figure A-5). When the square wave voltage from the function generator rises or falls, the Schmitt circuit input is forced up or down past the switching levels, so that a square wave of the same frequency is generated at the output plate. If switch S1 is switched opposite the position shown, the input is biased above or below the two switching levels, depending on the position of the manual control button S2, which determines the state of the Schmitt circuit for manual operation.

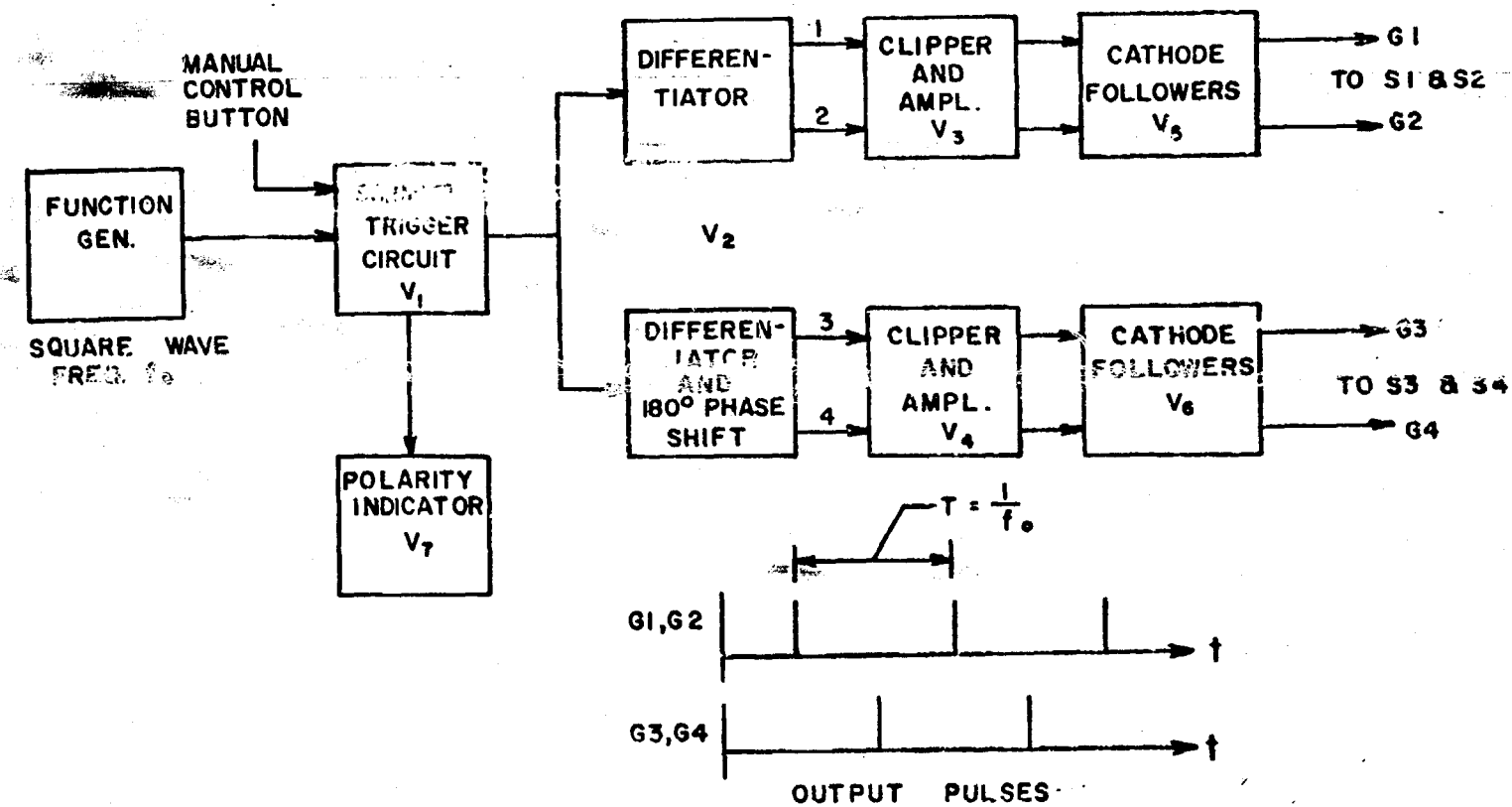

BLOCK DIAGRAM OF SWITCHING BRIDGE CONTROL

FIG. 24.

The output of the Schmitt circuit drives two pulse transformer-coupled amplifier stages, V_2 in the diagram, which differentiate the square wave and produce trains of 20 μsec pulses alternating in polarity. The secondaries of the pulse transformer in one differentiator are reversed relative to the other differentiator so that the output pulse trains of the two differentiators are 180° out of phase. Four identical output channels (channel 1 is shown) are driven by the two differentiator circuits. A diode clipping circuit removes the pulses of unwanted polarity in each channel. The pulse trains of each channel are passed through an over-driven amplifier stage to steepen the leading and trailing edges and flatten the tops. The final stage in each channel is the cathode follower which drives the SCR gate. As shown in Figure 24, outputs 1 and 2 are 180° out of phase with 3 and 4.

The polarity indicator, stage V_7 in the schematic, detects the state of the Schmitt circuit and lights one of two neon lamps marked A and B on the front panel. When the Schmitt circuit output plate jumps upward in potential, pulses are produced at outputs 3 and 4, turning on SCR's S3 and S4 so that the switching bridge output is positive at A. At the same time, the right side of the polarity indicator is turned on causing the "A" lamp to light. The "B" lamp lights when B is positive.

F. Transmitting Electrodes

The electrodes presently being used consist of 10 foot sections of galvanized 6-inch pipe. A brass block with a 3/8 inch hole is brazed to the center of each electrode; the electrode cables which are 1/0 stranded

copper wire, are inserted and soldered in a hole in the brass block to form a corrosion-free connection.

The electrodes are installed horizontally about 1 foot below the surface. A trench about 18 inches deep is first dug and filled with water, after which about 50 pounds of granular salt (sodium chloride) is added. The water and salt are stirred well and mixed with soil; and the electrode, with the cable attached, is lowered into the solution. The trench is then filled with the remainder of the dirt. In the Austin area, a total electrode resistance of around 6 ohms can be obtained in this way. A lower resistance may be obtained by paralleling several such electrodes spaced far enough apart to allow the potential distribution around each electrode to be appreciably unaffected by the other electrodes.

The two transmitting electrodes are usually spaced about a kilometer apart, and, due to the long connecting cables required, considerable inductance will be seen from the transmitter terminals. This inductance is minimized by laying the electrode cables along a line joining the electrodes, but an inductance on the order of 1 mh will still exist. This is enough to affect the operation of the switching bridge and must be corrected at the transmitter.

Consider the electrode equivalent circuit of Figure 25a with a resistance R and series inductance ℓ (for a 1 km or so line, ℓ can be considered a lumped constant). Let a step voltage $e(t) = u(t)$ be impressed. The current will be

$$i(t) = u(t)\,\frac{1}{R}\,(1 - e^{-\frac{R}{\ell}t}). \qquad (27)$$

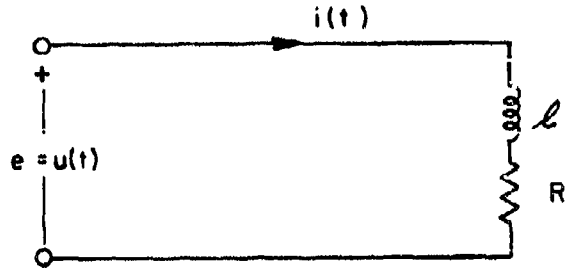

(a) EQUIVALENT CIRCUIT OF ELECTRODES

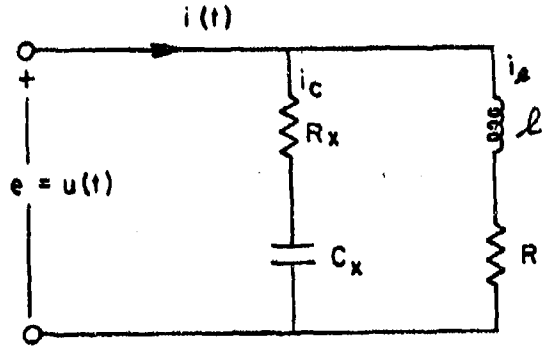

(b) CORRECTION FOR ELECTRODE INDUCTANCE

ELECTRODE IMPEDANCE CORRECTION

FIG.25.

If a series RC circuit composed of R_x and C_x of Figure 25b is shunted across the electrode input, the current i(t) for e(t) = u(t) becomes

$$i(t) = i_c + i_\ell = u(t)\,\frac{1}{R}\left(1 - e^{-\frac{R}{\ell}t}\right) + u(t)\,\frac{1}{R_x}\,e^{-\frac{1}{R_x C_x}t} . \qquad (28)$$

If the time constants of i_c and i_ℓ are made equal and $R_x = R$, the current becomes

$$i(t) = u(t)\,\frac{1}{R} . \qquad (29)$$

Since e(t) = u(t) contains all frequency components, this correction is good for all frequencies and the corrected electrode impedance appears as a pure resistance.

Equating the above time constants,

$$\frac{R}{\ell} = \frac{1}{R_x C_x} ,$$

where

$$R_x = R,$$

$$C_x = \frac{\ell}{R^2} \qquad (30)$$

This impedance correcting termination should be located near the transmitter.

For longer electrode cables where the inductance can no longer be considered lumped, the same correction circuit can be used; however, it is not exact since the inductive current i_ℓ will now increase in small steps so that the average value is rising exponentially toward $\frac{1}{R}$.

III. DESCRIPTION OF RECEIVING SYSTEM

A mobile van equipped to measure natural magneto-telluric fluctuations is used with a modification for the detecting equipment at the measuring dipole.[5] Two sets of measuring electrodes were used to measure the right angle components of the electric field and thus determine the direction of the field.

The measuring system is shown in block diagram form in Figure 26. After 60 cycle rejection, DC amplification, and broad band filtering, a superheterodyne circuit is used to take advantage of one of three fixed frequency high Q filters and make the system more frequency selective. This is especially necessary at large distances from the transmitter. The three narrow band filters used have center frequencies at .05, .5, and 5 cps, and each has a Q of 25. In the diagram, f_o is the transmitting frequency and f is the local oscillator frequency needed to translate f_o to the center frequency f_c of the filter. Both filtered and unfiltered data are recorded on the chart recorder.

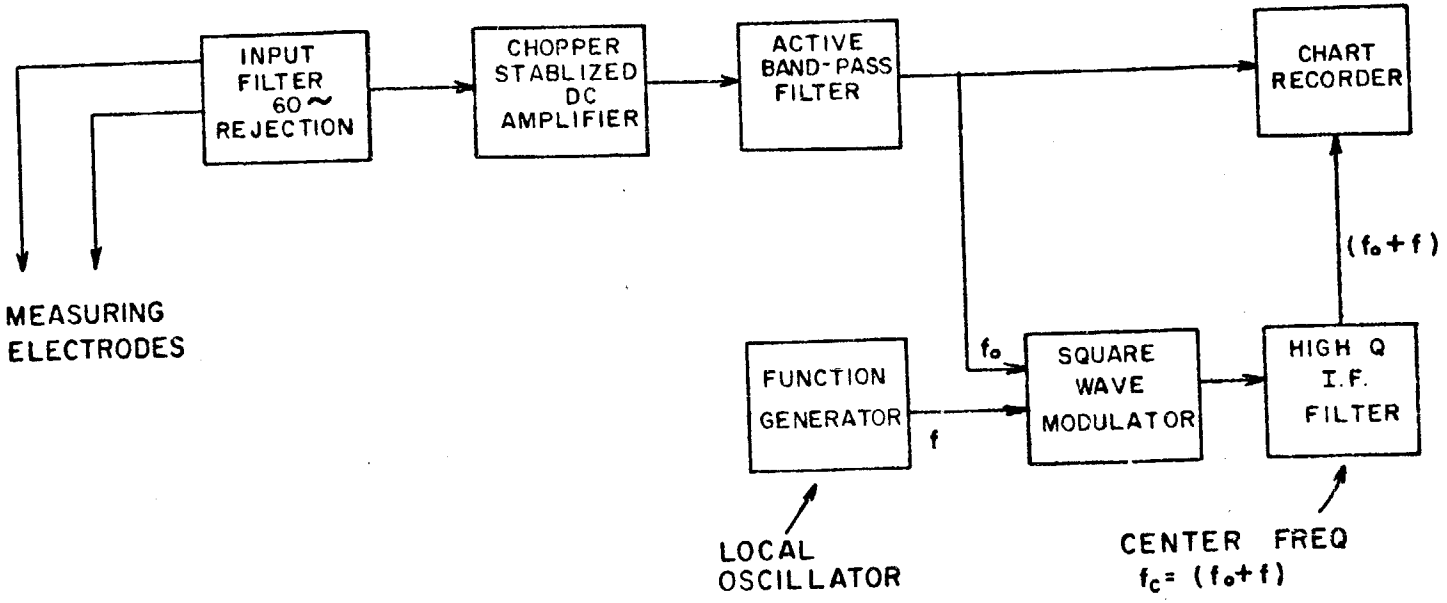

BLOCK DIAGRAM OF RECEIVING SYSTEM

FIG. 26

IV. COMMUNICATIONS AS RELATED TO A STRATIFIED EARTH MODEL

In recent years, interest has been shown in the development of a secure communications system using electromagnetic wave propagation through the crust of the earth.[6] The lossy characteristics of the earth restrict a system of this type to operation at low frequencies. The transmitter described previously in this report was designed to operate in the frequency range 0-200 cps. The purpose of this section is to estimate expected signal strengths for a dipole transmitter, located at the surface of the earth and operated in this frequency range.

Because the earth is a conductive medium, the field of a dipole will be a function of frequency. As will be shown later in this section, the character of the variation of signal strengths with frequency is largely determined by the electrical properties of the local geology. The rate at which information may be transmitted is a direct function of bandwidth. Although for the frequency range which this report is considering, this rate is low, the bandwidth is still an important quantity. In many locations, the earth may be approximated by a model consisting of homogeneous, horizontal stratified layers. For this reason, the model considered here is composed of two horizontal layers. Even though this model will usually be a gross simplification of the actual geology encountered, it is felt that it will illustrate most of the important phenomena associated with discontinuities in this range of frequencies.

For the purposes of communication, it will be shown that the greatest signal strength for a given dipole and input current occurs when a large strata of low conductivity material exists. The optimum frequency of signal transmission will be depend on the depth of this strata. The following analyses give the solutions for the general cases of one- and two-layer homogeneous stratified earths. The somewhat simpler case of a homogeneous earth is considered first and will be referred to as case (a). The two layer case will be case (b). Because the solution may be normalized with respect to the physical properties of the dipole transmitter itself, the natural quantity for the presentation of the solution is the apparent resistivity.

The apparent resistivity for a given model of the earth, position and frequency is the resistivity which would yield the same field as a d. c. dipole on a homogeneous earth.

For distances of interest the transmitter may be considered to be a horizontal dipole located just beneath the surface of the earth. The general solution for case (a) above was given by Sommerfeld in 1909.[7] This solution is in integral form and various approximations, depending on the wavelengths considered, are necessary in order to evaluate them. When the wavelength in air is much greater than the distances involved, displacement currents may be neglected. In this case, only the quasi-static and induction fields are present. This approximation is valid in the present case. The solution for this case was given by Foster in 1931. In the following derivation, the method of Foster is followed.

The electromagnetic field associated with the dipole must satisfy Maxwell's equations, which if sinusoidal time variations of the form expf ($j\omega t$) are assumed, become:

$$\text{curl } \bar{E} = -j\omega\mu_o \bar{H} \tag{31}$$

$$\text{curl } \bar{H} = j\omega\epsilon \bar{E} + \sigma \bar{E} \tag{32}$$

It follows that in the absence of free charges, the rectangular components of both $\bar{E}$ and $\bar{H}$ must satisfy the equations

$$\text{div grad } E = \gamma^2 E \tag{33}$$

$$\text{div grad } H = \gamma^2 H \tag{34}$$

where

$$\gamma^2 = j\omega\mu_o(j\omega\epsilon_o + \sigma) \tag{35}$$

The boundary conditions on the set of partial differential equations are that the fields must vanish at infinity and that the tangential components of $\bar{E}$ and $\bar{H}$ must be continuous across a discontinuous interface. It may be shown that both fields may be derived from a single vector function $\vec{\pi}$, called the Hertzian vector, where

$$\bar{E} = -\gamma^2 \vec{\pi} + \text{grad div } \vec{\pi} \tag{36}$$

$$\bar{H} = \frac{\gamma^2}{j\omega\mu_o} \text{ curl } \vec{\pi} \tag{37}$$

It may be easily verified that $\vec{E}$ and $\vec{H}$ satisfy Maxwell's equations if the rectangular components of $\vec{\pi}$ satisfy

$$\text{div grad } \pi = \gamma^2 \pi \tag{38}$$

Cylindrical coordinates are required due to the symmetry of the problem, and in these coordinates equation (38) becomes

$$\frac{1}{r}\frac{\partial}{\partial r}\left(r\frac{\partial \pi}{\partial r}\right) + \frac{1}{r^2}\frac{\partial^2 \pi}{\partial \phi^2} + \frac{\partial^2 \pi}{\partial z^2} = \gamma^2 \pi \tag{39}$$

where π represents any of the rectangular components of $\vec{\pi}$. The general solution to this equation may be expressed in integral form as

$$\pi = \begin{matrix} A_\phi \cos\psi \\ B_\phi \sin\psi \end{matrix} \int_0^\infty \left(f_1(\lambda) e^{-az} + g_1(\lambda) e^{+az} \right) \cdot \left(f_2(\lambda) J_n(\lambda r) + g_2(\lambda) Y_n(\lambda r) \right) d\lambda \tag{40}$$

where $a = \sqrt{\lambda^2 + \gamma^2}$ and $Jn(r\lambda)$ and $Yn(r\lambda)$ are Bessel functions of the first and second kinds, respectively. In the following discussion, the solution is obtained by assuming a primary field which induces a secondary field. The solution is the sum of these fields and must fit the boundary conditions. The primary field will be that of a dipole in an infinite homogeneous conductive medium. The expression for the Hertzian vector of such a dipole is well known and is given by

$$\pi = \frac{j\omega\mu_o I\ell}{4\pi\gamma^2} \frac{e^{-\gamma R}}{R} \tag{41}$$

where $I\ell$ is the dipole moment and $R^2 = r^2 + z^2$. This solution may be represented in the integral form of eq. (40) by a Fourier transformation as

$$\pi = \frac{j\omega\mu_o I\ell}{4\pi\gamma^2} \int_0^\infty \frac{\lambda}{a} e^{-az} J_o(\lambda r)\, d\lambda . \tag{42}$$

The functions $f(\lambda)$ and $g(\lambda)$ in eq. (40) are determined by the boundary conditions of the problem. For a horizontal dipole located at a plane interface of two differing media, the π vector must possess two components in order to satisfy the boundary conditions, one component perpendicular to the interface and another in the direction of the dipole. Let the coordinates be as in Figure 27, then the boundary conditions at the interface between any two media become

$$H_{ox} = H_{1x} \qquad \gamma_o^2 \pi_{oz} = \gamma_1^2 \pi_{1z} \tag{43}$$

$$H_{oy} = H_{1y} \qquad \gamma_o^2 \frac{\partial \pi_{ox}}{\partial z} = \frac{\partial \pi_{1x}}{\partial z} \tag{44}$$

$$E_{oy} = E_{1y} \qquad \frac{\partial \pi_{ox}}{\partial x} + \frac{\partial \pi_{oz}}{\partial z} = \frac{\partial \pi_{1x}}{\partial x} + \frac{\partial \pi_{1z}}{\partial z} \tag{45}$$

$$E_{ox} = E_{1x} \qquad \gamma_o^2 \pi_{ox} = \gamma_1^2 \pi_{1x} \tag{46}$$

In addition to these conditions one has the condition that the field must vanish at infinity. The application of these conditions to the total field due to the sum

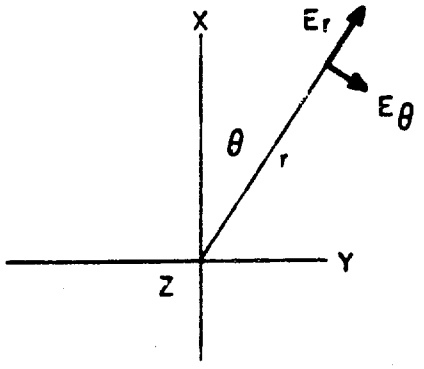

(a) COORDINATES

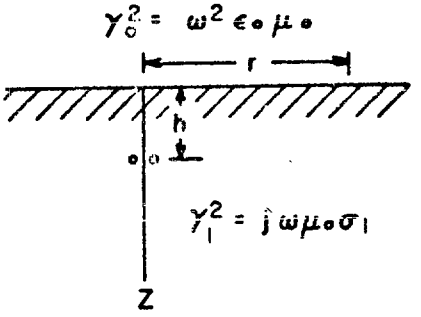

(b) CASE a

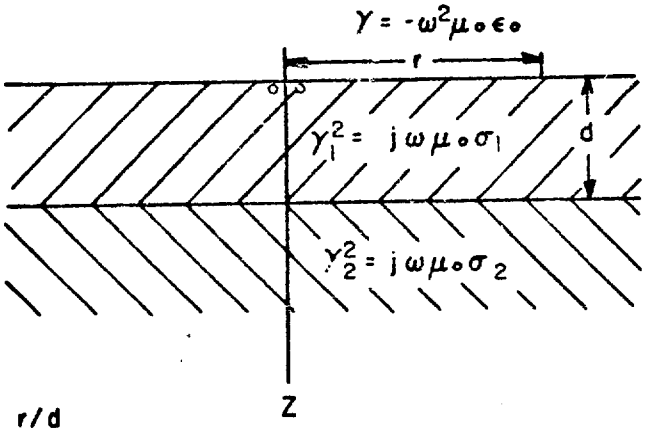

$\alpha = r/d$

$\beta = \rho_2/\rho_1$

$\Delta = \sqrt{\omega\mu_o\sigma_1}\ d$

(c) CASE b

COORDINATES AND EARTH MODELS

FIG. 27.

of the primary field and a secondary field of the form of eq. (40) yields the desired solution in each medium under consideration.

Case (a) discussed above is shown in Figure 27b. The dipole is considered to be a distance h beneath the surface. The solution in the region $o < z < h$ is given by

$$\pi_{ox} = \frac{i\omega\mu_o Il}{4\pi\gamma^2} \int_o^\infty \frac{2\lambda^2}{(a_1 + a_o)a_1} e^{a_1 z - a_1 h} J_o(\lambda r)\, d\lambda \qquad (47)$$

$$\pi_{oz} = \frac{i\omega\mu_o Il \cos\theta}{4\pi\gamma_o^2} \int_o^\infty \frac{2(\gamma_1^2 - \gamma_o^2)\lambda^2 e^{a_o z - a_1 h}}{(a_1\gamma_o^2 + a_o\gamma_1^2)(a_1 + a_o)} J_1(\lambda r)\, d\lambda \qquad (48)$$

In the air, the conductivity is zero, while in the earth, the displacement currents may be neglected, and the propagation constants will be given by

$$\gamma_o^2 = -\omega^2\mu_o\epsilon_o \qquad \gamma_1^2 = j\omega\mu_o\sigma_1 \qquad (49)$$

and for the frequency range of interest

$$\gamma^2 >> \gamma_o^2 . \qquad (50)$$

This is equivalent to neglecting displacement currents in the air, compared to conduction currents in the ground. With these assumptions, the eqs. (47) and (48) become

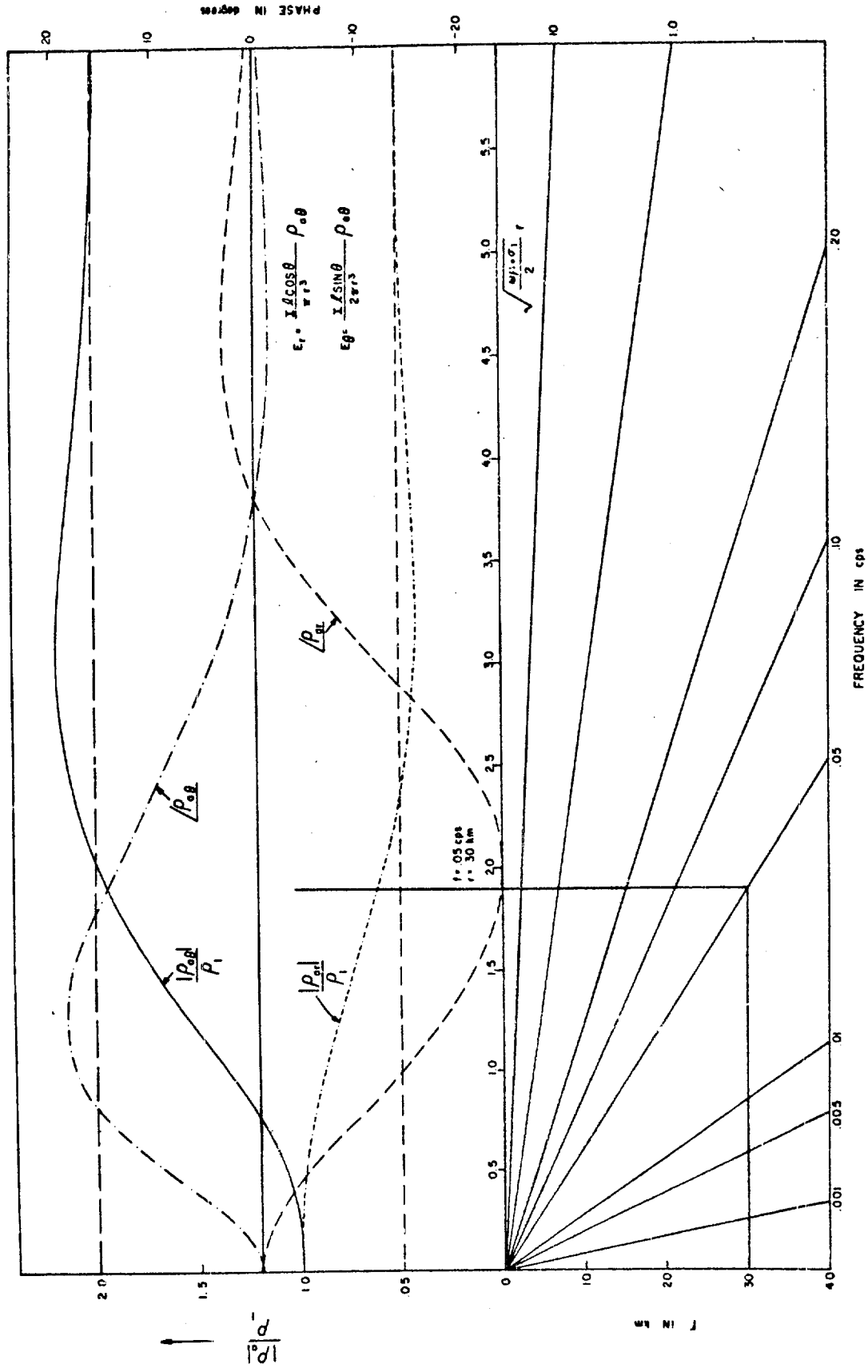

APPARENT RESISTIVITY VS FREQUENCY FOR SINGLE LAYER CASE

FIG. 28.

$$\pi_{ox} = \frac{i\omega\mu_o I\ell}{2\pi\gamma_o^2} \int_0^\infty \frac{\lambda}{\lambda + a_1} J_o(\lambda r)\, e^{a_1 z}\, d\lambda \tag{51}$$

$$\pi_{oz} = \frac{i\omega\mu_o I\ell}{2\pi\gamma_o^2} \frac{\partial}{\partial x} \int_0^\infty \frac{1}{\lambda + a_1} J_o(\lambda r)\, e^{a_1 z}\, d\lambda \tag{52}$$

These integrals may be evaluated and then if one substitutes eqs. (51) and (52) into eq. (36) one obtains for the components of the E field just beneath the surface of the interface:

$$E_R = \frac{I\ell \cos\theta}{2\pi r^3 \sigma_1} \left[1 + (1+\gamma_1 r) e^{-\gamma_1 r} \right] \tag{53}$$

$$E_\theta = \frac{I\ell \sin\theta}{2\pi r^3 \sigma_1} \left[2 - (1+\gamma_1 r) e^{-\gamma_1 r} \right] \tag{54}$$

As the frequency goes to zero, these formulas approach the well known functions for a static dipole. The quantities in brackets contain the frequency dependence and might be considered to be ratios of the apparent resistivity to the actual resistivity. Thus, one defines a distinct apparent resistivity for both components of the electric field. Although somewhat superficial now, the concept for having a distinct apparent resistivity associated with each component of the electric field becomes a necessity for multilayer cases. It is interesting to note that at frequencies high enough for the field due to current

penetration in the earth to become negligible compared to the field in the air, the relative strengths of the two components reverse. This phenomenon is due to the fact that the induced fields in the air are perpendicular to the fields directly dependent upon conduction currents. These functions are plotted in Figure 28 as a normalized resistivity as a function of the parameter $\sqrt{\frac{\omega\mu_o\sigma}{2}}\, r$.

Case (b) is shown in Figure 27c. Although the model is probably no more of an accurate picture of actual conditions than case (a), it does serve to illustrate the effects of discontinuities on signal strengths. This solution was obtained by Riordan and Sunde[8, 9] in 1933, although few numerical results were given. The solution is obtained, as in case (2), by applying the boundary conditions to the two interfaces, and then solving for the fields in the three media. One arrives at the following solution for the E field at the surface $z = 0$.

$$E_R = \frac{i\omega\mu_o I\ell \cos\theta}{2\pi} \int_0^\infty \left[\left\{ -f_p(\lambda) + \lambda^2 f_q(\lambda) \right\} J_o(\lambda r) - \frac{\lambda}{r} f_q(\lambda) J_1(\lambda r) \right] \quad (55)$$

$$E_\theta = \frac{i\omega\mu_o I\ell \sin\theta}{2\pi} \int_0^\infty \left\{ f_p(\lambda) J_o(\lambda r) + \frac{\lambda}{r} f_q(\lambda) J_1(\lambda r) \right\} d\lambda \quad (56)$$

where

$$f_p(\lambda) = \frac{\lambda}{D} \left\{ a_1 + a_2 + (a_1 - a_2)\, e^{-2da_1} \right\} \quad (57)$$

$$f_q(\lambda) = \frac{\lambda}{D D_1} \left\{ 4(\gamma_1^2 - \gamma_2^2) a_o a_1^2 \; e^{-2da_1} - D_2 \left[(a_1 + a_2) + (a_1 - a_2) \; e^{-2da_1} \right] \right\} \tag{58}$$

where

$$D = (\lambda + a_1)(a_1 + a_2) + (\lambda - a_1)(a_1 - a_2) \; e^{-2da_1} \tag{59}$$

$$D_1 = (a_o \gamma_1^2 + a_1 \gamma_o^2)(a_1 \gamma_2^2 + a_2 \gamma_1^2) + (a_o \gamma_1^2 - a_1 \gamma_o^2)(a_1 \gamma_2^2 - a_2 \gamma_1^2) \; e^{-2da_1} \tag{60}$$

$$D_2 = (a_o + a_1)(a_1 \gamma_2^2 + a_2 \gamma_1^2) + (a_o - a_1)(a_1 \gamma_2^2 - a_2 \gamma_1^2) \; e^{-2da_1} \tag{61}$$

where

$$a = \sqrt{\lambda^2 + \gamma^2}$$

and γ is chosen for the appropriate media. The r and θ components of the electric field have been chosen because for these components only, the field strengths may be normalized and plotted as apparent resistivity curves which are independent of the variable θ. In the d. c. case, all gammas are zero and the integral reduces to a form which may be evaluated exactly. Otherwise the results must be obtained by numerical integration. In presenting these results it will be necessary to normalize the variables which affect the apparent resistivity. Therefore, we now make the changes

$$\alpha = r/d \qquad \beta = \rho_2/\rho_1 \qquad \Delta = \sqrt{\omega \mu_o \sigma_1 d} \qquad \mu_1 = \frac{1 - \beta}{1 + \beta} \tag{62}$$

when the frequency is zero, $\Delta = 0$, and eqs. (55) and (56) reduce to

$$E_R = \frac{I\ell \cos\theta \rho_1}{2\pi r^3} \int_0^\infty \left\{ \frac{1 - \mu_1 e^{-\frac{2n}{a}}}{1 + \mu_1 e^{-\frac{2n}{a}}} \right\} n \left\{ J_1(n) - n J_o(n) \right\} dn \tag{63}$$

$$E_\theta = \frac{I\ell \sin\theta \rho_1}{2\pi r^3} \int_0^\infty \left\{ \frac{1 - \mu_1 e^{-\frac{2n}{a}}}{1 + \mu_1 e^{-\frac{2n}{a}}} \right\} n J_1(n)\, dn. \tag{64}$$

These integrals are easily evaluated. One obtains the solution

$$E_R = \frac{I\ell \cos\theta}{2\pi r^3} \rho_{ar} \qquad E_\theta = \frac{I\ell \sin\theta}{2\pi r^3} \rho_{a\theta} \tag{65}$$

where

$$\rho_{a_r}/\rho_1 = 1 + 2 \sum_{n=1}^{\infty} (-\mu_1)^n \left(\frac{a}{2n}\right)^3 \left\{ \frac{\left(\frac{a}{2n}\right)^2 - 1/2}{\left[\left(\frac{a}{2n}\right)^2 + 1\right]^{5/2}} \right\} \tag{66}$$

$$\rho_{a\theta}/\rho_1 = 1 + 2 \sum_{n=1}^{\infty} (-\mu_1)^n \left(\frac{a}{2n}\right)^3 \left\{ \frac{1}{\left[\left(\frac{a}{2n}\right)^2 + 1\right]^{3/2}} \right\} \tag{67}$$

The functions ρ_{ar}/ρ_1 and $\rho_{a\theta}/\rho_1$ are plotted in Figures 29 and 30 with respect to the variable a for various values of B. These curves are very similar to the curves used in the Wenner 4-pole method of geophysical prospecting.

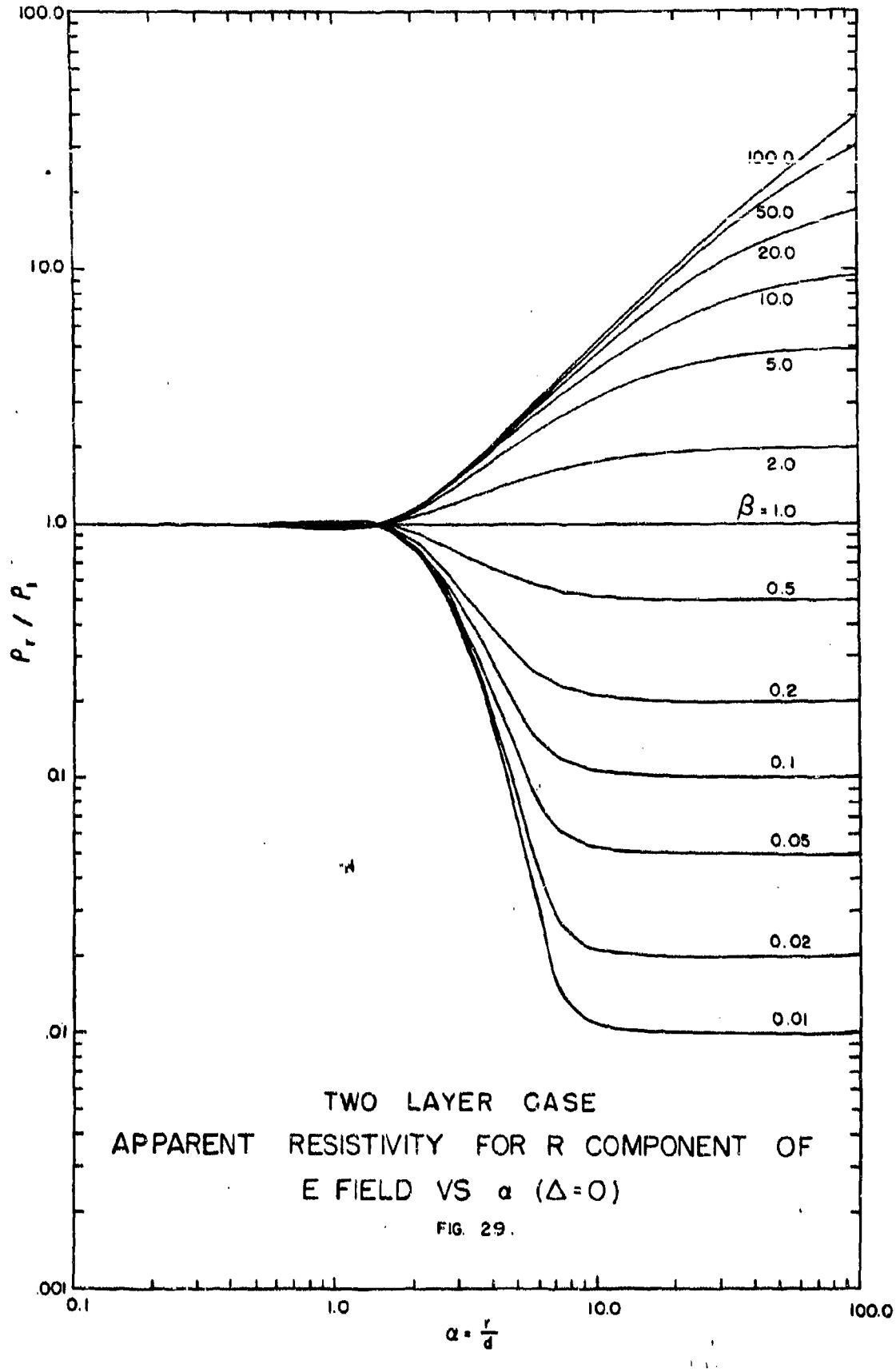

TWO LAYER CASE

APPARENT RESISTIVITY FOR R COMPONENT OF E FIELD VS α ($\Delta = 0$)

FIG. 29.

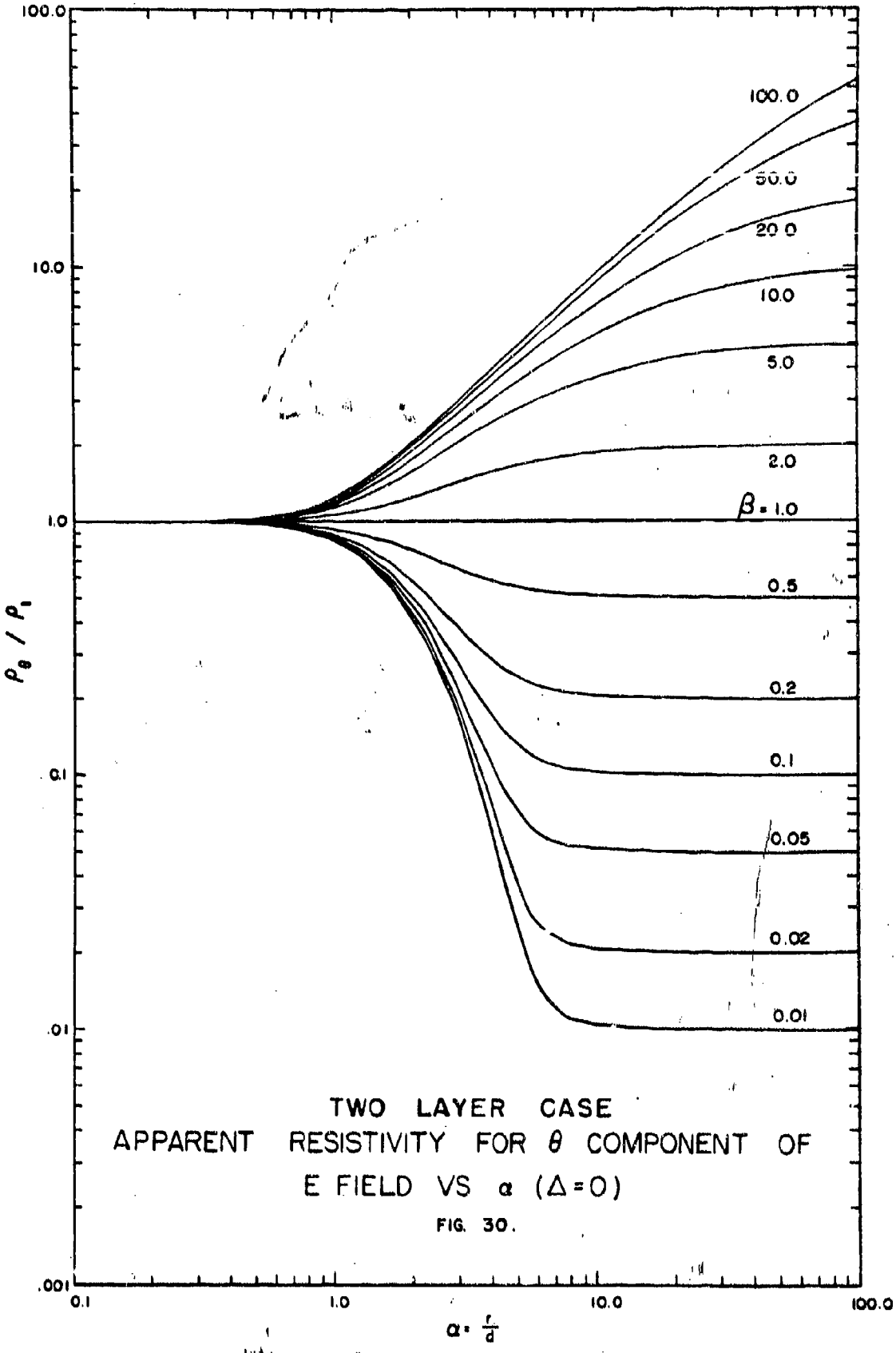

TWO LAYER CASE
APPARENT RESISTIVITY FOR θ COMPONENT OF E FIELD VS α ($\Delta = 0$)

FIG. 30.

The more interesting case is that for which induction fields are present. In this case, the integrals in equations (55) and (56) must be evaluated numerically. These integrations were performed for typical values of resistivity contrast on the CDC 1604 computer at the University of Texas. The results are shown in Figures 31 through 38. Figures 31 through 34 are for a resistivity contrast, i.e. β, equal to 20, corresponding to a more resistive second layer; while Figures 35 through 38 are for β, equal to .05, corresponding to a more conductive second layer. The apparent resistivities are plotted as functions of Δ, the normalized frequency, with α, the normalized distance as a parameter. The magnitudes and phases of both components of the electric field are on separate graphs. The phase is with respect to the input current at the transmitter.

The variable Δ may be interpreted as the ratio of d, the depth of the second layer, to the effective depth of penetration, and is proportional to the square root of the frequency. As the frequency is increased from zero Δ increases and the effective depth decreases. Figures 31 though 38 show that for frequencies such that the effective depth is much less than the depth of the interface, the second layer has no effect on the signal strength. However, for very low frequencies the second layer will have a definite effect, the magnitude of which depends on the distance of the receiver from the transmitter compared to the depth of the second layer and the resistivity contrast between the two layers. If one is using these curves to compute expected signal strengths, it should be remembered that they are normalized as in Eq. (65).

The effect of the layers on the signal strength may best be shown by considering an example. Suppose that the local geology may be approximated by a model which consists of a bed with a thickness of 1 km and a resistivity, ρ_1, equal to 50 Ω-meters, over a very deep strata with a resistivity, ρ_2, equal to 1000 Ω-meters. Suppose the receiver is located 7 km from the transmitter, at an angle of 30° with respect to the transmitting dipole axis. Let the transmitting electrodes be 770 meters apart and the current be 50 amperes. The electric field will be given by the two equations

$$E_R = \frac{I\ell \cos\theta}{\pi R^3} \rho_{aR} \qquad \text{and} \qquad E_\theta = \frac{I\ell \sin\theta}{2\pi R^3} \rho_{a\theta} \tag{65}$$

in which ρ_{aR} and $\rho_{a\theta}$ will be determined from theoretical apparent resistivity curves. In this case the resistivity contrast, β is equal to 20.0 and the curves of Figures 31 through 34 apply. The normalized distance, α, is 7.0. The parameter Δ is

$$\Delta = \frac{4\pi}{10}\sqrt{\frac{f}{10}}\ , \tag{68}$$

where f is the frequency of transmission.

Let f = .1 cps, then Δ = .126, and referring to Figures 31 and 33 we see that

$$\frac{\rho_{ar}}{\rho_1} = 3.2 \qquad \text{and} \qquad \frac{\rho_{a\theta}}{\rho_1} = 5.3, \tag{69}$$

which yield

$$\rho_{ar} = 160\ \Omega\text{-meters} \quad \text{and} \quad \rho_{a} = 265\ \Omega\text{-meters.}$$

Figures 32 and 34 show that for this frequency, the phase lag of the received electric field with respect to the current in the transmitting dipole will be negligible. Using these apparent resistivities the received electric field as computed from Eqs. 65 will be

$$E_R = 5.7\ \text{mv/km} \quad \text{and} \quad E_\theta = 4.7\ \text{mv/km.} \tag{70}$$

The effect of the discontinuity may be demonstrated by considering a frequency of 15 cps, instead of .1 cps: Δ is now equal to 1.54 and the apparent resistivities and the resulting field strengths are

$$\begin{aligned} \rho_{ar} &= 13.5\ \Omega\text{-meters} & \rho_{a\theta} &= 60\ \Omega\text{-meters} \\ E_R &= .48\ \text{mv/km} & E_\theta &= 1.06\ \text{mv/km.} \end{aligned} \tag{71}$$

From Figures 32 and 34 we see that the phase angle will be lagging by 65° for E_R and 55° fro E_θ.

If one is attempting to find a model from measured field strengths, the apparent resistivities are determined from Eq. (65) and then plotted on log paper versus the square root of the frequency. These curves may then be compared with the theoretical resistivity curves. The surface resistivity is then determined by the upper frequency limit. If measurements from a number of sites are available then the apparent resistivity for the low frequency limit

may be plotted versus distance and compared to the d. c. curves which are given in Figures 29 and 30 where the parameter is resistivity contrast. It should be noted that the parameter in Figures 31 through 38 for the a. c. case is α, the normalized distance, which corresponds to distance from the transmitter to the receiver. For large values of α the apparent resistivity will approach the resistivity of the second layer, while for small values of α it approaches the resistivity of the first layer.

As was stated at the first of this section, optimum signal transmission depends on the location of large deep strata of high resistivity. From Figures 31 through 38, it is apparent that if the high resistivity strata is located at the surface, then the optimum frequencies will be those which are high enough that the fields do not penetrate significantly into the more highly conductive substrata. In other words, frequencies such that the skin depth is less than the depth of this layer. As may be seen from the d. c. curves in Figures 29 and 30, this consideration will be necessary if the separation of the receiver from the transmitter is somewhat greater than the depth of this layer.

In the alternative case, when the highly resistive strata is beneath the surface and is overlaid by a more highly conductive strata, the maximum signal strength occurs at d. c. and the bandwidth is limited to frequencies such that the skin depth is somewhat greater than the depth of the second layer. Suppose that it were possible to vary the depth of the interface between the two media: it is apparent that for a given transmitter-receiver separation the upper frequency for a given field strength increases as the thickness of the

more conductive surface layer decreases. This is shown in Figure 29 where the value Δ at which the signal strengths are down to half-power points as function of Δ is shown. This locus was obtained from Figure 31.

From this discussion one may conclude that the optimum frequency for transmission and the useable bandwidth depend to a large extent on the local geology. Other factors which one might want to consider are the natural magnetotelluric signals and the local industrial noise as the signal strengths which are possible from a transmitter of this type are generally of the same order of magnitude as the natural signal.

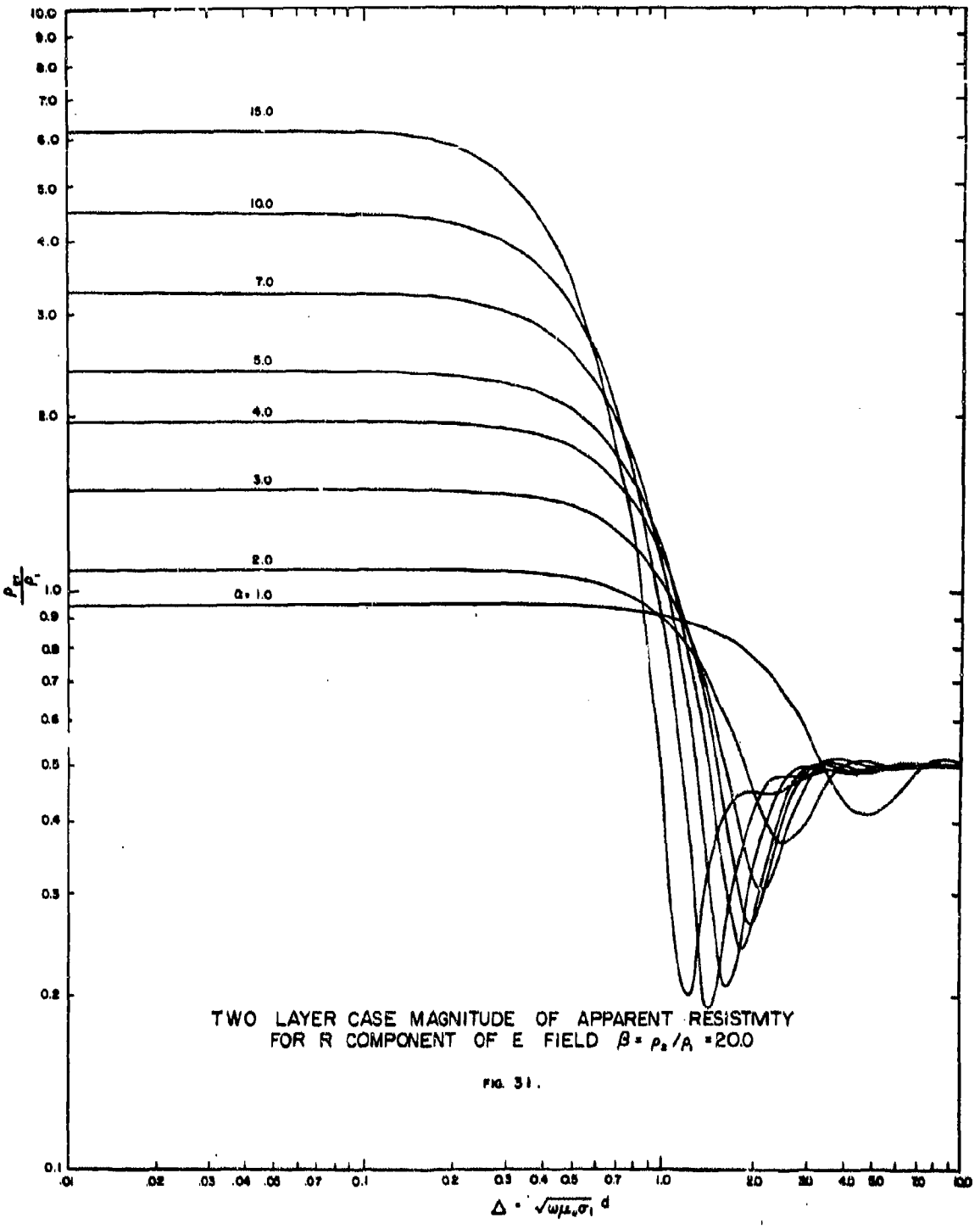

TWO LAYER CASE MAGNITUDE OF APPARENT RESISTIVITY
FOR R COMPONENT OF E FIELD $\beta = \rho_2/\rho_1 = 20.0$

FIG. 31.

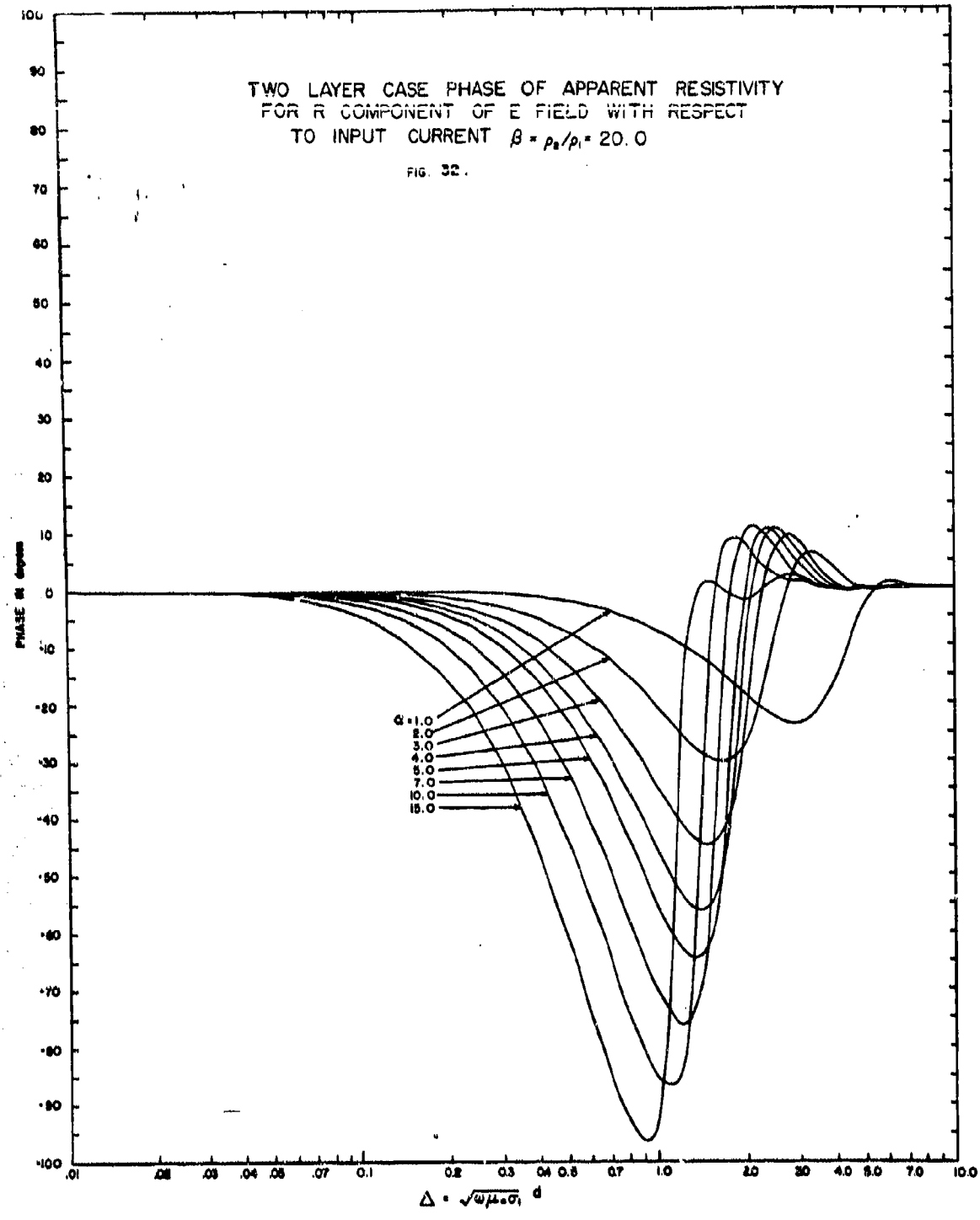
TWO LAYER CASE PHASE OF APPARENT RESISTIVITY
FOR R COMPONENT OF E FIELD WITH RESPECT
TO INPUT CURRENT $\beta = \rho_2/\rho_1 = 20.0$
PHASE in degrees
α = 1.0
2.0
3.0
4.0
5.0
7.0
10.0
15.0
$\Delta = \sqrt{\omega\mu_0\sigma_1}\, d$

FIG. 32.

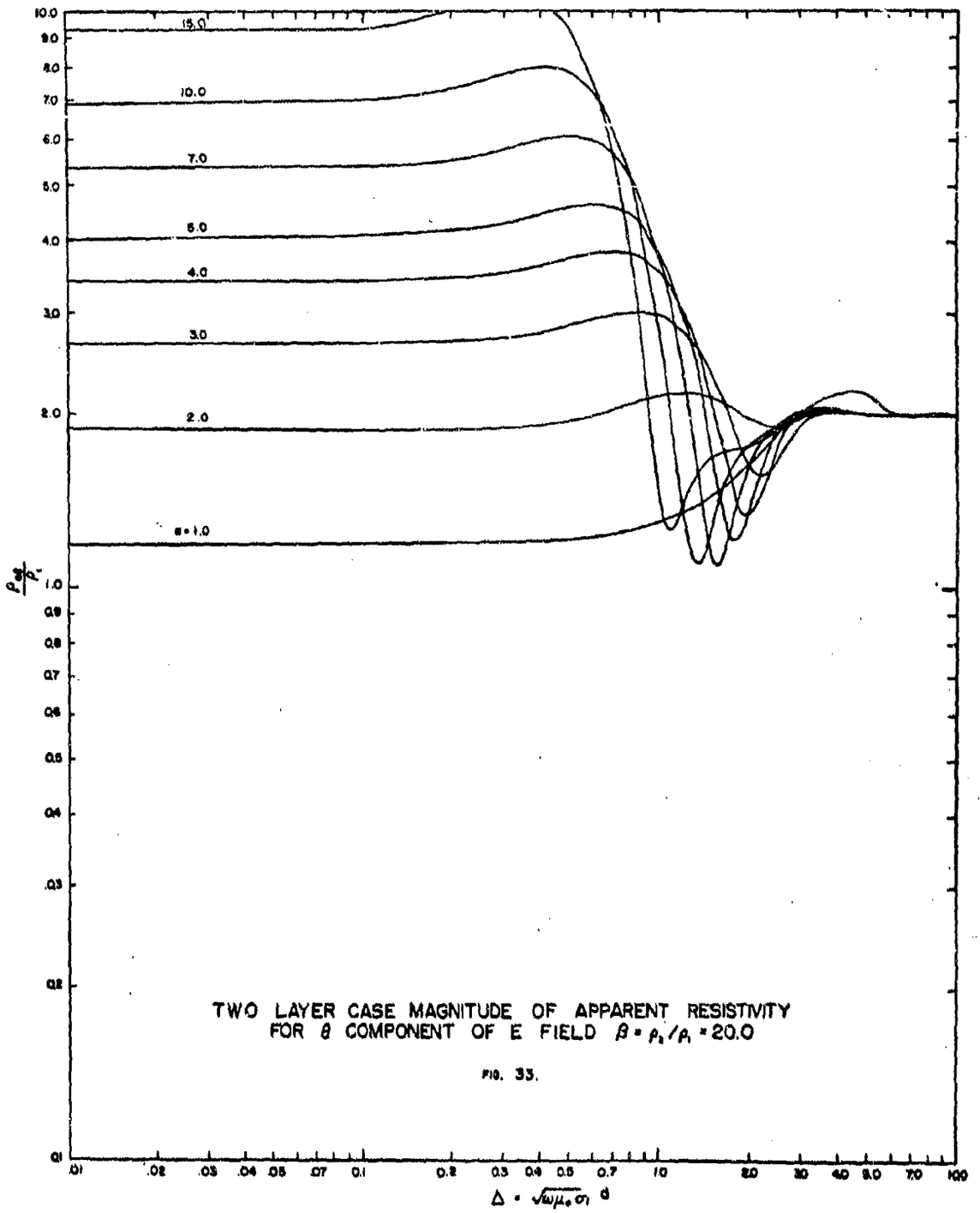

TWO LAYER CASE MAGNITUDE OF APPARENT RESISTIVITY
FOR θ COMPONENT OF E FIELD $\beta = \rho_2/\rho_1 = 20.0$

FIG. 33.

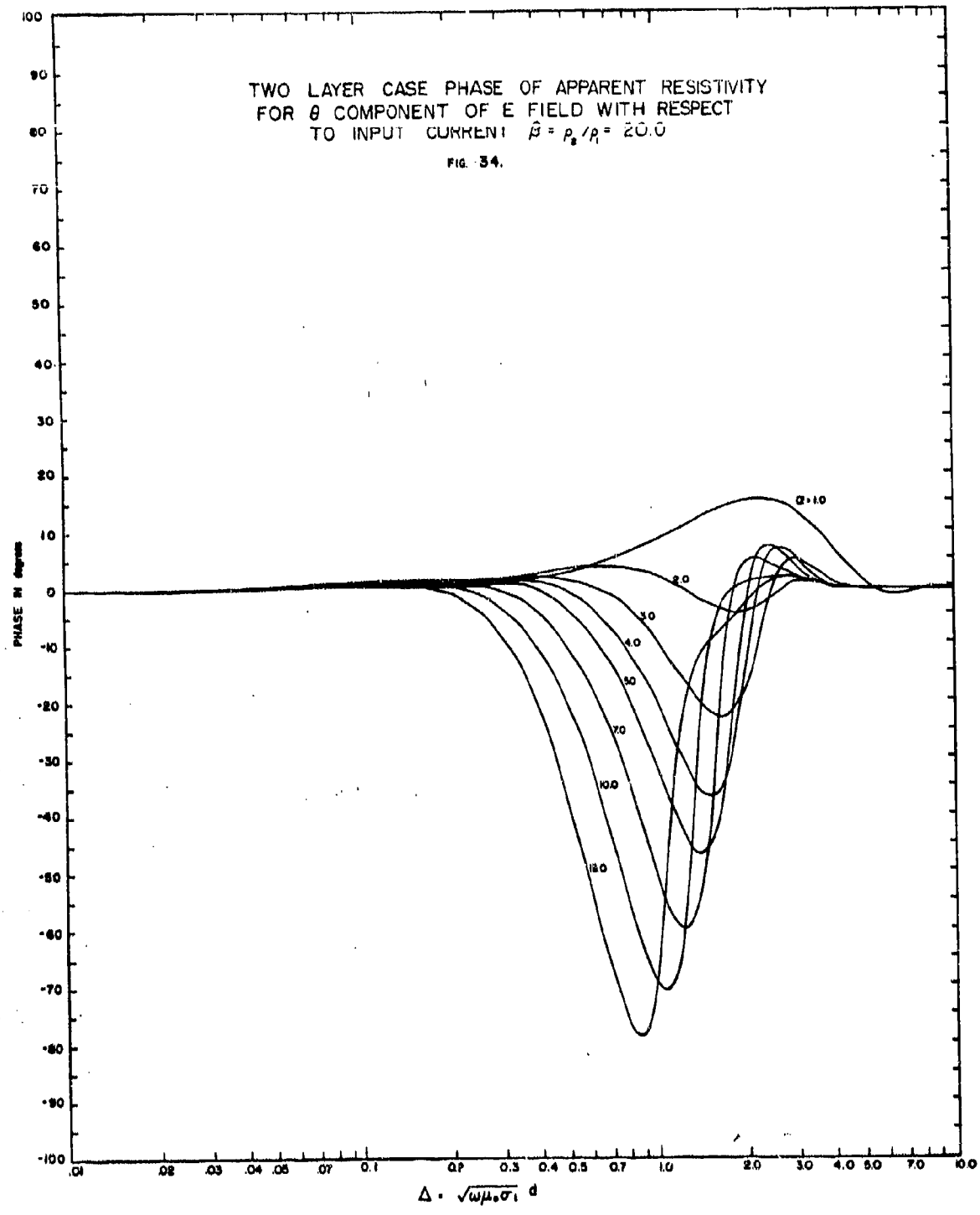
TWO LAYER CASE PHASE OF APPARENT RESISTIVITY
FOR θ COMPONENT OF E FIELD WITH RESPECT
TO INPUT CURRENT $\hat{\beta} = \rho_2/\rho_1 = 20.0$
FIG. 34.
PHASE IN degrees
α=1.0
2.0
3.0
4.0
5.0
7.0
10.0
12.0
$\Delta = \sqrt{\omega\mu_0\sigma_1}\, d$

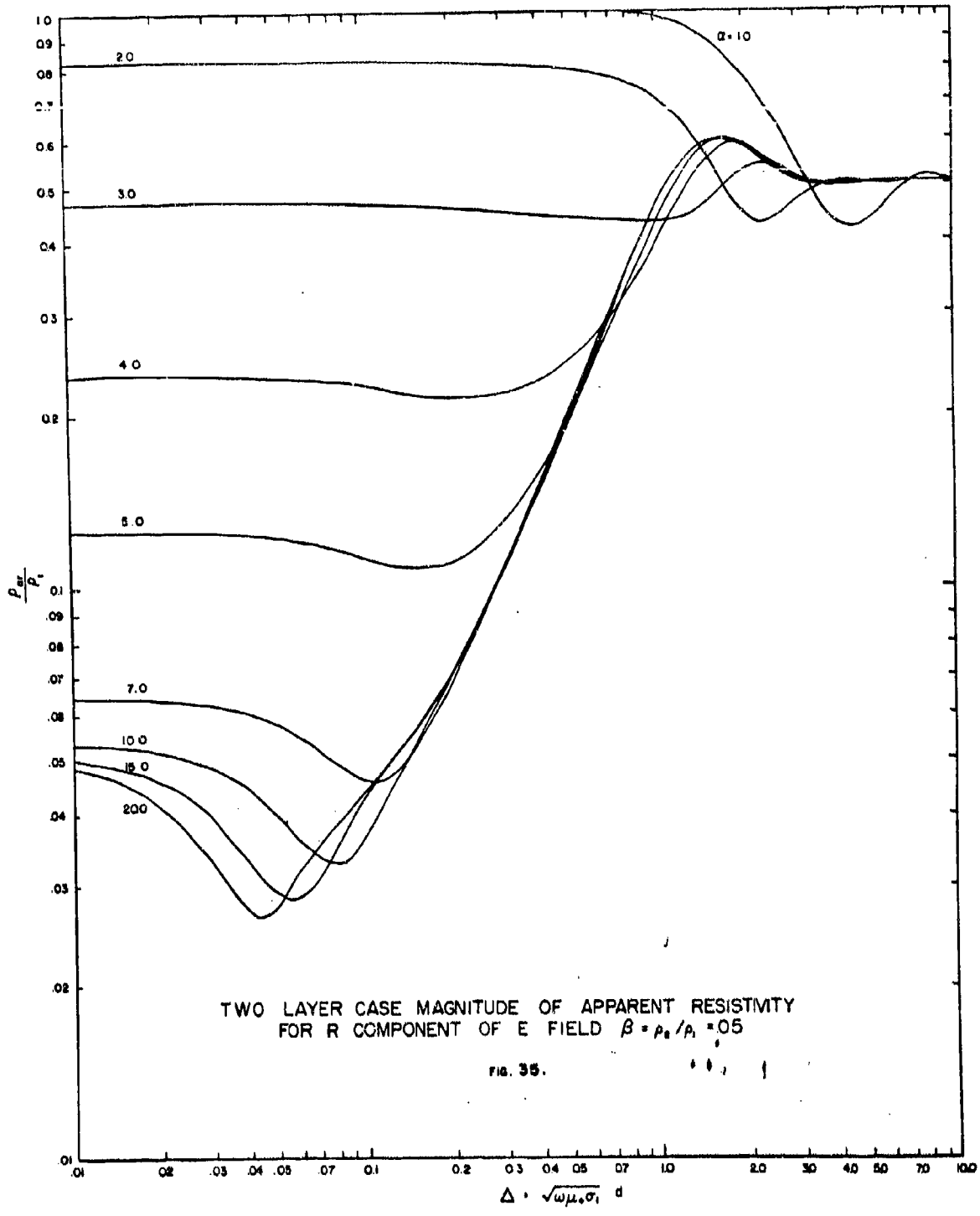

TWO LAYER CASE MAGNITUDE OF APPARENT RESISTIVITY
FOR R COMPONENT OF E FIELD $\beta = \rho_2/\rho_1 = .05$

FIG. 35.

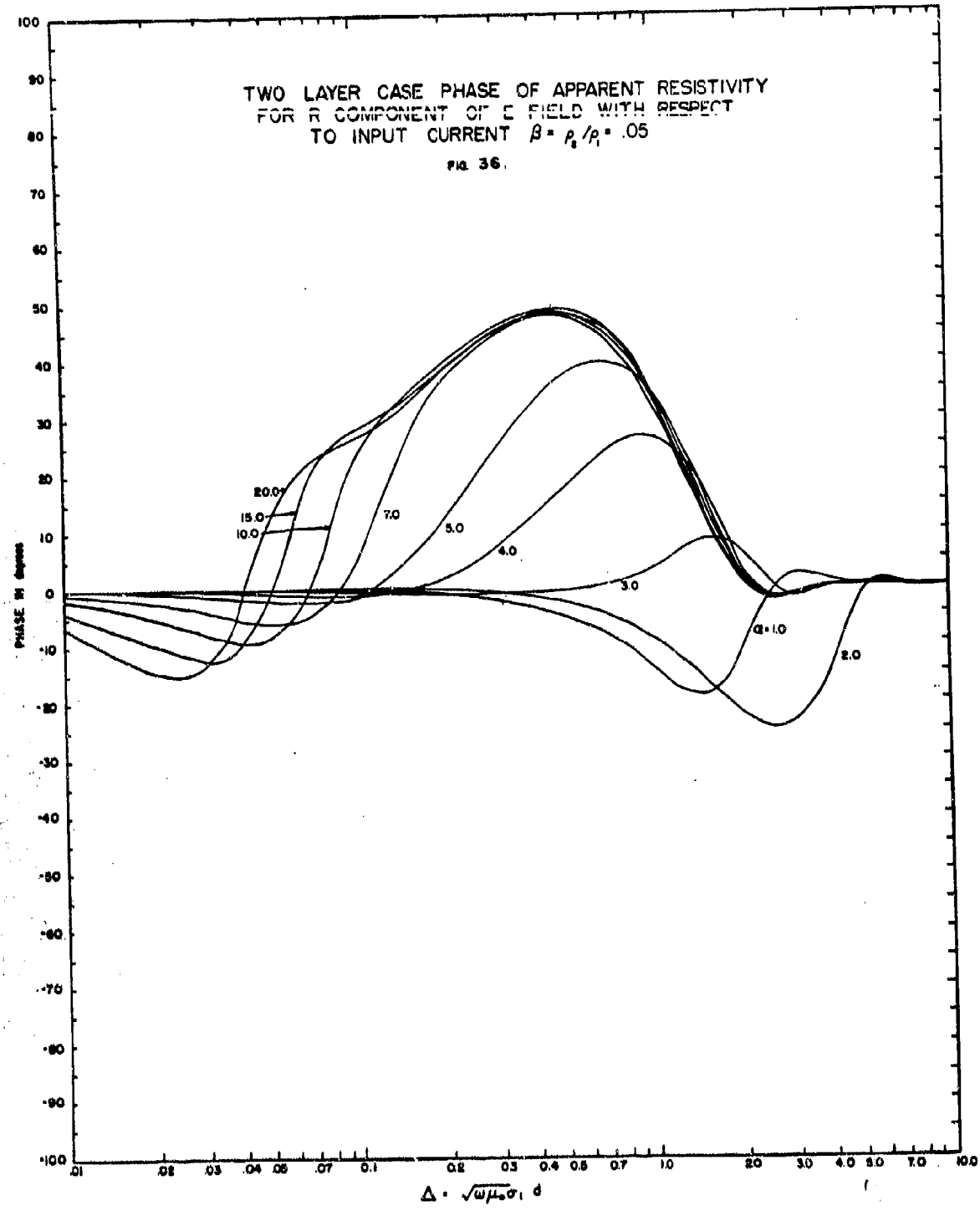
TWO LAYER CASE PHASE OF APPARENT RESISTIVITY
FOR R COMPONENT OF E FIELD WITH RESPECT
TO INPUT CURRENT $\beta = \rho_2/\rho_1 = .05$
FIG. 36.
PHASE IN degrees
20.0
15.0
10.0
7.0
5.0
4.0
3.0
α = 1.0
2.0
$\Delta = \sqrt{\omega\mu_0\sigma_1}\, d$

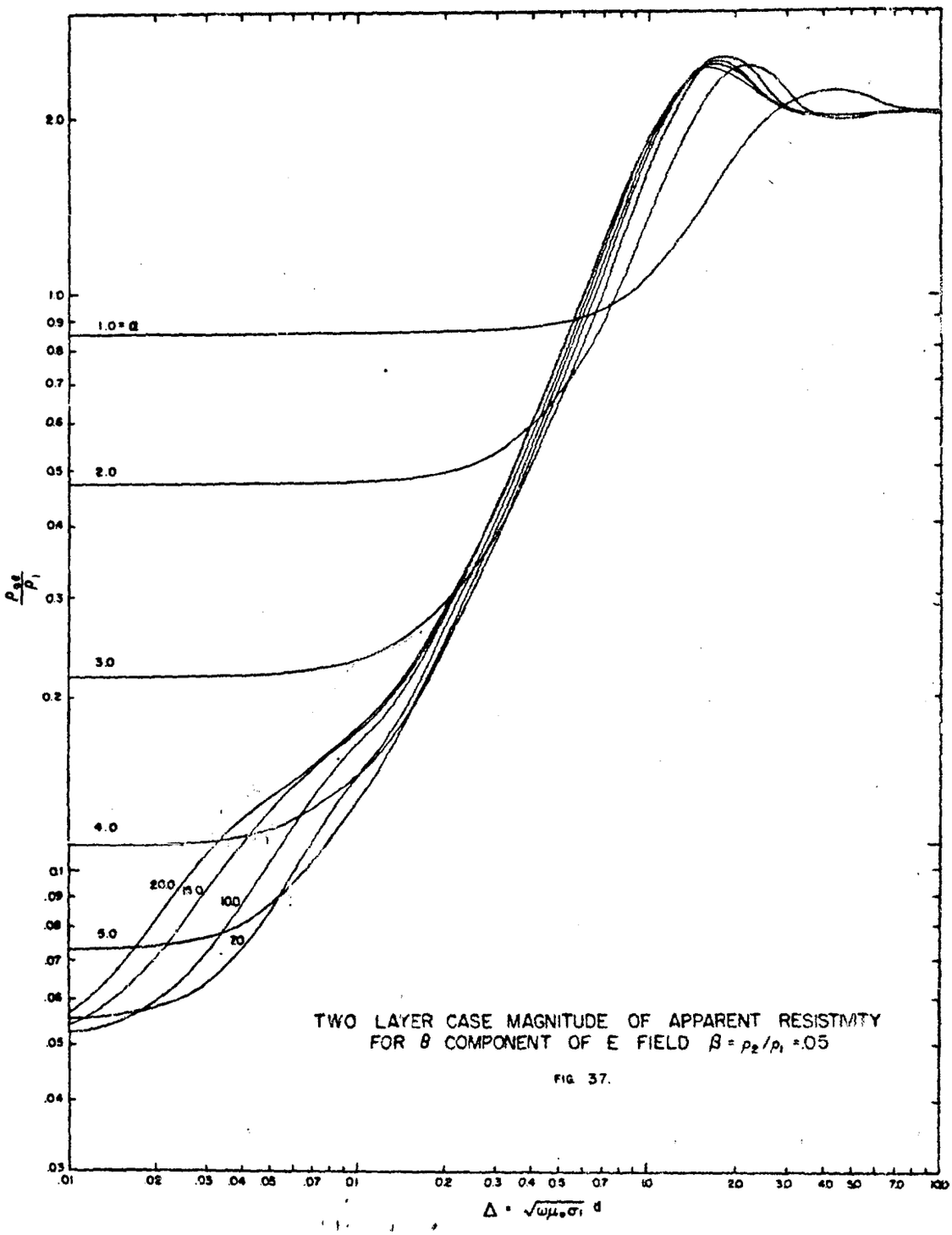

TWO LAYER CASE MAGNITUDE OF APPARENT RESISTIVITY
FOR θ COMPONENT OF E FIELD $\beta = \rho_2/\rho_1 = .05$

FIG. 37.

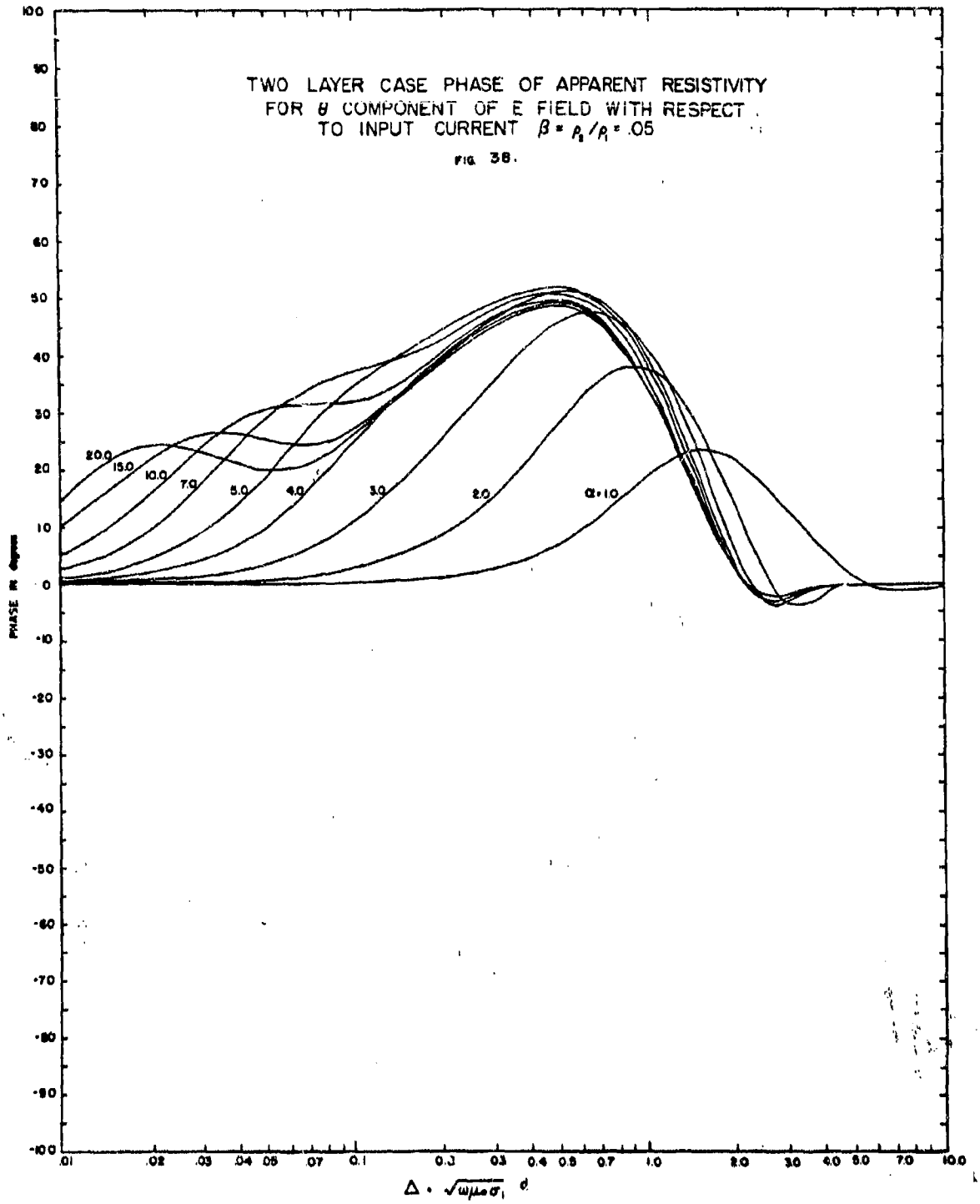
TWO LAYER CASE PHASE OF APPARENT RESISTIVITY
FOR θ COMPONENT OF E FIELD WITH RESPECT
TO INPUT CURRENT β = ρ2/ρ1 = .05
FIG. 38.
PHASE IN degrees
100
90
80
70
60
50
40
30
20
10
0
-10
-20
-30
-40
-50
-60
-70
-80
-90
-100
20.0
15.0
10.0
7.0
5.0
4.0
3.0
2.0
α=10
.01
.02
.03
.04
.05
.07
0.1
0.2
0.3
0.4
0.5
0.7
1.0
2.0
3.0
4.0
5.0
7.0
10.0
Δ = √ωμσ1 d

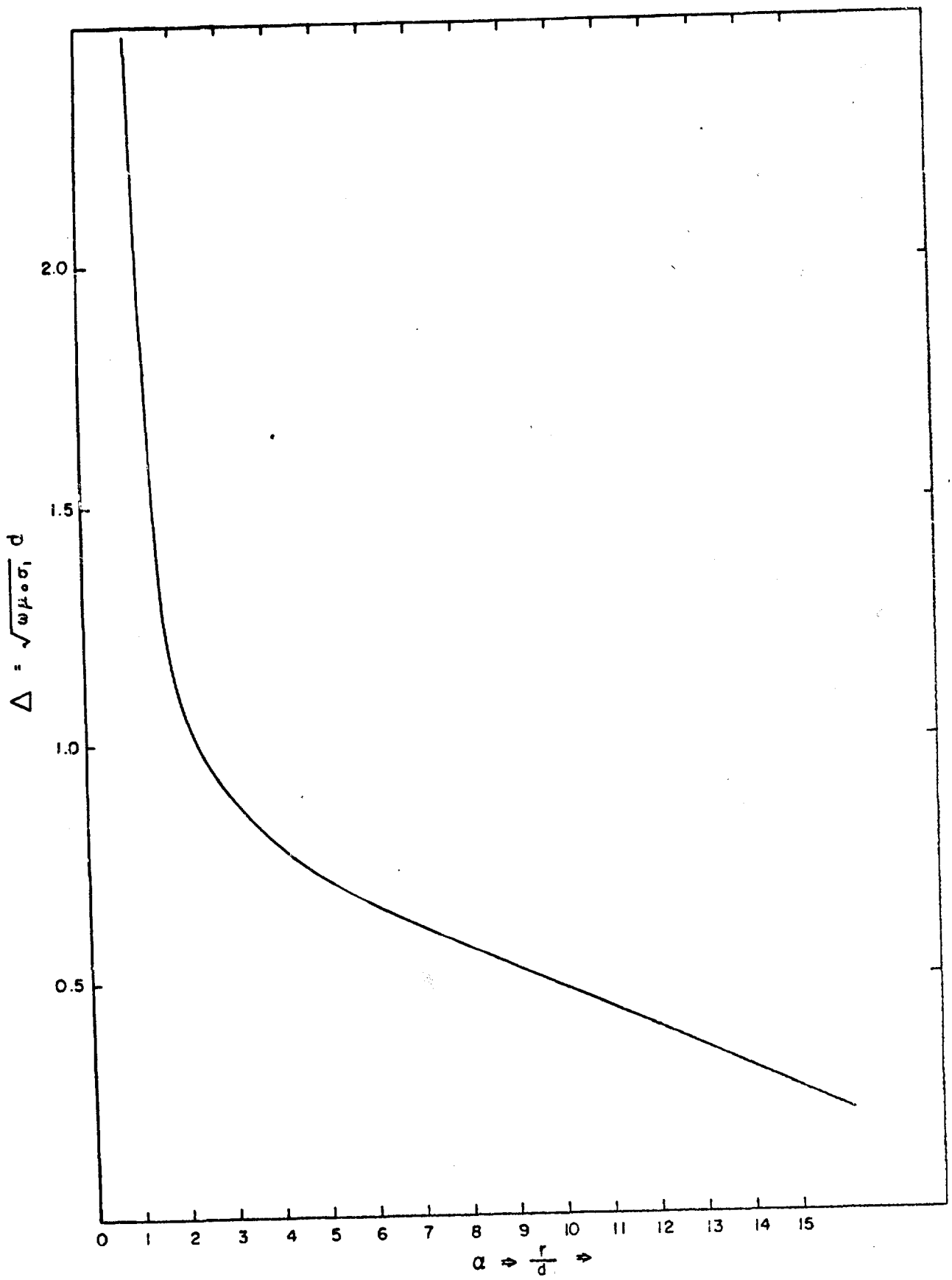

LOCUS OF $\frac{1}{2}$ POWER POINTS FOR $\beta = 20.0$
R-COMPONENT

FIG. 39.

V. EXPERIMENTAL PROCEDURE AND SAMPLE DATA

Signal strength measurements were conducted with the transmitter operating on the grounds of the Electrical Engineering Research Laboratory. The transmitting electrodes were spaced 0.77 kilometer apart on an east-west line, electrode resistance was about 8 ohms, and the current used was from 40 to 50 amperes.

The receiver was set up at four sites ranging in distance from 5 to 32 kilometers from the transmitter as shown in Figure 40, which also shows the measured field directions compared with the direction of a dipole field at each receiving site. Figure 41 gives plots of signal strength versus frequency at each site. The signal voltage shown was measured with 500 foot receiving electrode separation, and the data is corrected for system response and adjusted for a transmitting electrode current of 50 amperes. The signals at sites 1 and 2 were well above the noise due to magnetotellurics and the values shown are the actual signal amplitudes. The narrow band filter was used only at sites 3 and 4, at which the signals were nearer the noise levels; for these sites, Figure 41 shows the signal plus noise and the corresponding noise levels in the filter bandpass as a function of frequency. The Q of the system response can be considered to be 25 when the narrow band filter is used.

The experimental data may be interpreted on the basis of the theory presented in Section IV, if one assumes a two-layer horizontally stratified earth. For the frequency range, 0 to 200 cps, the electric field will be given by

$$E_R = \frac{I\ell \cos\theta}{\pi R^3} \rho_{ar} \qquad E_\theta = \frac{I\ell \sin\theta}{2\pi R^3} \rho_{a\theta} \tag{65}$$

where I is the transmitter current, ℓ the dipole length, and R and θ are the cylindrical coordinates of the receiver with respect to the transmitter, and $\rho_{a\theta}$ and ρ_{ar} are the apparent resistivities. It should be noted that the electric field explicitly varies in inverse proportion to the cube of the distance from the transmitter. However, the apparent resistivity is also a function of R, as shown in Section IV, in addition to being a function of frequency. If one resolves the field into its R and θ components, and assumes a distinct apparent resistivity for each component then these apparent resistivities are not a function of the bearing of the receiver with respect to the transmitting dipole, but only of the distance to the receiver, the frequency, and the parameters necessary to describe the earth.

As shown in Section IV, variations in the field from the inverse radius cubed dependence may be quite large, depending on the structure of the earth. For this reason, the data might be advantageously presented as plot of apparent resistivity versus frequency for various distances from the transmitter. The apparent resistivities, computed from the fields given in Figure 41 for the locations shown in Figure 40 are plotted in Figures 42 and 43. In the optimal case, when the structure of the earth is known to be two layers, the experimental apparent resistivities may be compared to a set of curves as given in Figures 31 through 38 and from a best fit, the depth of the interface and resistivity contrast between the first and second layers determined. Or, conversely, if the exact

structure is known, the theoretical apparent resistivities for a given location and frequency may be determined from the curves, and the expected electric field for a given dipole transmitter computed.

In general, the earth may not be modeled as a homogeneous horizontally stratified medium, and quite probably is not known with any degree of exactness. However, for the two layer case, certain characteristics are common for all values of resistivity contrast. For a given location, as the frequency is increased from d. c., the apparent resistivity remains approximately constant until the skin depth approaches the depth of the interface, at which point it rapidly becomes that which would be expected from a semi-infinite homogeneous earth with the apparent resistivity equal to that of the first layer. In other words, as the frequency becomes large ρ_{aR} approaches $\rho_1/2$, and $\rho_{a\theta}$ approaches $2\rho_1$.

In the Austin area the geology is known to be different from that of a two-layer stratified earth. The Balcones Fault runs directly by the transmitting electrodes. Site 2 is across the fault and the surface resistivity at this site is known to be considerably higher than that at the other sites. Only Site 3 may be considered to be a reasonable distance from the fault. Making a rough comparison between the experimental apparent resistivity curves plotted in Figure 42 and the typical theoretical apparent resistivity curves in Section IV, we see that the data apparently indicate a substratum whose resistivity is somewhat greater than that of the surface and which is located at a depth equal to the skin depth of the first layer at approximately 1 cps. If one were to assume a surface resistivity of about 50 ohm-meters, then this would indicate

a more resistive substratum at a depth of approximately 2.5 kms. Unfortunately, the data is limited to low frequencies, and due to the Oregon transmission tests (Appendix B) there was not time to make more tests. The failure of the data to be consistent for the low frequencies may be attributed to the extreme irregularities in the local geology.

With an operating current on the order of 50 amps, and with a transmitting electrode spacing of about 1 km, the maximum distance over which a typical magnetotelluric measuring system, without special filters, would be able to detect the signal would be on the order of 15 to 20 kms. The major limitation to reception is not noise or gain of receiving equipment but the level of the natural magnetotelluric signal, and for high frequencies, industrial and 60 cps noise. This situation may be improved considerably by the use of band-pass filters. The fact that for an homogeneous semi-infinite earth decreases inversely proportional to the cube of the distance implies that with the input used in these experiments the signal level will be approximately that of natural magnetotellurics at 15 kms. Doubling the input current increases the effective distance by a factor of only the $\sqrt[3]{2}$ or 1.27. The same is true for increasing the spacing between the transmitting electrodes. It is thought that the use of bandpass filters or a synchronous detection system might increase the maximum distance of reception to about 40 km, when operating the transmitter as was done in Austin. However, it accurate data were desired for purposes of determining apparent resistivities, 30 kms would probably be the maximum distance.

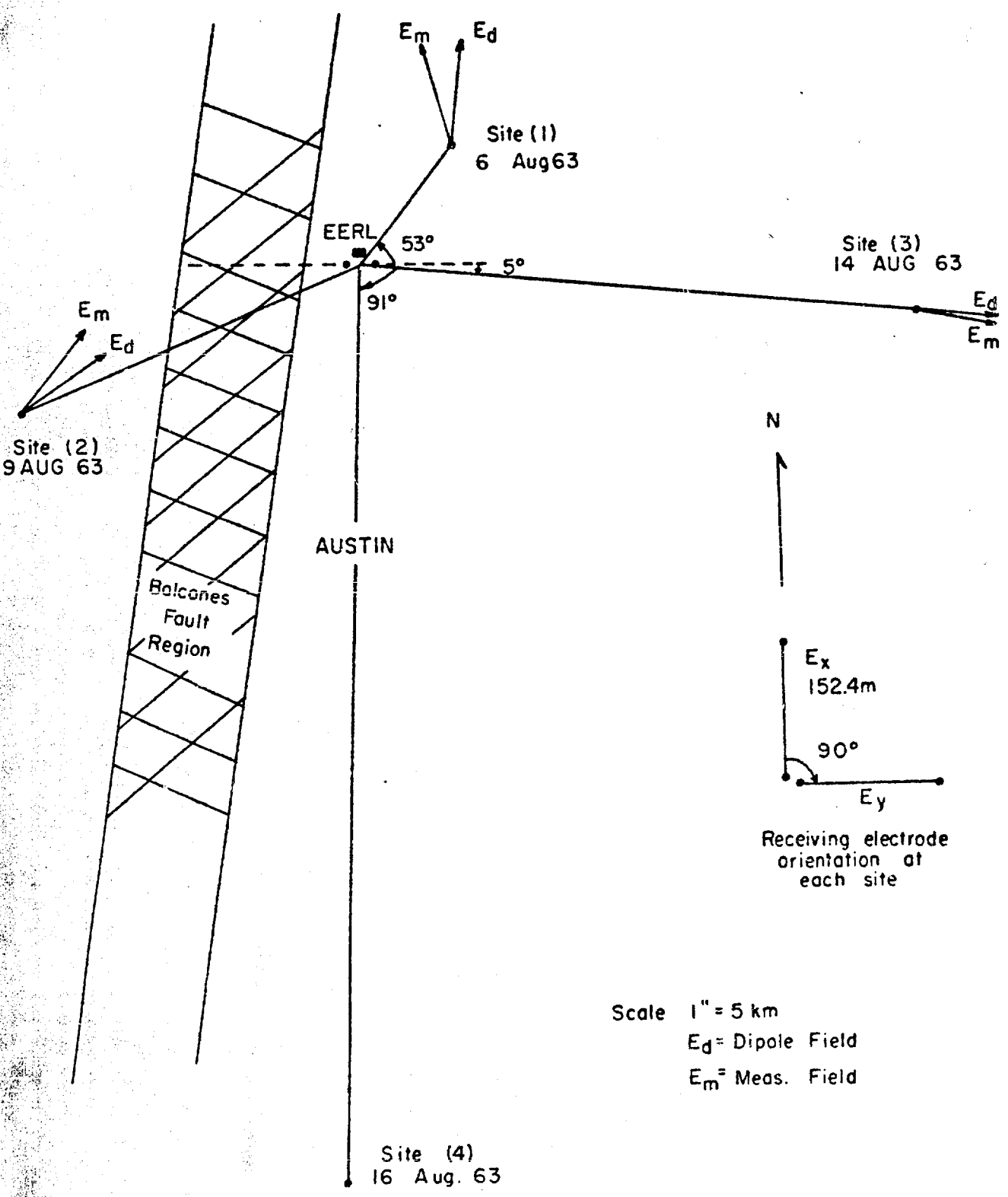

TRANSMITTING AND RECEIVING SITES
IN THE AUSTIN AREA

FIG. 40.

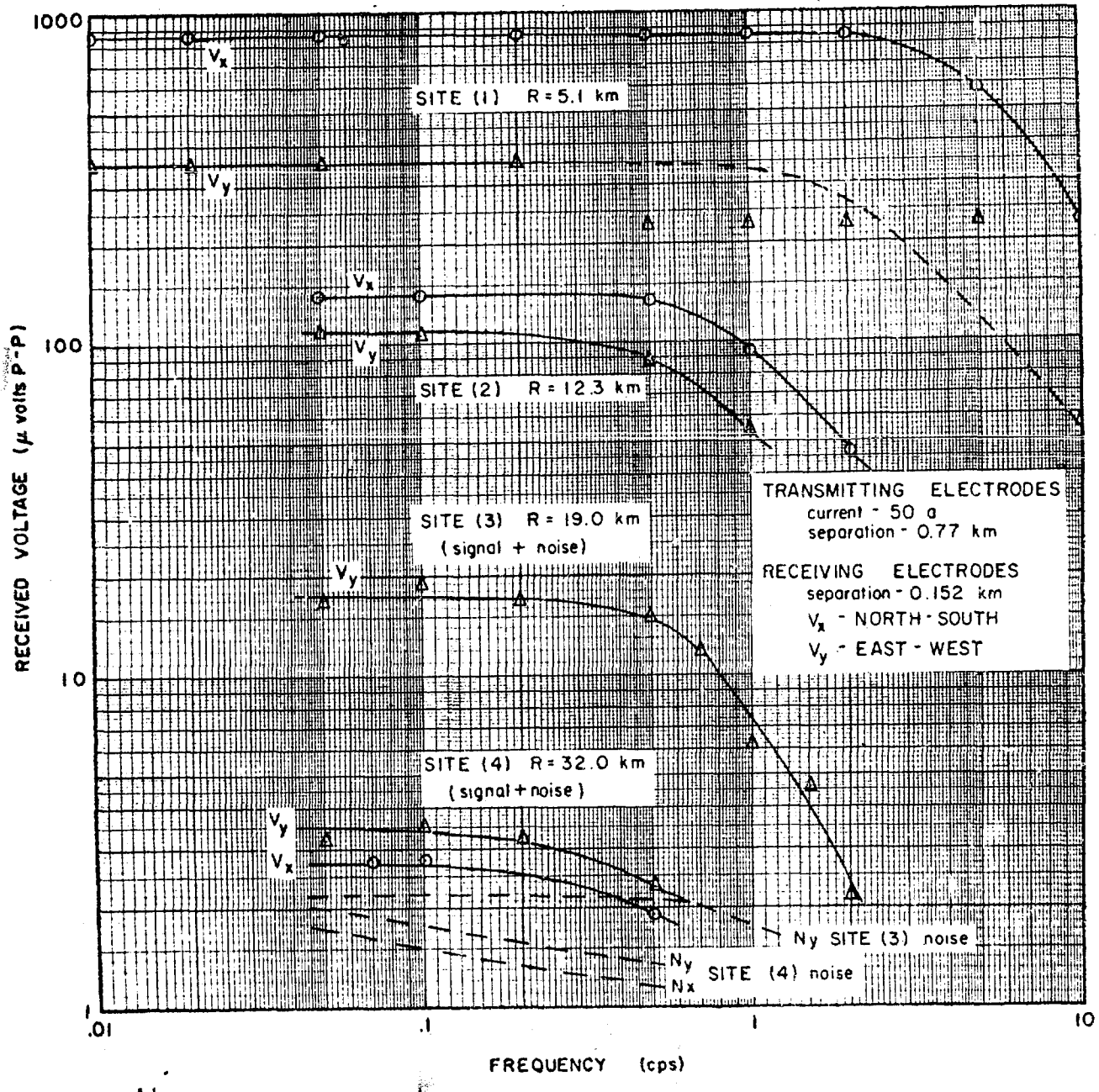

PLOT OF RECEIVED SIGNAL VS FREQUENCY

FIG. 41.

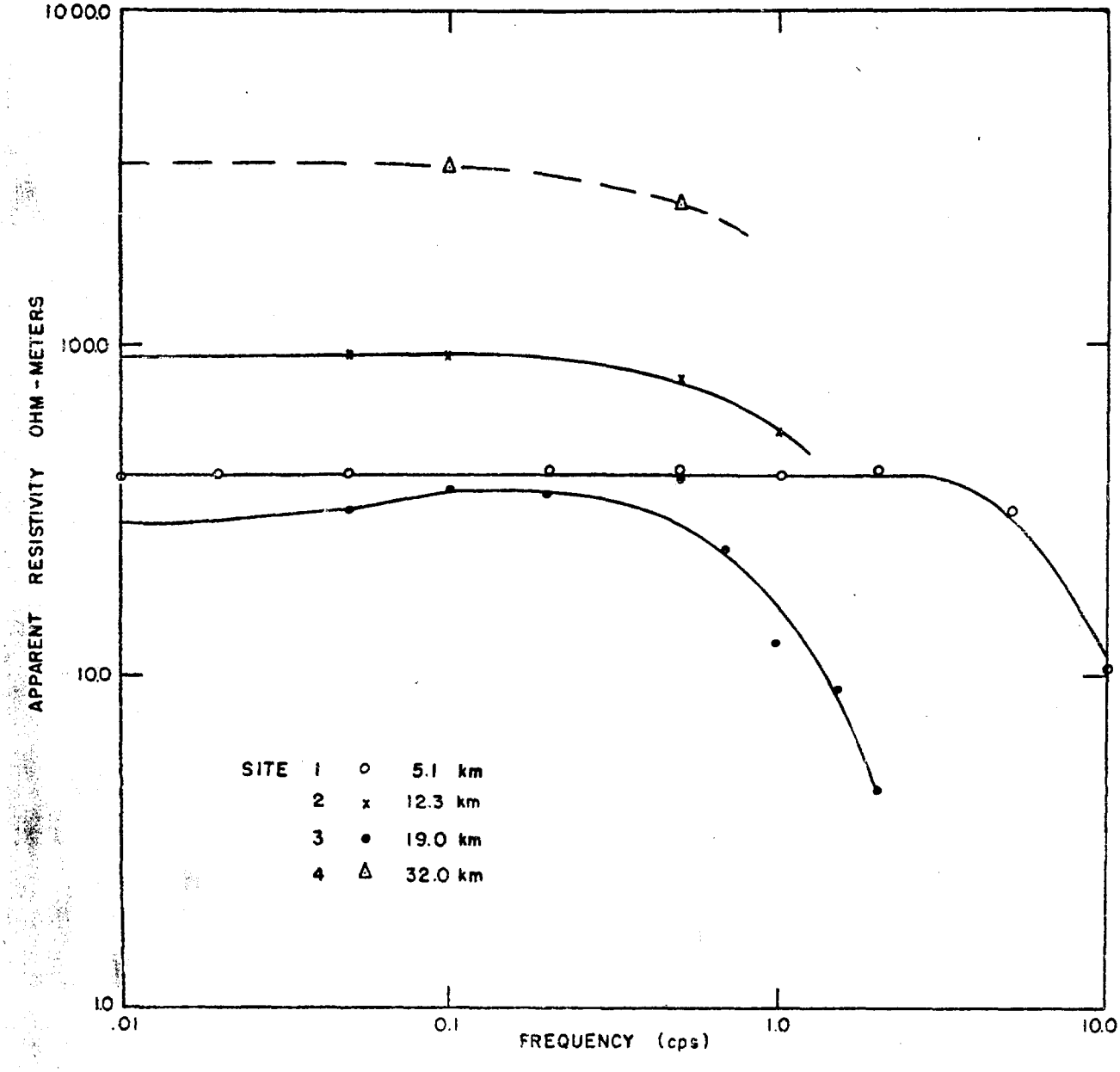

EXPERIMENTAL APPARENT RESISTIVITIES
R-COMPONENT

FIG. 42.

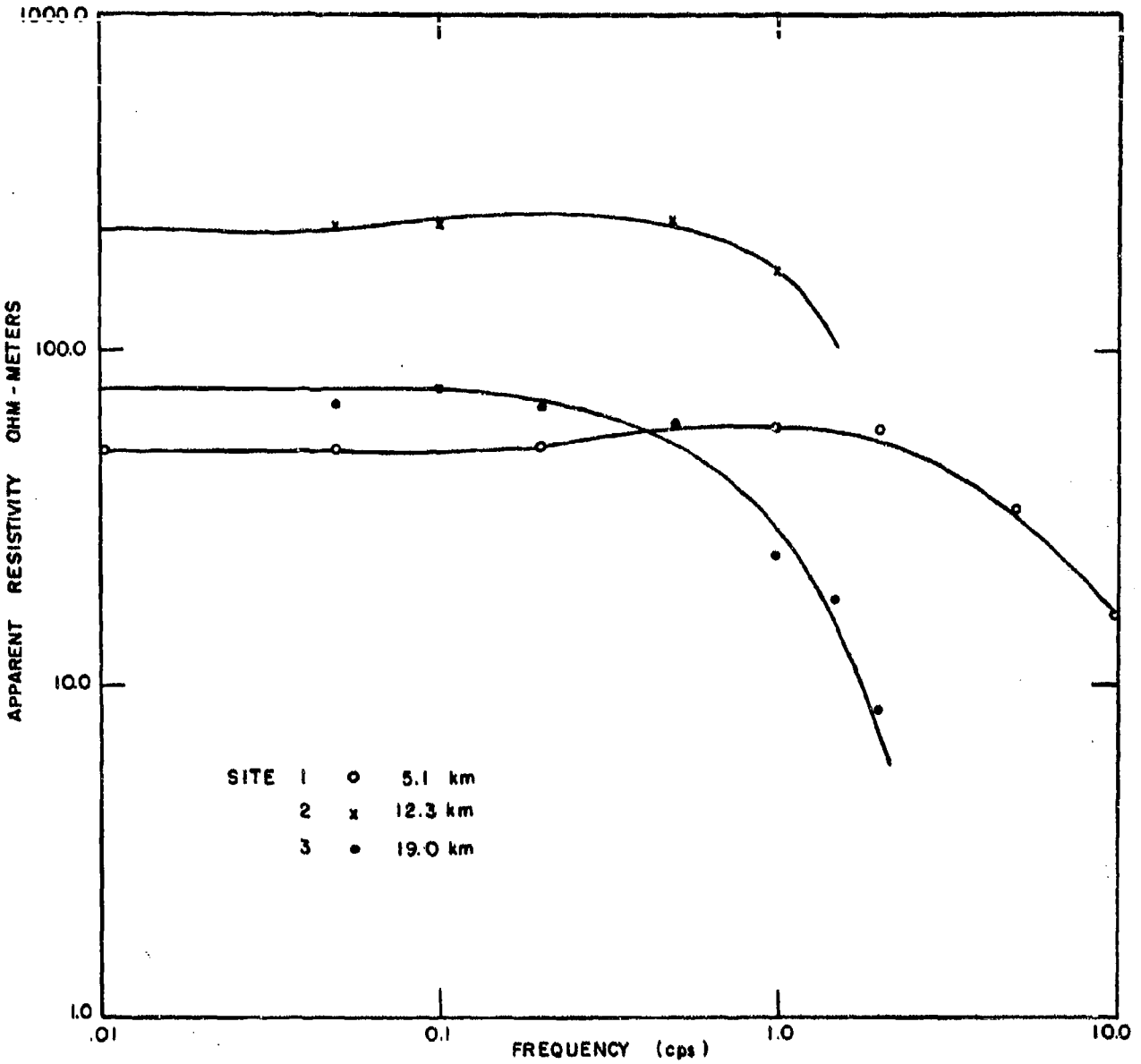

EXPERIMENTAL APPARENT RESISTIVITIES
R-COMPONENT

FIG. 43.

BIBLIOGRAPHY

1. Dunn, G. R., "An Experimental Investigation of EM Wave Propagation at 400 cps," Report No. 42R-7, Space-General Corporation, 2 April 1962.

2. Keller, G. V., "Electrical Properties in the Deep Crust," IEEE Trans., Vol. AP-11, No. 3, pp. 352-355, May 1963.

3. Sunde, Erling D., Earth Conduction Effects in Transmission Systems, p. 38, D. Van Nostrand Company, Inc. (1949).

4. Reference Data for Radio Engineers, Fourth Edition, International Telephone and Telegraph Corporation, pp. 60-70, American Book-Stafford Press, Inc., New York, N. Y., (1956).

5. Williams, F. U., and G. H. Hopkins, Jr., "Instrumentation and Techniques for Simultaneous Measurement and Synchronous Transcription of Tellurics," Report No. 123, Electrical Engineering Research Laboratory, The University of Texas, 31 May 1961.

6. "Special Issue on Electromagnetic Waves in the Earth," IEEE Trans., Vol. AP-11, No. 3, May 1953.

7. Sommerfeld, A., "Partial Differential Equations in Physics," Academic Press, Inc., New York, N. Y. (1949).

8. Foster, R. M., "Mutual Impedance of Grounded Wires Lying on or Above the Surface of the Earth," Bell Syst. Tech. Jour., 12 April 1933.

9. Riordan, J., and E. O. Sunde, "Mutual Impedance of Grounder Wires for Stratified Two Layer Earth," Bell Syst. Tech. Jour., 12 April 1933.

10. Sunde, E. D., "Earth Conduction Effects in Transmission Systems," D. Van Nostrand Co., Inc., New York, N. Y. (1949).

APPENDIX A

Silicon Controlled Rectifier Data and Schematic Diagrams of Transmitter

TENTATIVE SPECIFICATIONS

70 Ampere (110 A R.M.S.) Silicon Controlled Rectifiers*

JEDEC 2N1909 SERIES (with Single Control Lead)
IR 71RC Series (with Dual Control Leads)

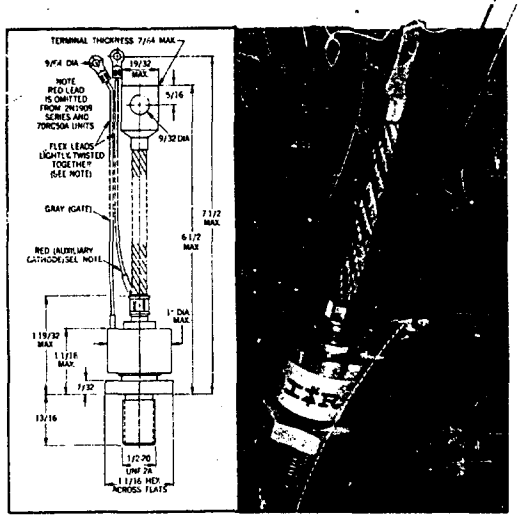

ELECTRICAL CHARACTERISTICS

(Resistive or Inductive Load, 50 to 400 cps)
(Temperatures listed refer to junction temperature unless otherwise specified)

FORWARD CONDUCTION CHARACTERISTICS

Max. Peak Forward Voltage (V_F) @ 25°C @ 70 amps average, (220A peak), 180° conduction angle: 1.80 volts
Max. RMS Forward Current (I_F) (for all conduction angles): 110 amps
Max. Average Forward Current ($I_{F(AV)}$): 70 amps @ -40 to +62°C T_{Stud}, 180 deg. cond. angle
Max. Peak One Cycle Non-recurrent Surge Current (I_{surge}): 1000 amps. (1/2 Cycle sine wave (60 cps) or 5 millisec. rectangular pulse, SCR full on)
Max. Peak Surge Current During Turn-on Interval:

Switching from	Amps Surge
200 V	400 A
300 V	270 A
400 V	200 A

Max. I^2t (for fusing): 4000 Amp^2 secs. for 0.0083 sec.
Max. Internal Thermal Resistance: 0.4 °C/Watt, junction to stud.
Typical Holding Current (I_H) @ 25°C: 10 mA
Typical Turn-On Time (t_d+t_r) @ 25°C: 2.5 to 6 μ secs. for 50A dc, resistive load.
Typical Delay Time (t_d) @25°C: .5-1.5 μ sec.
Typical Rise Time (t_r) @ 25°C: 2-4.5 μ secs.
Typical Turn-off Time (t_{off}) @ 125°C: 15 to 25 μ sec. (I_F= 50A, i_r = 10A, dV/dt = 20V/μ sec.)
Operating Temperature Range: -40°C to +125°C.

FIRING CHARACTERISTICS

Max. Peak Gate Power (P_G): 5 watts.
Max. Average Gate Power (P_G): 0.5 watts.
Max. Peak Gate Current (i_G): 2 amperes
Max. Peak Forward Gate Voltage (v_G) 10 volts.
Max. Peak Reverse Gate Voltage (v_G) 5 volts.
Max. Required Gate Current to Fire (I_{GF})* @ -40°C: 130 mA; @ 25°C: 70 mA.; @ 125°C: 40 mA.
Max. Required Gate Voltage to Fire (V_{GF})* @-40 °C: 3.0 volts.
Min. Required Gate Voltage to Fire (V_{GF})** @ 125°C: 0.25 volts.
Typical Gate Current to Fire (I_{GF}) @ 25°C: 25 mA. @ + 1.5 Volts Gate to Cathode.

MECHANICAL CHARACTERISTICS

Max. Mounting Torque on Stud: 100 pound-inches.
Weight: Approximately 3.5 ounces.
Storage Temperature: -40°C to +125°C.
Outline Dimensions: 2N1909 Series & 70RC50A - *JEDEC TO-49.*
71RC--Series-TO-49 with auxiliary cathode lead. Gate and aux. cathode lead twisted together, and color coded.
Gate lead: Grey; Aux. Cathode lead: Red.

ABSOLUTE MAXIMUM RATINGS

JEDEC TYPE SERIES (Single Control Lead)		2N1909	2N1910	2N1911	2N1912	2N1913	2N1914	2N1915	2N1916	70RC50A
IR TYPE SERIES (Dual Control Leads)	UNIT	71RC2A	71RC5A	71RC10A	71RC15A	71RC20A	71RC25A	71RC30A	71RC40A	71RC50A
Maximum Repetitive Peak Reverse Voltage (PRV)***	Volts	25	50	100	150	200	250	300	400	500
Max. allowable Transient Peak Reverse Voltage (Non-recurrent, 5 millisecond max. duration) ***	Volts	35	75	150	225	300	350	400	500	600
Minimum Peak Forward Breakover Voltage (V_{BO})	Volts	25	50	100	150	200	250	300	400	500
Maximum Reverse (I_R) or Forward (I_s) Leakage Current at PRV, at 125°C (full cycle average, Vg=0, gate open circuited)	mA	6.5	6.5	6.5	6.5	6.0	5.5	5.0	4.0	3.0

ELECTRICAL AND MECHANICAL CHARACTERISTICS FOR THE INTERNATIONAL SILICON CONTROLLED RECTIFIER 70RC50A

FIG. A-1.

*Permission for use of reprint granted by International Rectifier Corporation

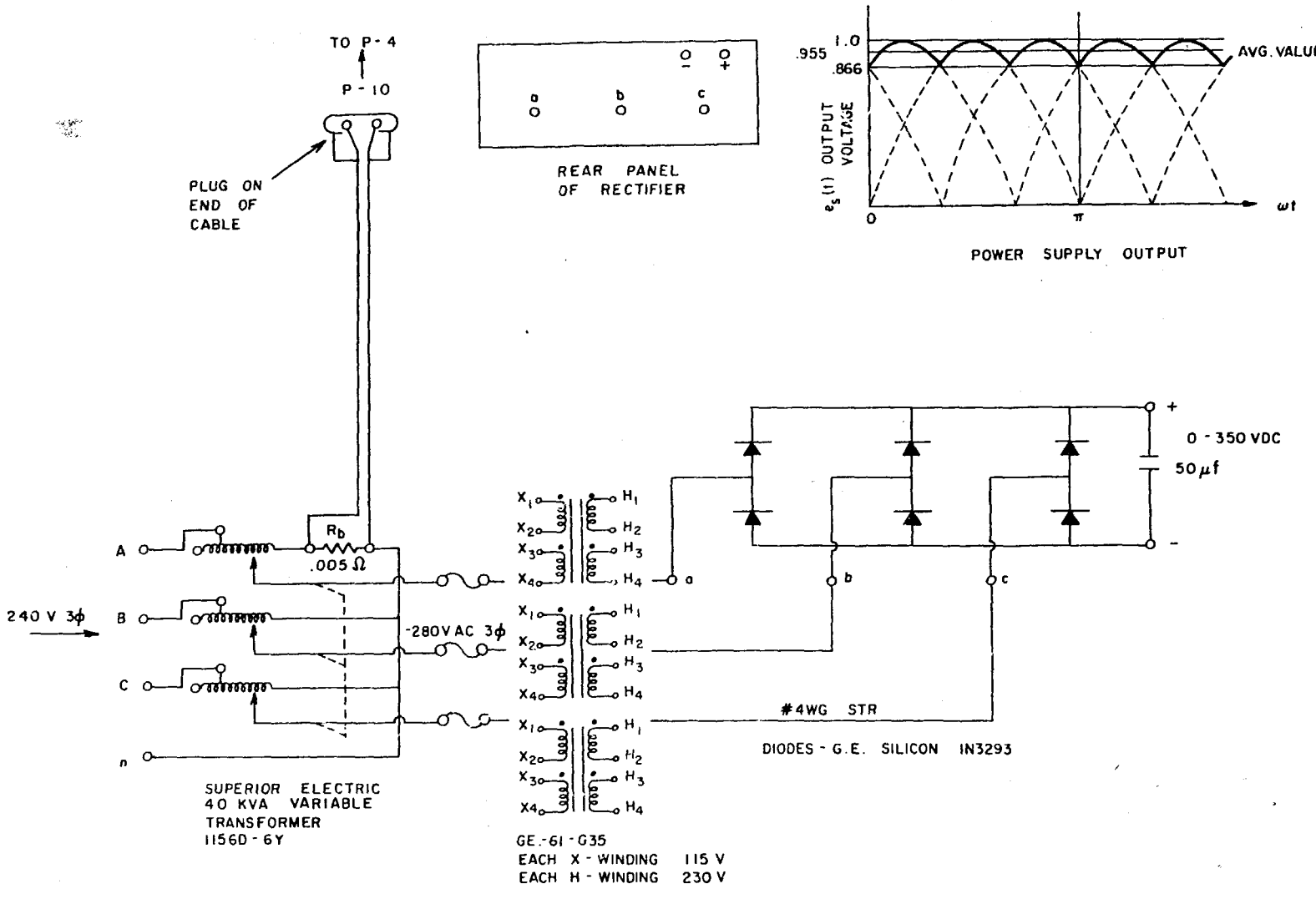

MAIN POWER SUPPLY

FIG. A-2.

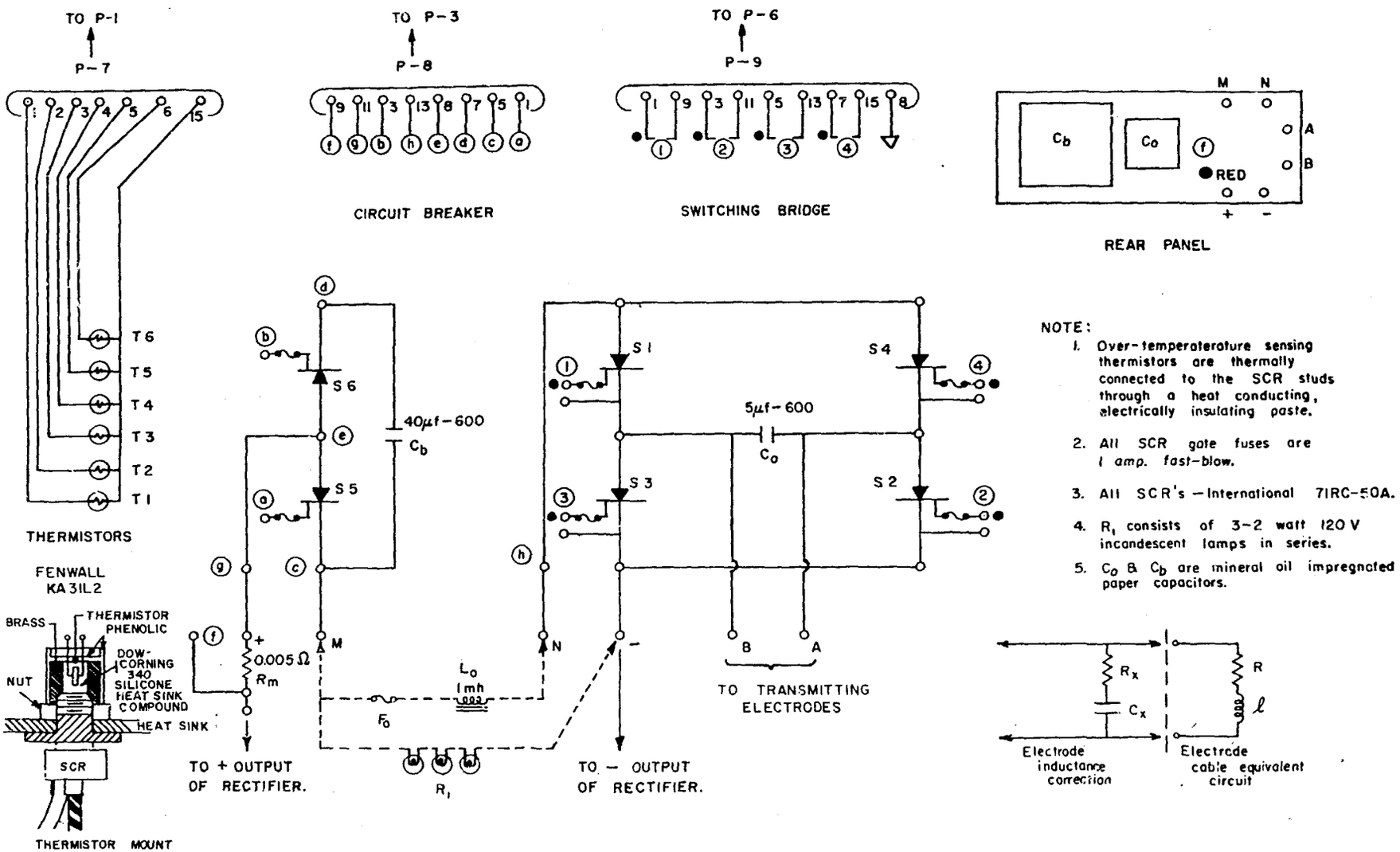

NOTE:

1. Over-temperaterature sensing thermistors are thermally connected to the SCR studs through a heat conducting, electrically insulating paste.
2. All SCR gate fuses are *1 amp. fast-blow.*
3. All SCR's — International 71RC-50A.
4. R_1 consists of 3-2 watt 120 V incandescent lamps in series.
5. C_o & C_b are mineral oil impregnated paper capacitors.

SCR SWITCHING BRIDGE AND CIRCUIT BREAKER

FIG. A-3.

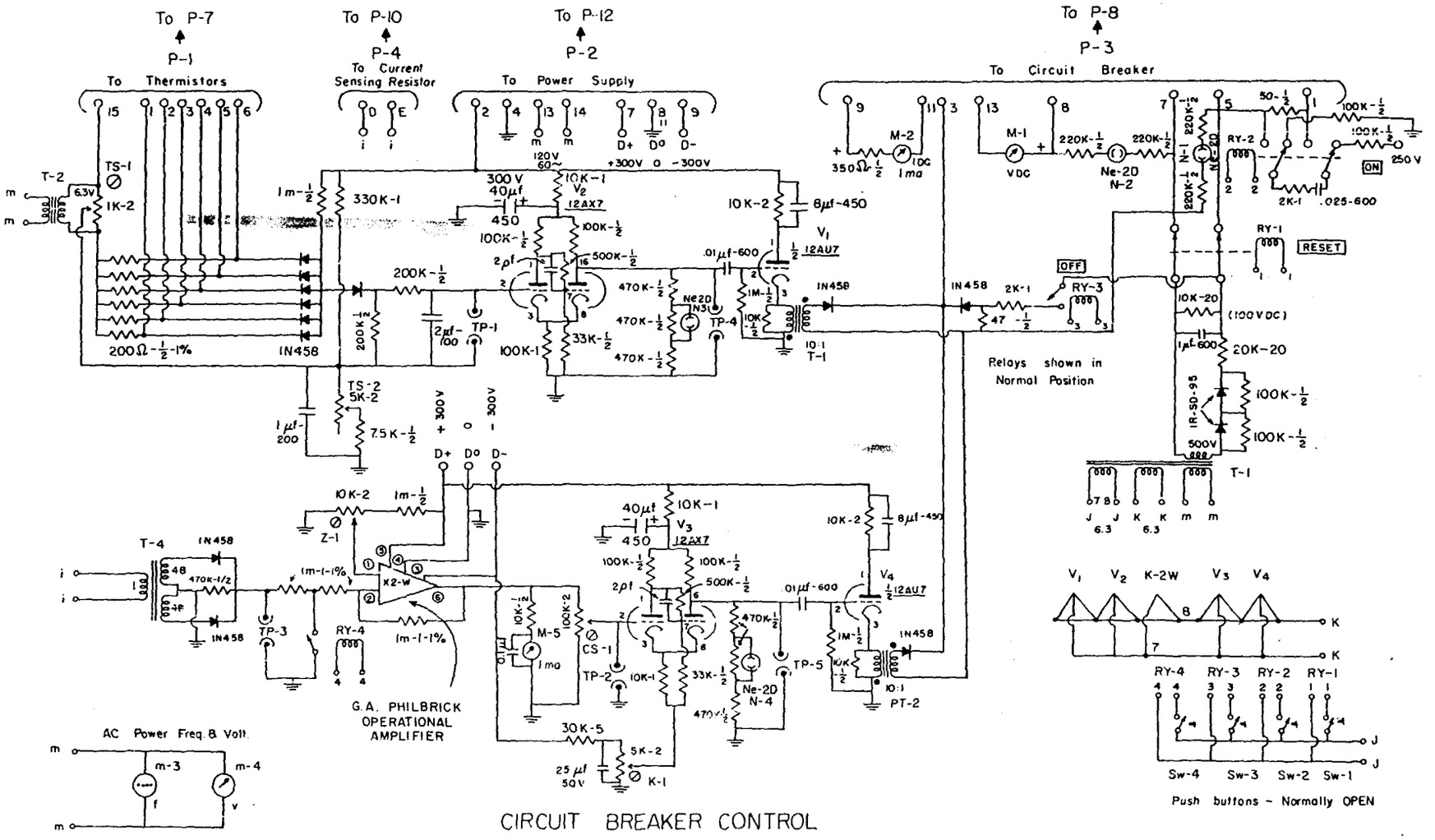

CIRCUIT BREAKER CONTROL

FIG A-4.

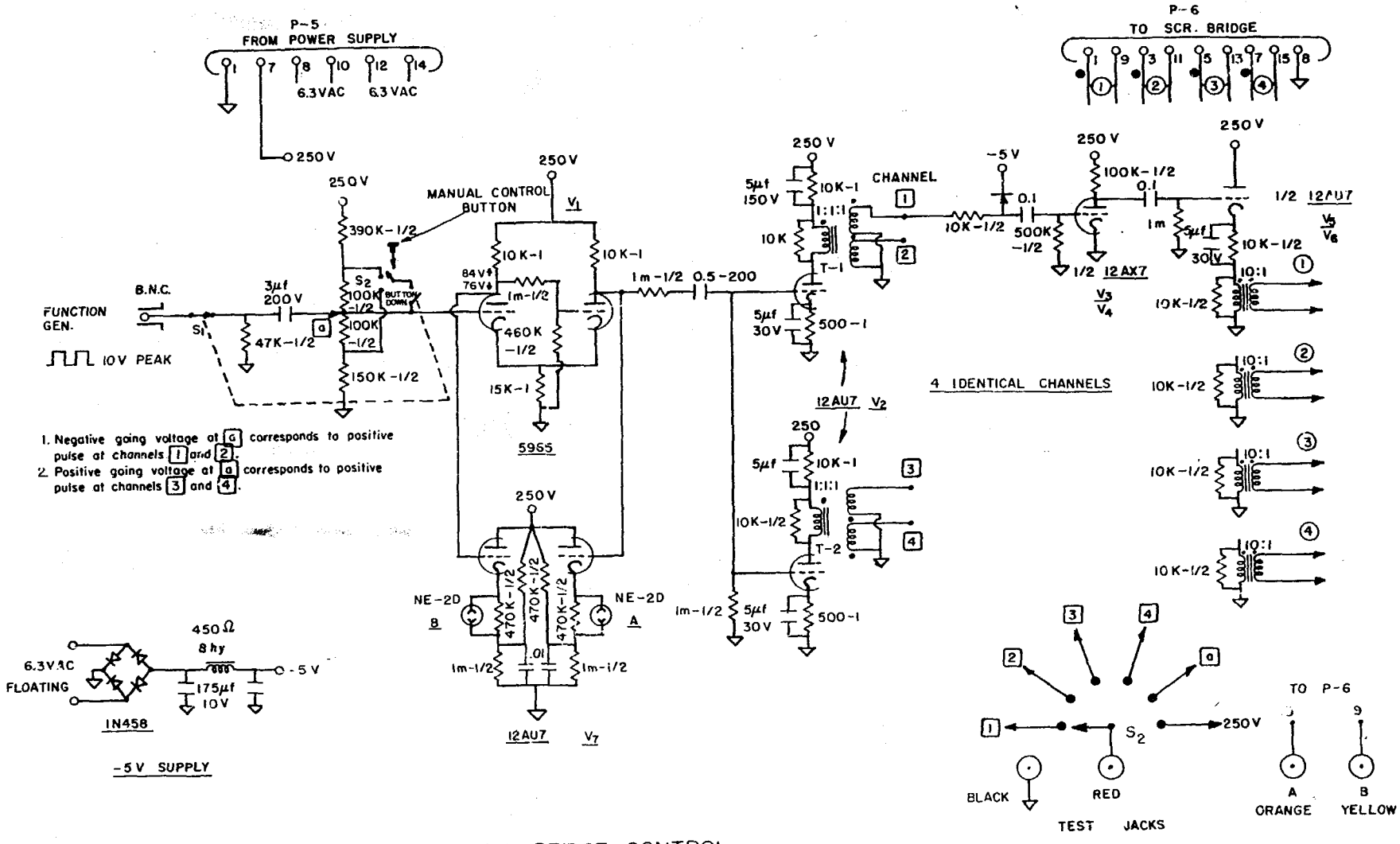

SWITCHING BRIDGE CONTROL

FIG. A-5

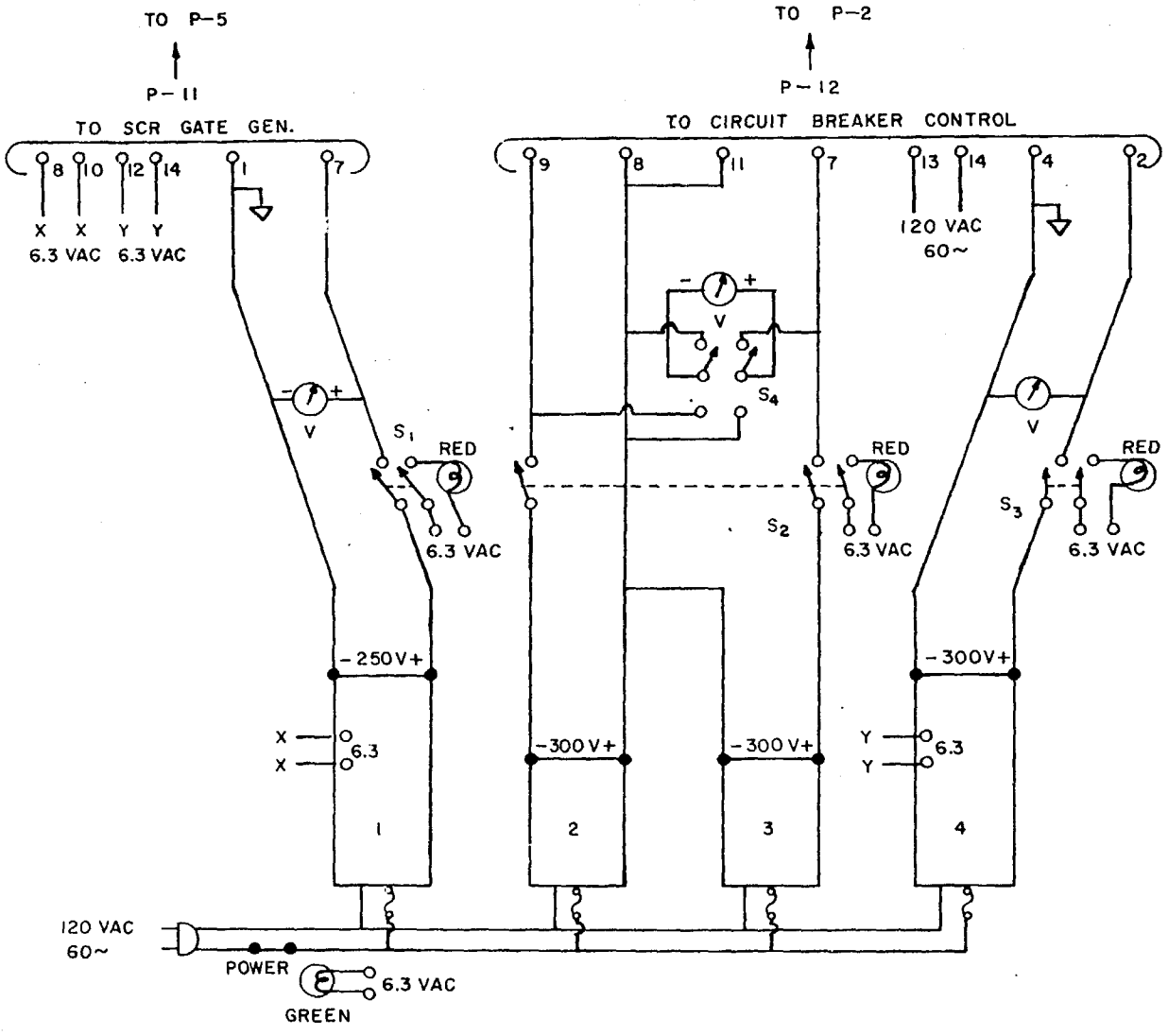

NOTE:

Power supplies are Dressen-Barnes,

1 & 4 Mod. 22-106

2 & 3 Mod. 22-104

CONTROL CIRCUITRY POWER SUPPLY

FIG. A-6.

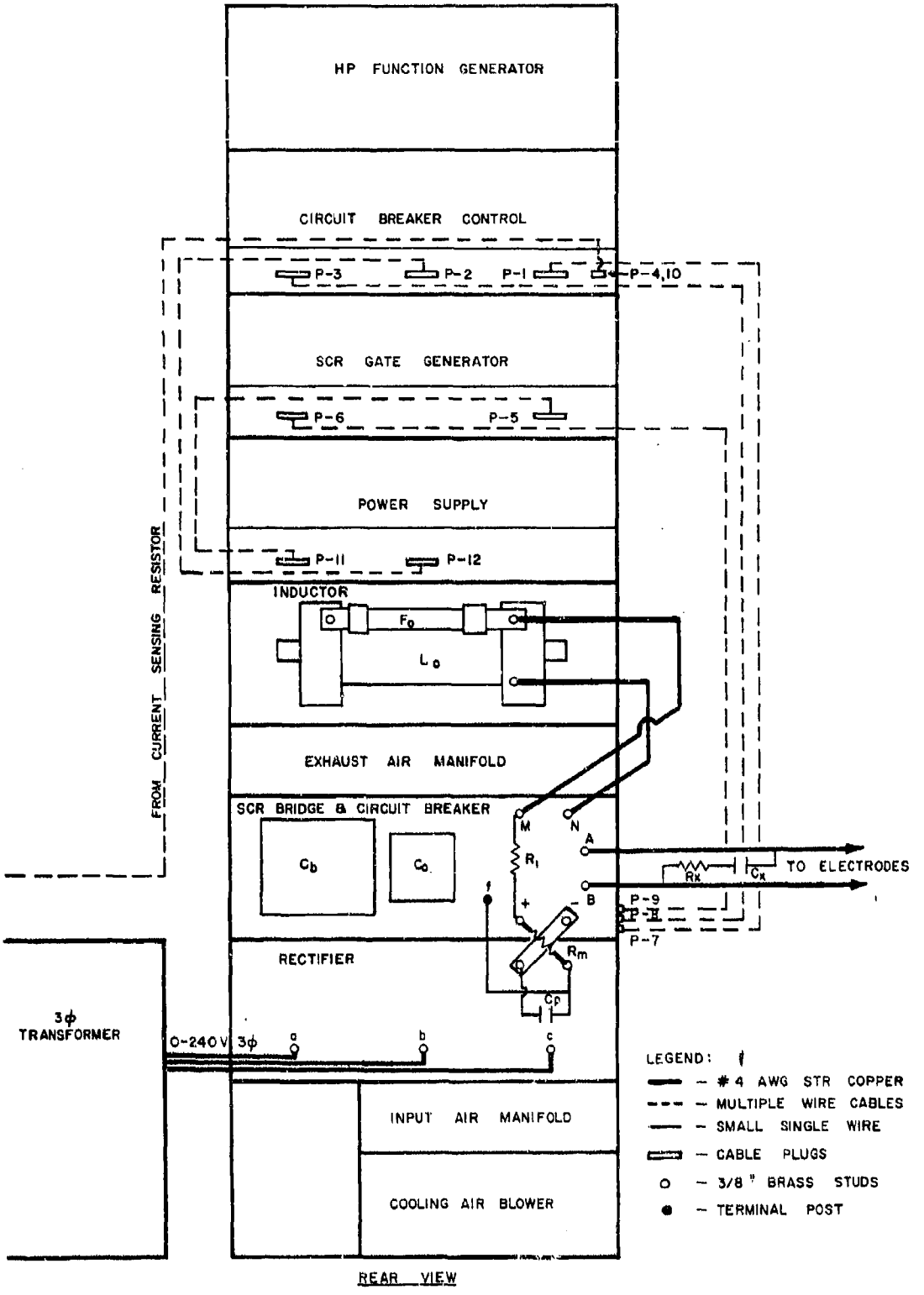

CABLE DIAGRAM

FIG. A-7.

APPENDIX B

Subsurface Resistivity Sounding in Washington-Oregon Area

Under an extension of Contract AF 19(604)-8513, during October and November of 1963, the Electrical Engineering Research Laboratory cooperated with Dr. Tom Cantwell of Geoscience, Inc., Air Force Cambridge Research Laboratories, and the Bonneville Power Administration in a project to measure subsurface resistivities in the Washington-Oregon area using the dipole-dipole method. Four transmitting electrodes were located in The Dalles, Oregon; McNary, Oregon; Redmond, Oregon; and Midway, Washington. Three transmitting dipoles were used. They consisted of The Dalles electrode used in conjunction with each of the other three. The transmitter in every case was located in The Dalles and connection to the electrodes was made through sections of 230 kv power transmission lines belonging to the Bonneville Power Administration. The transmitting electrode locations, with the exception of the Midway electrode, are shown in Figure B-1.

The receiving dipoles, some of which are indicated in the figure, consisted of electrodes connected by sections of telephone lines leased for the purpose, and ranged from about 7 to 15 miles in length. Positioning of the receiving electrodes in Figure B-1 is only approximate; however, they should be within a two-mile radius of their actual location.

The mobile earth-current measuring system from the Electrical Engineering Research Laboratory was located near LaGrande, Oregon, for the primary purpose of measuring the background noise due to natural magneto-telluric fluctuations.

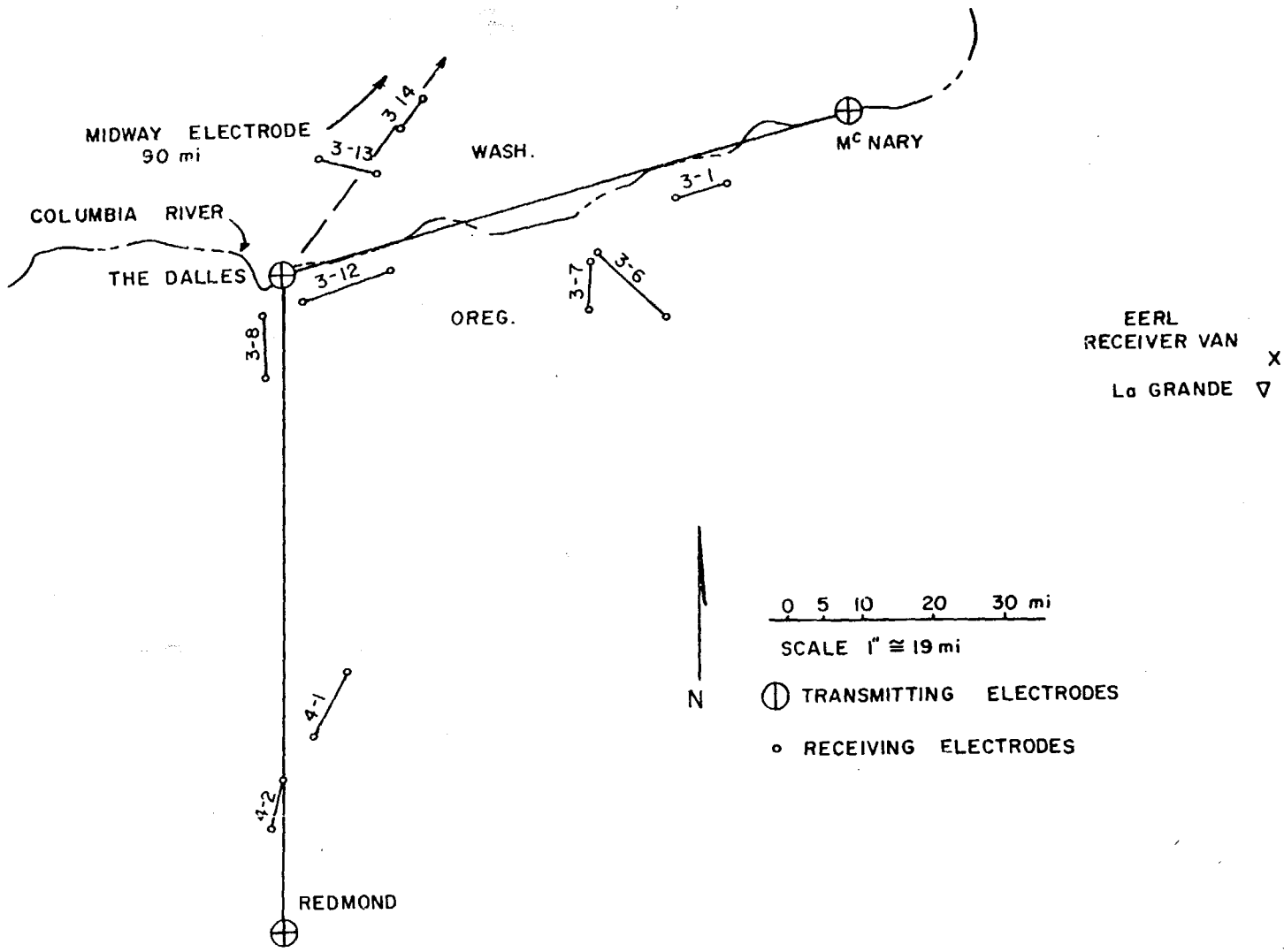

TRANSMITTING AND RECEIVING DIPOLES
IN WASHINGTON OREGON AREA

FIG. B-1.

A transmitter capable of about 300 amperes direct current with 10 ohms electrode resistance was used by the Bonneville Power Administration to energize the transmitting dipoles. The transmitter current was mechanically switched off and on to produce a square wave with a two-minute period.

Receiving dipole potentials were measured with portable systems furnished by Geoscience, Inc., which could be moved from one to the other during the course of the transmitting sessions.

Prior to the availability of the Bonneville transmitter, the Electrical Engineering Research Laboratory transmitter, described in the foregoing text, was used to energize the McNary and Redmond lines shown in Figure B-1, and measurements were made at that time at the receiving dipoles shown in the figure.

Before the EERL transmitter could be used to drive the transmitting dipoles, special attention had to be given the transmission line connecting the electrodes. The McNary and Redmond lines were about 85 and 90 miles long, respectively, and the distributed inductance and capacitance L and C were estimated by handbook formulae to be

$$L = 1.2 \times 10^{-6} \text{ hy/M}$$

$$C = 10 \times 10^{-12} \text{ f/M}$$

This gives a line characteristic impedance of $Z_o = 350$ ohms, and a total inductance of about 20 mh for a 90-mile line.

Consider the equivalent circuit of Figures B-2a, which was assumed to represent the system. The total electrode resistance plus line resistance is

R and is represented by R/2 at each end of the line. Now, if a voltage change V is applied by the transmitter to the input of the line, this change propagates down the line and is reflected with a high negative reflection coefficient ($\rho = -0.97$ for R = 10 ohms). For a 90-mile line, the time for the wave front to travel down the line and back is about 950 μsec; consequently, the input current change will rise in small steps every 950 μsec and will approach V/R with a time constant of about $\frac{L}{R}$ = 20 m sec. Note that during the first 950 μsec the voltage change at the line input or transmitter output sees a resistive load of 350 ohms. With a commutating inductor of around 1 mh, the damping factor of the transmitter commutating circuit will be very low, and proper switching, as described in Section II-D of this report, cannot occur. An R-C correction circuit with a series resistance R and a time constant of 20 m sec was placed across the transmitter output as shown in Figure B-2b. A capacitance of 2000 μf was required. With the impedance correction, the transmitter output current change, with a change in voltage of V, is the sum of the line current and the correction circuit current, and is essentially V/R as shown in the sketch of Figure B-2c.

Table 1 gives the results of measurements made while the EERL transmitter was operating. The dipole numbers refer to Figure B-1, and the apparent resistivity values, computed by Dr. Cantwell, are based on a homogeneous earth.

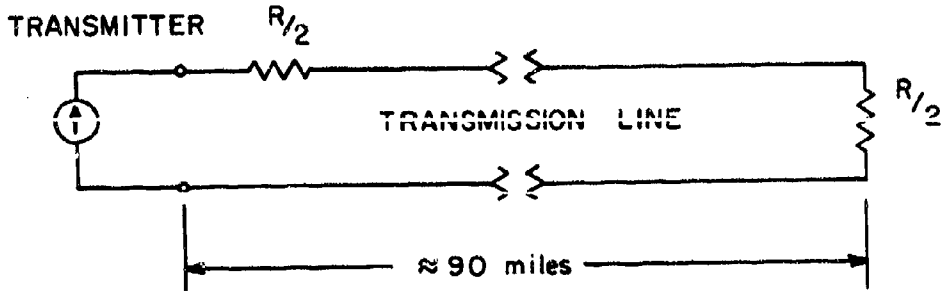

(a) EQUIVALENT CIRCUIT

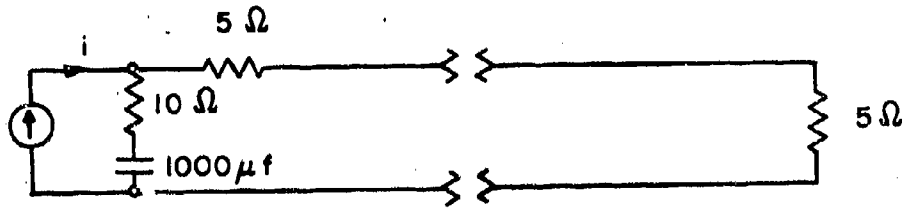

(b) IMPEDANCE CORRECTION FOR R = 10 Ω

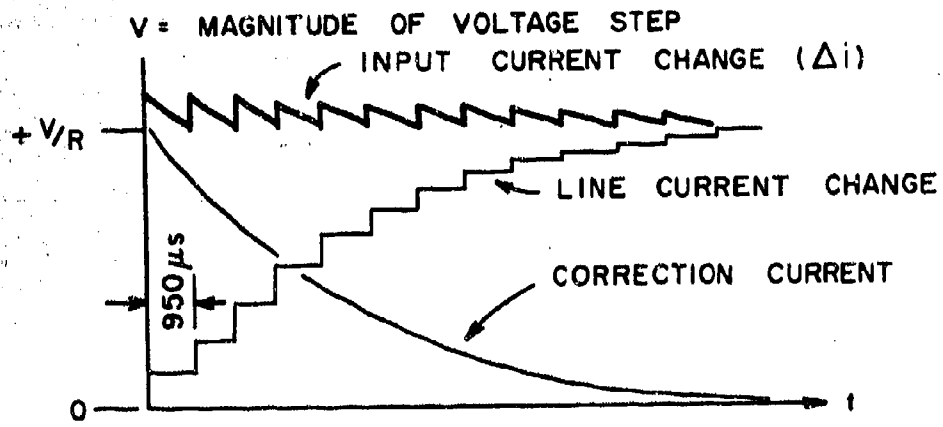

(c) TRANSMITTER CURRENT

TRANSMISSION LINE IMPEDANCE CORRECTION

FIG. B-2.

Table I

Date	Dipole	Transmitter Current (Amperes P/P)	Signal (mv)	Apparent Resistivity (Ohm-meters)
Nov. 6	3-8	104	17.0	60
Nov. 7	3-1	110	2.3	<1
	3-6	104	7.2	190
	3-7	110	5.7	13
	3-12	100	155.0	100
	3-13	100	7.5	35
	3-14	100	7.5	50
Nov. 8	4-1	100	108.0	110
	4-2	100	69.5	30

During the tests of 16 Nov. and 18 Nov., while the Bonneville transmitter was operating, the signals given in Table II were measured by the EERL mobile van in LaGrande. The numbers represent positive intensity vectors to the north and east. Electrodes were separated 1000 feet.

Table II

Date	Component	Signal
Nov. 16	E_x (North-South)	36 μv/km
	E_y (East-West)	30 μv/km
Nov. 18	E_x	30 μv/km
	E_y	9 μv/km

The transmitting electrodes were: The Dalles-McNary on Nov. 16, and the Dalles-Midway on Nov. 18. Electrode current was switched on and off with a two-minute period and was positive at The Dalles. The magnitude was 230 amperes.

This appendix is meant to be only a brief description of the participation of the Electrical Engineering Research Laboratory in the project. Geoscience, Inc. was primarily responsible, and can supply detailed information.